

Aus dem Labor für Tissue Engineering  
am BIH Center für Regenerative Therapien und der Klinik für Rheumatologie m.S. medizinische Immunologie der Medizinischen Fakultät Charité  
– Universitätsmedizin Berlin

DISSERTATION

In vitro pharmacological risk assessment of new therapeutic agents for osteoarthritis on osteochondral tissue cultures – a risk profile of CCL25

/

In vitro pharmakologische Risikobewertung neuer therapeutischer Wirkstoffe gegen Osteoarthritis an osteochondralen Gewebekulturen - ein Risikoprofil von CCL25

zur Erlangung des akademischen Grades  
Medical Doctor - Doctor of Philosophy (MD/PhD)

vorgelegt der Medizinischen Fakultät  
Charité – Universitätsmedizin Berlin

von

Jacob Burkhard Spinnen

**Datum der Promotion: 25.06.2023**

Abstract – English version.....	4
Abstract - Deutsche Version.....	5
1. Introduction.....	6
1.1 Emerging therapies for osteoarthritis.....	6
1.2 Methods and limitations of preclinical analysis for adverse Effects of experimental therapeutic approaches for osteoarthritis.....	7
1.3 Aim of the study.....	8
2. Methods.....	9
2.1. Experimental growth of osseous tissue in 3D printed scaffolds. ....	9
2.1.1. Isolation- and cultivation of different osseous cells .....	9
2.1.2. Bioprinting and cultivation .....	9
2.1.3. Analysis of vitality-/viability.....	10
2.1.4. Mineralisation assay .....	10
2.1.5. Gene expression .....	10
2.2. Studies on osteochondral thin-section cultures.....	11
2.2.1. Establishment of thin-section method.....	11
Immune cell culture from synovial fluid.....	12
2.2.2. Analysis of cell vitality- / viability.....	13
2.2.3. Histological analysis .....	13
2.2.4. Transcriptomic analysis.....	14
2.3. Immunological studies of CCL25 on human immune cell subclasses.....	14
2.3.1. Manufacturing of CCL25-containing PLGA microparticles .....	14
2.3.2. Determination of the previously established quality criteria of the produced particles	15
2.3.3. Cytokine secretion quantification.....	16
2.3.4. Analysis of surface marker expression.....	16
2.3.5. Analysis of chemotactic potential.....	16
2.4. Statistical analysis.....	16
3. Results.....	17
3.1. Bioprinting and analysis of osteoid constructs from native human bone cells .....	17
3.1.1. Different bone entities have different cell out-growth kinetics and cell yields .....	17
3.1.2. Stereolithography is suited to print highly viable cell laden 3D scaffolds.....	17
3.1.3. Periosteal cells show the strongest osteogenic potential.....	17

3.2.	Establishment of osteochondral thin section cultures .....	20
3.2.1.	Tissue slice cultures can be obtained in large quantities from single samples and exhibit stable histologic and gene expression long-term behavior .....	20
3.2.2.	Immune cells from synovial fluid and whole blood show low viability in tissue culture medium.....	22
3.2.3.	Osteochondral live slice cultures stayed highly reactive towards anabolic and catabolic stimuli without additional serum .....	23
3.3.	Stimulation of osteochondral explant cultures with CCL25.....	24
3.3.1.	CCL25 shows no cell-toxic effects on osteochondral cells .....	24
3.3.2.	Histology shows CCR9 receptor in superficial cartilage layers but no catabolic or anabolic reactions towards CCL25 stimulation.....	25
3.3.3.	Low doses of CCL25 cause proliferation marker spikes in chondrocytes while high dosages result in a mild catabolic reaction.....	25
3.4.	Analysis regarding inflammatory potential of CCL25 .....	26
3.4.1.	Direct CCL25 stimulation causes unspecific inflammatory activation and migration of different leukocyte subsets .....	26
3.4.2.	Neither CCL25 loaded- nor unloaded PLGA microparticles show strong inflammatory potential.29	
3.4.3.	Degradation products from CCL25 loaded- and unloaded PLGA microparticles cause a mild inflammatory reaction .....	31
4.	Discussion.....	33
4.1.	Bioprinting is a promising method for the development of tissue grafts but of limited use for manufacturing high numbers of pharmacological screening tissue cultures .....	33
4.2.	Thin sectioned osteochondral explant cultures prove to be highly feasible as pharmacological testing device .....	34
4.3.	Presence of CCR9 receptor and paradox effect of different CCL25 dosages on osteochondral tissue suggest an alternative/new/different mode of action .....	36
4.4.	Encapsulation of CCL25 in PLGA microparticles prevents strong inflammatory activation of different immunecell subsets.....	36
5.	Conclusion .....	37
6.	References .....	39
7.	Affidavit .....	44
	Publication 2: <b>Amler A-K, Dinkelborg PH, Schlauch D, Spinnen J, Stich S, Lauster R, Sittinger M, Nahles S, Heiland M, Kloke L, Rendenbach C, Beck-Broichsitter B, Dehne T</b> (2021). Comparison of the Translational Potential of Human Mesenchymal Progenitor Cells from Different Bone Entities for Autologous 3D Bioprinted Bone Grafts <i>Int J Mol Sci.</i> 2021 Jan 14;22(2):796.....	45
8.	Publications .....	47
8.1.	<b>Spinnen J, Shopperly LK, Rendenbach C, Kühl AA, Sentürk U, Kendoff D, Hemmati-Sadeghi S, Sittinger M, Dehne T.</b> A Novel Method Facilitating the Simple and Low-Cost Preparation of Human Osteochondral Slice Explants for Large-Scale Native Tissue Analysis. <i>Int J Mol Sci.</i> 2021 Jun 15;22(12):6394. ....	47

8.2.	<b>Spinnen J, Fröhlich K, Sinner N, Stolk M, Ringe J, Shopperly L, Sittinger M, Dehne T, Seifert M.</b> Therapies with CCL25 require controlled release via microparticles to avoid strong inflammatory reactions. <i>J Nanobiotechnology</i> . 2021 Dec 25;19(1):83.....	67
8.3.	<b>Amler A-K, Dinkelborg PH, Schlauch D, Spinnen J, Stich S, Lauster R, Sittinger M, Nahles S, Heiland M, Kloke L, Rendenbach C, Beck-Broichsitter B, Dehne T</b> (2021). Comparison of the Translational Potential of Human Mesenchymal Progenitor Cells from Different Bone Entities for Autologous 3D Bioprinted Bone Grafts <i>Int J Mol Sci</i> . 2021 Jan 14;22(2):796. ....	85
9.	Curriculum Vitae .....	109
10.	Acknowledgements.....	110

## Abstract – English version

In the field of arthritic joint diseases, numerous new therapeutic substances such as BMP-2, FGF-18 and the chemokine CCL25 are currently being investigated for the regeneration of cartilage tissue. However, the unknown clinical side effect profiles of these compounds pose a high economic development risk for a potential manufacturer. Preclinical options for risk stratification of new therapeutics are limited to either poorly informative cell culture models or logistically immensely costly and ethically questionable animal studies. Therefore, there is a clear need for informative preclinical models that can be produced in large quantities and at low cost to evaluate side effects and toxicity of experimental therapeutic approaches for joint diseases.

The goal of this work was to establish such a joint model and subsequently evaluate it for potential side effects of CCL25 on tissue.

For this purpose, a novel method for the preparation of osteochondral explant cultures from native human joint tissue was established, which can obtain up to 100 tissue cultures from a single tissue sample. To include in vitro-produced tissues as a potential pharmacological screening tool, osteoid tissue cultures were 3D printed stereolithographically from various human bone cells. After comparing both methods for their applicability, the explant models were stimulated with different concentrations of CCL25 for 21 days and subsequently evaluated for adverse effects. Furthermore, the inflammatory potential of CCL25 was analyzed in a separate experimental setup with human immune cell subclasses.

In the pharmacological analysis of CCL25 on tissue cultures, no direct toxic or strong metabolic effects on osteochondral tissue were found. However, the CCL25-specific receptor CCR9 was detected in the superficial cartilage layer, and gene expression analyses showed pro-proliferative influences at low concentrations and mild catabolic influences at high CCL25 concentrations. Immunological analysis of CCL25 revealed that CCL25 has immense pro-inflammatory potential from concentrations of 50-100 nM and this must be considered as an important source of side effects in the context of therapeutic application.

In conclusion, the thin section cultures proved to be a very suitable pharmacological screening tool with high production capacity and long tissue stability at the same time. The investigation of CCL25 did not show any direct tissue toxicity or metabolism alterations, but nevertheless a paradoxical proliferation stimulation and a high inflammatory potential, which underlines the absolute necessity of a dosage control during application in case of a possible translation of CCL25 as therapeutic agent.



## Abstract - Deutsche Version

Auf dem Gebiet der arthritischen Gelenkerkrankungen werden es derzeit zahlreiche neue therapeutische Stoffe wie z.B. BMP-2, FGF-18 sowie das Chemokin CCL25 zur Regeneration von Knorpelgewebe untersucht. Die unbekanntenen klinischen Nebenwirkungsprofile dieser Stoffe stellen jedoch für einen potenziellen Hersteller ein hohes wirtschaftliches Entwicklungsrisiko dar. Präklinische Optionen zur Risikostratifizierung neuer Therapeutika beschränken sich entweder auf wenig aussagekräftige Zellkulturmodelle oder auf logistisch immens kostspielige und ethisch fragwürdige Tierversuche. Daher besteht ein deutlicher Bedarf an aussagekräftigen präklinischen Modellen, die in großen Mengen und zu geringen Kosten hergestellt werden können, um Nebenwirkungen und Toxizität experimenteller therapeutischer Ansätze für Gelenkerkrankungen zu bewerten.

Ziel dieser Arbeit war es, ein solches Gelenkmodell zu etablieren und es anschließend auf mögliche Nebenwirkungen von CCL25 auf das Gewebe zu untersuchen.

Dafür wurde eine neuartige Methode zur Herstellung von osteochondralen Explantatkulturen aus nativem menschlichem Gelenksgewebe etabliert, die aus einer einzigen Gewebeprobe bis zu 100 Gewebekulturen gewinnen kann. Um in-vitro hergestellte Gewebe als potenzielles pharmakologisches Screening-Instrument einzubeziehen, wurden Osteoid-Gewebekulturen aus verschiedenen menschlichen Knochenzellen stereolithografisch 3D-gedruckt. Nach dem Vergleich beider Methoden auf ihre Anwendbarkeit, wurden die Explantmodelle 21 Tage lang mit verschiedenen Konzentrationen von CCL25 stimuliert und anschließend auf schädliche Auswirkungen untersucht. Weiterhin wurde das inflammatorische Potential von CCL25 in einem separaten Versuchsaufbau mit menschliche Immunzellsubklassen analysiert.

In der pharmakologischen Analyse von CCL25 an Gewebekulturen wurden keine direkten toxischen oder starke metabolische Einflüsse auf osteochondrales Gewebe festgestellt. Der CCL25-spezifische Rezeptor CCR9 konnte jedoch in der oberflächlichen Knorpelschicht nachgewiesen werden und genetische Analysen zeigten proliferative Einflüsse bei niedrigen Konzentrationen- und leicht katabole Einflüsse bei hohen CCL25-Konzentrationen.

Die immunologische Untersuchung von CCL25 ergaben, dass CCL25 ab Konzentrationen von 50-100 nM ein immenses pro-inflammatorisches Potential besitzt und dies als wichtige Quelle von Nebenwirkungen im Rahmen einer therapeutischen Anwendung betrachtet werden muss. Zusammenfassend erwiesen sich die Dünnschnittkulturen als ein sehr geeignetes pharmakologisches Screeninginstrument mit hoher Herstellungskapazität bei gleichzeitig langer Gewebestabilität. Die Untersuchung an CCL25 zeigten keine direkten Gewebetoxizität- oder Metabolismusalterationen, gleichwohl aber eine paradoxe Proliferationsstimulation und ein hohes inflammatorisches Potential, welches bei einer möglichen Translation dieses Wirkstoffes die absolute Notwendigkeit einer Dosierungskontrolle bei Applikation unterstreicht.

# 1. Introduction

## 1.1 Emerging therapies for osteoarthritis

Osteoarthritis (OA) is the most common joint disease worldwide, affecting 5 million patients in Germany alone (Europe 40 million, U.S.A. 27 million) (prevalence: women 27%, men 18%)(1)(2). The available conservative therapy consists of anti-inflammatory and analgesic drugs as well as symptomatic injection of hyaluronic acid into the joint space. Due to the chronic progressive course, surgical procedures for joint or cartilage transplantation are usually the last therapeutic options left(3)(4)(5). In 2015, a total of approximately 398,000 joint replacement prostheses due to OA were implanted in Germany. The pure surgical costs for these were about 4,378,000,000€ in 2014; assuming mean surgical costs of 11,000€, costs of pre-treatments, complications and rehabilitation not included. This makes osteoarthritis one of the most burdensome diseases for society in economic terms - not only because of treatment costs, but also because of sick days. Due to the increasing prevalence of risk factors such as obesity and demographic change, costs are expected to rise even further (6).

In recent years, a paradigm shift has occurred in the therapeutic prospects for degenerative cartilage diseases. The former belief that cartilage is a non-regenerative tissue has been changed by clinical experience with transplantation of autologous cartilage, chondrogenic matrices and in vitro studies on cartilage matrix cultures(7,8). It is now known that chondrocytes require a special pro-regenerative microenvironment in addition to mechanical prerequisites to initiate matrix regeneration processes. The natural production of this microenvironment is often prevented by chronic inflammatory processes(9–11). Since then, there have been a number of research efforts to identify and characterize new agents and methods for regenerative stimulation of chondrocytes or cartilage tissue. The majority of studies in this area are based either on so-called growth factor proteins such as fibroblast growth factor 18 (FGF-18) and bone morphogenic protein 2 (BMP-2) or on specific cell therapies(12,13). With regard to cell therapies, numerous experimental projects have shown that a specific form of stem cells, called mesenchymal stromal cells (MSCs) hold therapeutic potential due to their highly regenerative secretome, which induces anabolic processes and regulates the local immune response - in the case of cartilage, precisely the microenvironment necessary to regenerate the matrix(14–17).

A promising approach to combine the simplicity of protein-based therapy with the regenerative potential of MSCs is in-situ tissue engineering. The concept is based on refraining from harvesting and culturing cells and instead recruit autologous stem cells to the site of the lesion - which would prove to be much more economical and less invasive than an autologous cell therapy(18). The Tissue Engineering Laboratory at Charité – Universitätsmedizin Berlin is currently developing a chemokine-based attractant for MSCs that recruits a sufficient amount of autologous stem cells by injection into the damaged tissue. In broad migration assays, the C-C motif chemokine ligand 25 (CCL25) was identified as a potent candidate for therapeutic chemoattraction of MSCs (19). Using osteoarthritic Dunkin-Hartley guinea pigs as animal model a weekly intra-articular injection of CCL25 dissolved in hyaluronic acid for five weeks resulted in a 25% mean reduction in cartilage degeneration compared to the untreated counterpart(20). To eliminate the need for frequent injections while maintaining a constant level of biologically active CCL25 in the joint space, a poly(lactide-co-glycolide) (PLGA)-based microparticle was developed in which the chemokine can be encapsulated and released in a controlled manner over a longer period of time(21,22). If successful, this could achieve a concentration which constantly recruits cells over 40-60 days and, through their secretome, establishes a pro-regenerative milieu in the joint.

This poses the possibility of a therapeutic option that is able to effectively to counteract the progression of osteoarthritis, which would at the same time be economically feasible and applicable on an outpatient basis.

## 1.2 Methods and limitations of preclinical analysis for adverse Effects of experimental therapeutic approaches for osteoarthritis

A major drawback of all growth factor- or chemokine based, innovative therapeutic strategies is the lack of clinical data regarding the safety or possible side effects of their application. This poses an obstacle in the translation of new therapeutic approaches, as further clinical development is an verycostly undertaking and for any potential investor the possibility of unforeseen side effects represents a major financial risk. Therefore, existing products are often simply improved slightly instead of investing many resources in the development of completely new strategies(23). This also applies to the drug candidate CCL25. Until now, no chemokine has been used therapeutically and it is therefore completely unclear from an empirical point of view which side effects could occur through intra-articular injection. A published literature search on our part revealed that the CCR9/CCL25 signaling axis is involved in numerous immunological and neoplastic processes(24). Increased expression of CCR9 and secretion of CCL25 is found in pathological conditions such as endometriosis, inflammatory bowel disease, rheumatoid arthritis, as well as in various neoplasms such as colorectal carcinoma and non-small cell lung cancer(25–29). It can therefore be assumed that the application of CCL25 could possibly cause serious inflammatory as well as hyperplastic side effects which in turn renders the further translation of the therapy very risky. To decide whether further translation of the active ingredient makes clinical and economic sense, a targeted risk analysis is required which allows the probability of occurrence of side effects to be calculated. Traditionally, in the case of joint tissue, two-dimensional chondrocyte cultures in monolayer and OA animal models are available for preclinical testing of the efficacy and side effects of such substances(30–32). Unfortunately, the former often leads to limited findings due to the lack of representation of the complex joint tissue composition (33), while the latter is associated with high costs and time expenditure and is therefore usually only applied when a basic efficacy seems to be very likely(15,34,35). Moreover, animal experiments are increasingly considered unethical and no longer appropriate for a modern society. There is therefore a general impetus, especially in the field of pharmaceutical research, to develop alternative research methods that can both answer complex questions and at the same time do not involve physical or psychological suffering for sentient beings(36). Recently, this spectrum has expanded to include sophisticated 3D cultures and organ-on-chip applications. However, 3D cultures are either costly to maintain or, in the case of joint-on-a-chip, not yet commercially available. Therefore, these methods are rather unsuitable for large-scale pharmacological studies with multiple doses and time points(37–39).

One possibility currently opening up for the large-scale production of tissue cultures is the so-called bioprinting: a interdisciplinary field between additive manufacturing and tissue engineering. This process technology is very heterogeneous; however, all individual processes are based on the fact that the architecture of the desired tissue scaffold is digitally pre-designed with computer assisted design (CAD) software and then reproducibly produced by a computer numerical control system. The process of bioprinting consist of an layer-by layer build up of biological matrices which hardens to provide enough structural integrity for the following layer. These biomaterials can often be populated with cells prior to printing and can retain their vitality during the printing process by using cell-friendly printing methods. In contrast to tissue cultures such

as bone or cartilage micromasses, which are costly to produce, large quantities of identical tissue cultures could be produced and used for pharmacological testing in a short time thanks to the automation capability of this process(40–43).

Another very sustainable middle ground between cell- and animal models in joint modeling, however, is the use of tissue explants. Explants are living, native, and functional parts of organs obtained from donor tissues or cadavers. In contrast to monolayer cell cultures, explants can accurately represent part of the tissue composition and architecture(44)(45). In particular, tissue cells remain in their native extracellular matrix configuration and questions about their response to biological stimuli can be answered much more reliably in the native situation than, for example, with monolayer cultures containing only one, heavily altered cell type. As early as 2009, Pretzel et al. published a highly regarded bovine explant in vitro model that they co-cultured with synoviocytes and were able to observe excellent cross-reactions of the different tissues over a longer period of time.(45),(46). However, in osteochondral research this modeling technique is severely limited by the availability of human donor tissue. With the commonly used technique of vertical punching of the joint tissue and subsequent fabrication of osteochondral punches with a diameter of at least 3 mm, only a very small number of explants can be fabricated from a tissue sample, depending on the tissue properties. In addition, the diffusion of nutrients and potentially interacting proteins is strongly hindered by the amount of glycosaminoglycans in the tissue. Therefore, explant thickness correlates negatively with the information that can be obtained about the behavior of cells located deeper in the tissue. These limitations make explants attractive for basic science but have prevented their use in larger-scale pharmacological studies.

### 1.3 Aim of the study

The aims of this study were

- I. The identification of appropriate tissue and cell culture forms for pharmacological risk assessment of new therapeutics for OA in specific comparison of tissue engineered tissue and native tissue culture
- II. The subsequent risk profiling and determination of possible therapeutic range of CCL25 application on osteochondral tissue.

For this purpose, stereolithographic bioprinting was used to rapidly produce osteoid cultures from various native human bone cells, which can also serve for large-scale pharmacological analysis. Following printing, the constructs were cultured for 28 days and examined histologically and on gene expression level for tissue formation.

In a comparative work, a novel method for the preparation of osteochondral explant cultures from human native tissue was established, allowing large numbers of cultures to be prepared from a small number of human samples. Subsequently, this tissue model was investigated for its suitability as a pharmacological testing tool - including the possibility of co-culturing the tissue cultures with immune cells from autologous synovial fluid. Following these experiments, the explant cultures were inoculated with three different concentrations of CCL25 and examined for changes in viability, histology, and gene expression.

To complete the CCL25 risk profile in terms of immunological components regarding potential side effects, human leukocytes were isolated from whole blood in a second experimental set-

up, cultured and inoculated with three different concentrations, as well as the components of the PLGA-based release system. Following this, the expression of activation-indicating surface markers on the leukocytes was measured via flow cytometry, the secretion of pro-inflammatory proteins was quantified by protein assay, and the chemoattractive potential of CCL25 on the different immune cell subclasses was recorded by migration assay.

## 2. Methods

### 2.1. Experimental growth of osseous tissue in 3D printed scaffolds.

#### 2.1.1. Isolation- and cultivation of different osseous cells

A central part of the study was the evaluation of the osteogenic potential of different native cell sources. Therefore, cells were isolated from the following collection sites: (I) human bone marrow aspirate from the iliac crest, (II) cancellous fibula bone from remnants of a free tissue flap as part of a mandibular Maxillo-Facial surgical reconstruction, and (III) periosteal cells from mastoid tissue obtained during a mastoidectomy (Fig. 1 (a)). Periosteal cells were extracted from human mastoid by digesting the tissue samples with collagenase and subsequent seeding into cell culture. Fibula bone cells were grown out from cancellous bone by mincing and seeding the bone in tissue culture flasks containing cell culture medium containing fibroblast growth factor 2 (FGF-2). Bone marrow cells were isolated from bone marrow aspirates in the same manner as cancellous bone cells. In total, 30 million cells per donor site were cultivated. Due to the rather unspecific outgrowth culture, in which the cells grow out of the tissue via the nutrient gradient, the cells were first named mesenchymal progenitor cells (MPCs) and subsequently characterized more precisely via flow cytometry.

#### 2.1.2. Bioprinting and cultivation

Following cell expansion of the cells in the monolayer, the MPCs of different donor sites were placed in a suspension of methacrylated gelatin concentrated at  $20 \times 10^6$  cells at  $\text{ml}^{-1}$  (GelMA) (Fig 2 (b)). A concave disk-shaped matrix with the diameter of 4mm and depth of 0.6mm was designed via CAD and exported as a stereolithographic file. Subsequently, projection-based stereolithography was used to print a solid construct from the model and the prepared GelMA solution by projecting high-precision photomasks onto the printing dish (Fig 1 (c) and (d)). The different constructs were cultured and analyzed in osteogenic medium (DMEM with  $1 \text{ g L}^{-1}$  glucose, 10% FCS, 2.5% HEPES,  $100 \text{ U mL}^{-1}$  penicillin,  $10 \text{ } \mu\text{g mL}^{-1}$  streptomycin,  $100 \text{ nM}$  dexamethasone) for 28 days. In total, 70 replicates were printed per cell type plus 70 non-laden constructs.

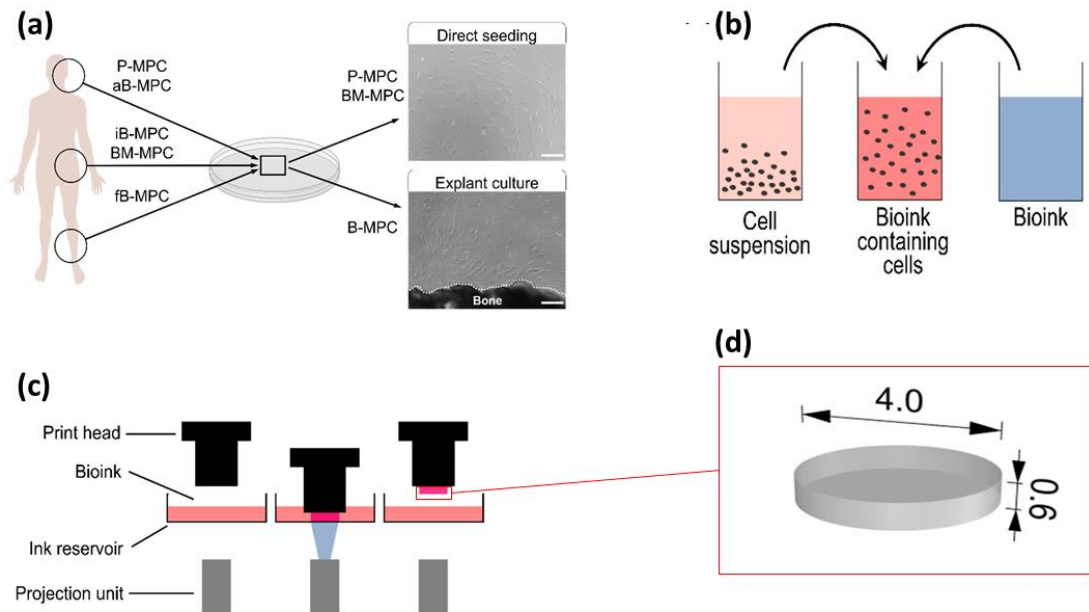


**Figure 1. Experimental setup.** (a) Human mesenchymal progenitor cells were isolated from different body tissues (alveolar bone (aB-MPC), fibula bone (fB-MPC), iliac crest bone (iB-MPC), iliac crest bone marrow (BM-MPC), periosteum of the mastoid (P-MPC)). Scale bar = 200  $\mu$ m. (b) Preparation of bioink prior to bioprinting. (c) The bioprinting process. The print head is lowered into the ink reservoir and the bioink is solidified by projecting photomasks. (d) 3D model of printed construct which was previously designed with computer-assisted design (CAD) software and exported as an stereolithography (STL) file. Measurements are given in mm.

**Figure adapted from co-authored publication in International Journal of molecular science:**

**Amler A-K, Dinkelborg PH, Schlauch D, Spinnen J, Stich S, Lauster R, Sittinger M, Nahles S, Heiland M, Kloke L, Rendenbach C, Beck-Broichsitter B, Dehne T.** Comparison of the Translational Potential of Human Mesenchymal Progenitor Cells from Different Bone Entities for Autologous 3D Bioprinted Bone Grafts. *Int J Mol Sci.* 2021 Jan 14;22(2):796, (47).

### 2.1.3. Analysis of vitality-/viability

On day 1, 7 and 28, the constructs were stained by PI/FDA and analyzed by fluorescence microscopy for the ratio of live to dead cells. Furthermore, a metabolic resazurin assay was performed on day 1, 10 and 28 to assess metabolic cell activity and individual cell viability progression.

### 2.1.4. Mineralisation assay

The most significant analytical parameter for the suitability of the individual cell sources is the rapid deposition of calcium phosphate crystals in the soft matrix environment. Therefore, the constructs were analyzed by osteoimage mineralization assay to quantify the hydroxyapatite content present. Staining intensity was determined in darkfield using a BIOREVO BZ-9000 microscope.

### 2.1.5. Gene expression

Analogous to the thin section model, the gene expressing phenotype of the bone cells in their matrix was determined at the gene expression level. For this purpose, RNA was isolated from the constructs and the following osseous-specific genes were analysed by Real Time – quantitative Polymerase Chain Reaction (RT-qPCR): Alkaline Phosphatase (*ALPL*), Collagen I (*COL1A1*), Runt-related transcription factor 2 (*RUNX2*), Secreted protein acidic and cysteine rich (*SPARC*) and Secreted phosphoprotein 1 (*SPP1*). The transcript for the ribosomal housekeeping gene Tata-Box Binding Protein (*TBP*) was used as the reference gene.

## 2.2. Studies on osteochondral thin-section cultures.

The experiments on the thin-section explants are divided into three different phases. In the first phase, the production of the explant cultures was established and the culture form was examined for its suitability for long-term cultivation. For this purpose, the sections were cultured in a stimulus-free environment for 21 days and examined for their natural behavior in cell viability, histological integrity and gene expression phenotype. Furthermore, we isolated local leukocytes from the synovial fluid of tissue donors to evaluate the possibility of osteochondral - leukocyte co-culture.

In a second series of experiments, we examined whether the tissue responded adequately to catabolic and anabolic stimuli in order to determine its utility for biologic pharmacological studies. To this end, cultures were inoculated with varying concentrations of the catabolic protein TNF- $\alpha$  and the anabolic protein TGF- $\beta$  and re-examined after 7 days for cell viability, histology, and gene expression. Experiments were performed both with and without the addition of fetal bovine serum (FBS) to investigate whether the tissue requires additional co-stimulators to respond adequately to external stimuli. After confirmation by the first two series of experiments that osteochondral thin-section explants are suited for large-scale pharmacological experiments, cultures were now inoculated with different concentrations of CCL25 in the third series of experiments. The cultures were constantly stimulated with either 1 nM, 5 nM or 50 nM CCL25 for 21 days and then subsequently examined for cell viability, as well as histological and transcriptomic alterations.

### *2.2.1. Establishment of thin-section method*

The quantity limitation in the production of explant cultures is mainly due to the complicated and time-consuming preparation. Since both the cartilaginous and the bony tissues have to be cut, so far tissue punches have mainly been used for explant preparation in order to preserve the integrity of the tissue inside the punch. Therefore, the first step was to establish a cutting technique that could produce the thinnest possible pieces of tissue without damaging the integrity of the osteochondral junction. Tibial plateaus from patients with grade III osteoarthritis were removed during surgical knee arthroplasty which served as donor tissue. Tissue removal was performed in cooperation with the Center for Musculoskeletal Surgery of the Charité and the Clinic for Orthopedics of the Helios Klinikum Berlin Buch. Instead of punching out the tissue vertically from above, the tissue punch was placed laterally at the edge of the plateau, to punch out a cylinder parallel to the surface. This cylinder was subsequently cut vertically into 500 $\mu$ m thin slices.

To enable reproducible and effective cutting of the osteochondral tissue, the punching cylinder had to be firmly fixed in the tray of a rotary microtome. Therefore, a special workpiece was 3D-printed of resin with the same dimensions as a normal paraffin mold normally used in such microtomes, which was made in collaboration with the Charité workshop. In the center of the workpiece are four cylindrical wells with dimensions 9.6 - 10 x 20 mm, into which the punched-out tissue-cylinders can be inserted and fixed. The cylinders are produced with a special tissue punch (OATS<sup>®</sup>, Arthrex), which are clinically used for mosaic plastics for cartilage reconstruction. It ensures low-injury punching safety via both, blade and handle design, and have an integrated ejection system (Fig 2 (a)). After punching out a cylinder, measuring 2 x 1 x 1 cm, the cylinder is fixed in the custom-made microtome insert and placed in the microtome. The microtome is then set to a cut thickness of 500  $\mu$ m and cut with a N35 axial microtome blade with a swing.

The cut is then divided into three equal parts with a scalpel (Fig 3. (b)). The sections are placed in so-called hanging inserts in 24 well cell culture plates. These inserts allow an upright position of the explant culture with simultaneous 360° mass transfer (Fig. 2 (c)). To increase diffusion efficiency, the plates are placed on a horizontal shaker that tilts 45° in both directions at a rate of 10 iterations per minute. The shaker and plates are placed in an incubator under cell culture conditions at a temperature of 37°C and 5%/CO<sub>2</sub>.

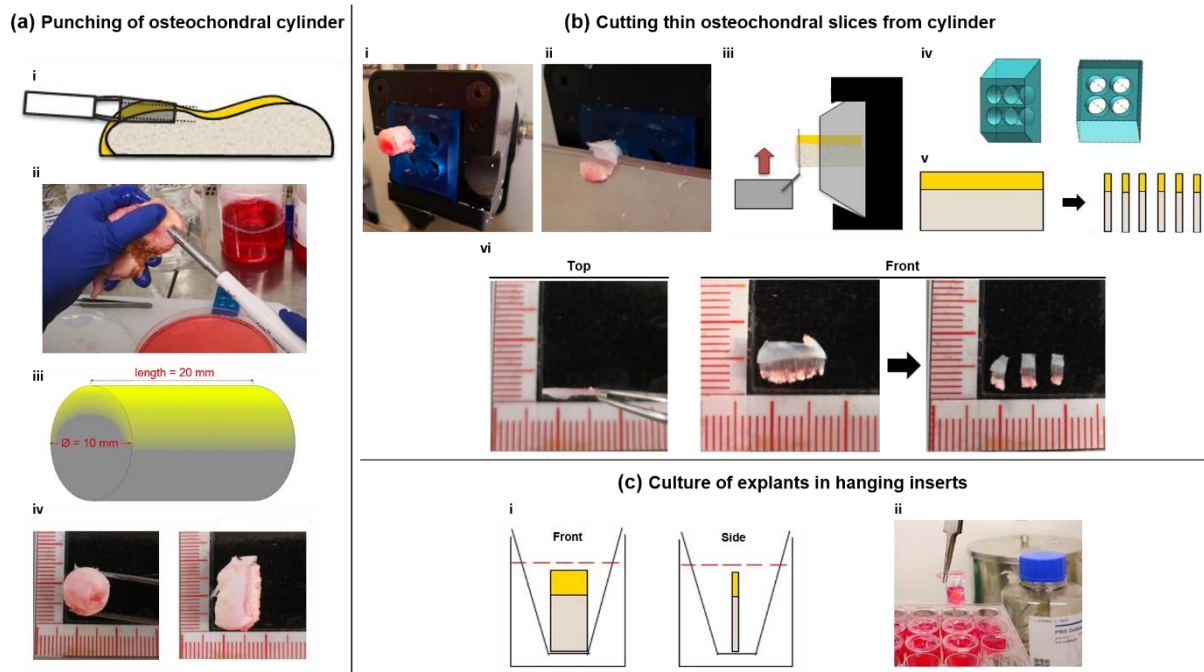


**Figure 2. Fabrication and culture of osteochondral live slices.** (a) *Punching of osteochondral cylinders.* A 2cm thick with a 1cm diameter 1 x 1 sized osteochondral cylinder is punched out of the macroscopically unaffected area of a recently explanted human tibial plateau under sterile conditions using an orthopedic OATS® Tissue Punch (i, ii). The resulting cylinder is shown schematically in iii, cartilaginous areas are highlighted in yellow. Front and side views of the cylinder are shown in iv. (b) *Cutting of osteochondral slices from the cylinder.* The cylinder is inserted into a 3D-printed microtome insert (iv) with no additional fixation (i), and 500 - 800 µm thick cuts are cut out from the cylinder (ii). Fixation of the cylinder is shown schematically in iii. The resulting disc-shaped cuts (schematic: v) are cut into three parallel-pipedal slices using a scalpel (vi). (c) *Slices are immediately transferred to a hanging insert of a multi-well cell culture plate and covered in cell culture medium (i,ii).* Plates are then placed on a horizontal shaker for culture at 37 °C and 5% CO<sub>2</sub>.

Figure is obtained from own publication in International Journal of Molecular Science:

Spinnen J, Shopperly LK, Rendenbach C, Kühl AA, Sentürk U, Kendoff D, Hemmati-Sadeghi S, Sittinger M, Dehne T. A Novel Method Facilitating the Simple and Low-Cost Preparation of Human Osteochondral Slice Explants for Large-Scale Native Tissue Analysis. *Int J Mol Sci.* 2021 Jun 15;22(12):6394, (48).

#### Immune cell culture from synovial fluid

CCL25 is mainly known in the context of chronic inflammatory diseases. Therefore, it was tested whether it is possible to simulate the immunological environment of the joint and to co-culture the osteochondral explants with their local immune cells. For this purpose, the synovial fluid of the patients was aspirated intraoperatively with a sterile cannula before removal of the joint. All cells were isolated, analyzed by flow cytometry and cultured in the possible low-stimulus media for the tissue culture (Dulbeccos modified eagle medium (DMEM) with 5% HEPES Buffer and 1% Penicillin/Streptomycin / Roswell Park Memorial Institute (RPMI) with 5% HEPES Buffer and 1% Penicillin/Streptomycin). Subsequently, the various immune cell subclasses were examined by flow cytometry for their individual survival in the respective media.



To distinguish the different subclasses we used antibodies against CD45-FITC (general leukocytes), CD3-PE (T-cells), CD14-PE (Monocytes), CD16-PE (neutrophile granulocytes), CD56-FITC (natural killer cells) and CD19-FITC (B-cells). LIVE/DEAD™ Fixable Aqua Dead Cell Stain Kit (Thermo Fisher Scientific, Waltham, USA) was used to exclude dead cells.

### 2.2.2. Analysis of cell vitality- / viability

Essential for the usability of the thin-section explant culture is the certainty that the cells within the tissue usually remain vital over the entire cultivation period. However, optical methods for determining vitality are generally only suitable as endpoint analysis due to the mostly toxic dyes or stimulation methods. Therefore, a non-toxic, metabolic assay would be much more suitable, as a progression analysis for pharmacological testing. To simultaneously determine long-term cell viability and the applicability of a metabolic assay, a total of 13 cultures from 2 different donors were cultured for 21 days. At the end of the cultivation period, two cultures of each donor were heated at 60°C for 30 minutes or 60 minutes to reduce cell viability and to achieve a homogeneous distribution of different viability levels within the samples. Subsequently, samples were incubated in a 10% resazurin DMEM cell culture medium mixture at 37°C in the dark for 2 hours. Resazurin is an oxidized, non-fluorescent blue dye that reduces to the fluorescent purple resorufin in human mitochondria. The amount of vital cells can be quantified indirectly via the fluorescence of the medium. To verify that this assumption can also be made for cells within solid tissues, the cell viability of samples measured in this manner were verified optically. For this purpose, the tissues were stained with the live/dead staining mixture propidium iodide/fluorescein diacetate, the former staining exclusively avital cells and the latter vice versa staining exclusively vital cells. When excited in a wavelength of 475 nm, avital cells fluoresce red and vital cells fluoresce green at an emission wavelength of 535 nm, allowing a direct relationship of cell viability to total cell quantity. To simultaneously penetrate deep enough into the cartilage tissue and bypass its autofluorescence, a Nikon Scanning Confocal A1Rs1+ (Nikon, Tokyo, Japan) confocal laser microscope was used, which is capable of rendering a high-resolution three-dimensional image of the cell distribution - and its vitality status - through field-of-view shifts in the  $\mu\text{m}$  range. To test the coherence of the metabolic resazurin assay with the optical analysis of cell viability, the cell density of the vital cell per  $\text{mm}^3$  was first determined using a script for the ImageJ image analysis program. Subsequently, these values were statistically compared with the fluorometric measurements of the resazurin assays and correlated regressively. Due to a sufficient correlation of about 88%, further long term cultures were tested exclusively with the metabolic resazurin assay for cell viability.

### 2.2.3. Histological analysis

Integral to the usability of tissue culture is the long-term stability of the native tissue configuration to guarantee reliable readout. Of greatest interest here is whether the cutting process damages the integrity of the cartilaginous connective tissue to such an extent that the proteoglycans of the matrix flow out into the surrounding medium. This process is known *in vivo* from cartilage damage and osteoarthritis and alters the tissue enormously - so would be limiting for the usability of the cultures(49). To detect tissue proteoglycan concentration, tissue cultures from 15 donors were cryopreserved in embedding medium and liquid nitrogen on days zero, seven, fourteen, and twenty-one, respectively, and then cut into 4  $\mu\text{m}$  thick sections on a cryotome. The sections were then stained with Safranin-O/Fast-Green histochemical stain, which stains sulfated proteoglycans red and is suggested by the Osteoarthritis Research Society International (OARSI) for histopathological classification of cartilage damage(50). The stained sections were

photographed under a histologic microscope and proteoglycan content was analyzed by histomorphometry. Briefly, pictures were taken and all pixels in the areas of interest were valued in the RGB color mode with a tool based on Xcode (Apple inc., Sunnyvale, CA, USA). Histomorphometry was performed by using the following macro on the software:

$$\text{Pixel counted as red} = (\text{Value}_{\text{Red}} * 2) > \text{Value}_{\text{Green}} + \text{Value}_{\text{Blue}}$$

$$\text{Intensity of red pixel} = 2 * \text{Value}_{\text{Red}} - \text{Value}_{\text{Blue}} - \text{Value}_{\text{Green}}$$

Values of the intensity ranged between 1 and 508, and reporting images depicting the intensity distribution were created (see Supplemental Figure S3). The mean intensity (sum of intensities/area of interest) was calculated from each image.

#### 2.2.4. Transcriptomic analysis

Gene expression analysis was performed aiming to assess whether the cell-specific gene expressing phenotype is maintained and whether any observed effects are a response to a stimulus or a culture artefact. For this purpose, mRNA was isolated from the native cartilage samples by shock freezing and disruption using a special column system. This was then transcribed into cDNA by reverse transcriptase and subsequently quantified using RT-qPCR. The succinate dehydrogenase complex flavoprotein subunit A (SDHA) was used as a reference gene, since this mitochondrial protein is not directly involved in the synthesis of matrix proteins, in contrast to common housekeeping genes such as GAPDH, and is therefore suited for the gene expression analysis of connective and supporting tissue cells. The mRNA of following matrix proteins was analyzed: the cartilage-specific collagen II (*COL2A1*), the more bone-specific collagen I (*COL1A1*), the proteoglycan aggrecan (*ACAN*), the cartilage support protein cartilage oligomeric matrix protein (*COMP*) and the cell division marker KI-67 (*Ki67*).

### 2.3. Immunological studies of CCL25 on human immune cell subclasses.

Due to the previously determined insufficient coverage of immunological physiology of the joint by the explant model, additional studies on the effects of CCL25 on immunological human cells are necessary. For this purpose, blood was collected from human donors and peripheral blood monocyctic cells (PBMCs) were isolated. These were placed in different culture forms and inoculated with three different stimuli. In the first group, the immune cell subclasses were inoculated with 3 different concentrations of CCL25, in the second group with CCL25-loaded and unloaded PLGA microparticles, and in the third with the supernatants of degraded PLGA microparticles (CCL25-loaded and unloaded). Subsequently, the secretion of pro-inflammatory cytokines was quantified in the supernatants of the immune cell cultures. Furthermore, the cells were examined for the expression of activation/polarization markers by flow cytometry and the chemotactic effect of the individual stimulation components on the different immune cells was measured via migration assay.

#### 2.3.1. Manufacturing of CCL25-containing PLGA microparticles

To incorporate the hydrophilic chemokine CCL25 (Peprotech, Rockyhill USA) into the biodegradable polymer PLGA (Sigma-Aldrich, St. Louis USA), a water-in-oil-in-water (w1/o/w2) double emulsion followed by solvent evaporation was performed. For this, PLGA polymer was immersed in methylene chloride and served as the organic (o) phase. The internal aqueous phase consisted of 1 µg CCL25 per mg PLGA dissolved in lactose, bovine serum albumin and (300 mM)/BSA (0%

or Tris- buffer. After preparation, the particles were freeze-dried overnight and stored at 4° C. After removal of the supernatant, fresh medium was added to the particle solution and it was placed back in the shaker. Samples were collected every seven days, starting with day 7, and every 14 days from day 35 to day 63.

**2.3.2. Determination of the previously established quality criteria of the produced particles**  
Scanning electron microscopy (SEM) analysis of the size and surface morphology of the particles was performed using a JFM-6000 electron microscope (Jeol, Akishima, Japan) for quality control of the prepared particles. On day 1 and day 63, images of the current batch of particles were acquired using the backscatter electron (BSE) detector at 200x and 1000x magnification. SEM analysis at day 1 showed consistently round particles of only slightly pronounced pore formation on an otherwise smooth surface. After a degradation period of 63 days, the shape of the previously round particles had been completely lost, leaving only fragments or deformed particles. This indicates that the degradation process is a prerequisite for the functional release of CCL25 (Fig. 3a). The release kinetics were in accordance with the quality criteria for successful protein encapsulation previously determined by our research group: The amount of CCL25 released from the PLGA microparticles was measured using the human CCL25/TECK DuoSet® enzyme-linked immunosorbent assay (ELISA) kit (R&D Systems, Minneapolis, USA). The onset of the release process could be identified around day 14, with more than 90% of the total CCL25 detected between day 21 and day 28. The strongest release was observed between days 14 and 21. Recovery of CCL25 amounted to 77% of the incorporated CCL25 (Fig. 3b)(21).

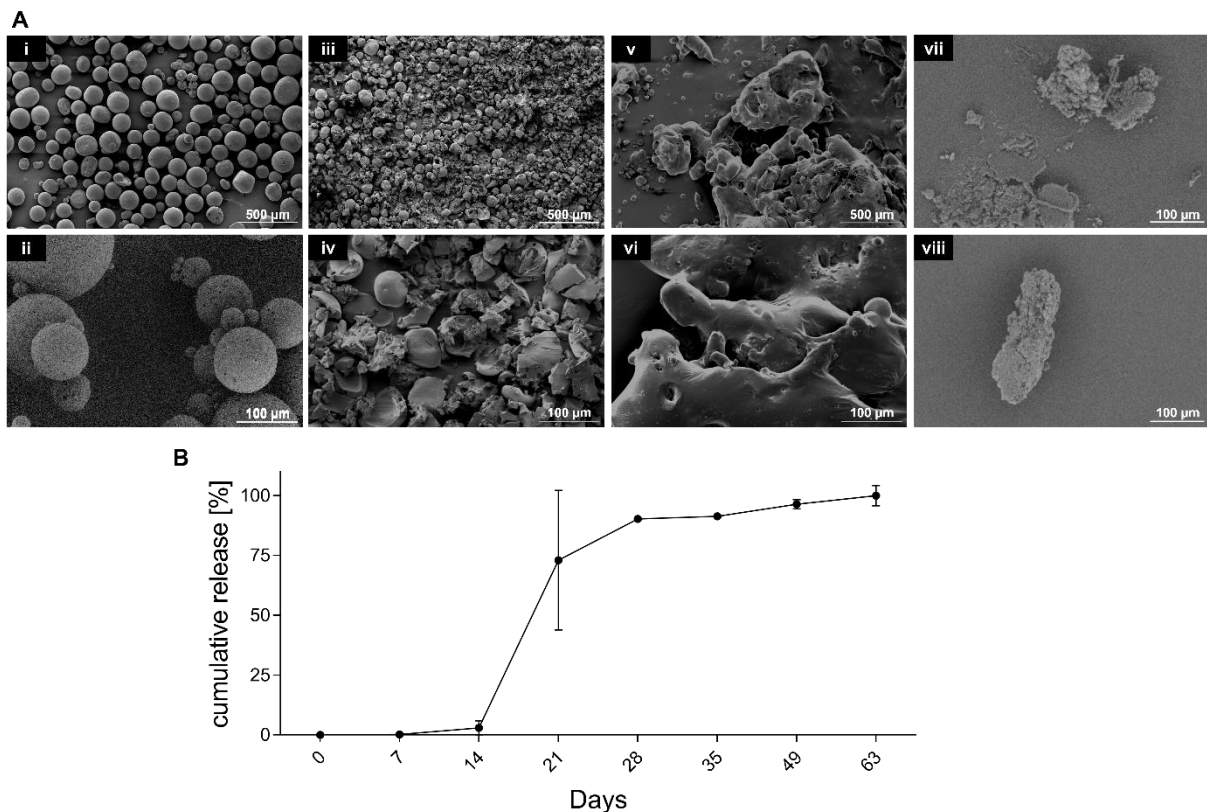


**Figure 3. A** Characteristic features of PLGA particles. PLGA particles were analyzed morphologically with SEM, and functionally assessed by their CCL25 release profile. Representative SEM images of the PLGA particles generated are shown in **a i, ii** with  $\times 40$  and  $200\times$  magnification at day one, **iii, iv** with  $\times 40/\times 200$  magnification after 14 days of degradation, **v, vi** with  $\times 40/\times 200$  magnification after 28 days of degradation and **vii, viii** with  $\times 1000$  magnification after 63 days of degradation. Scale bars represent 500 and 100  $\mu\text{m}$ , respectively **B** The cumulative release in percent  $\pm$  SD

of CCL25 from PLGA particles over time until day 63 ( $n = 3$ ) was determined by ELISA. CL CCL25-loaded, PLGA Poly (lactic-co-glycolic acid)

**Figure partly consists of images from own publication in Journal of Nanobiotechnology:**

**Spinnen J, Fröhlich K, Sinner N, Stolk M, Ringe J, Shopperly L, Sittinger M, Dehne T, Seifert M.** Therapies with CCL25 require controlled release via microparticles to avoid strong inflammatory reactions. *J Nanobiotechnology*. 2021 Dec 25;19(1):83, (51).

### 2.3.3. Cytokine secretion quantification

Cytokine secretion was quantified by analysis of cell culture supernatants after one, three, and five days. For this a LEGENDplex™ human inflammation cytokine protein array was used. This array quantifies known pro-inflammatory signaling proteins; in our case with particular focus on the following: IFN- $\gamma$ , TNF- $\alpha$ , MCP-1, IL-6, IL-8, IL-10. All samples were measured in a FACS Canto II cytometer and analyzed using Legendplex software.

### 2.3.4. Analysis of surface marker expression

After investigating the purity of the different PBMC subclasses with the antibodies CD3 FITC, CD4 PE, CD8 PE, CD14 PE, and CD15 FITC, the inflammatory activation-inducing surface marker HLA-DR was detected on all of them with the antibody HLA-DR PECy7. CCR9 expression was assessed on all cell types separately with an antibody against CCR9 (CD199 APC). PBMCs contained 60% T lymphocytes (CD3+), 46% CD4+ T lymphocytes, 26% CD8+ T lymphocytes, and 19% monocytes (CD14+). Changes in surface markers on macrophages were analyzed using the antibodies CD14 APCCy7 and CD16 PerCPCy5.5 (general monocyte/macrophage markers), CD80 PE and HLA-DR PECy7 (M1 macrophage polarization markers), and CD206 APC (M2 polarization marker).

### 2.3.5. Analysis of chemotactic potential

The migration behavior was investigated using a modified Boyden-Chamber assay. The principle is based on two-chamber systems separated by a microporous polycarbonate membrane. In one chamber the cultured cells are seeded, in the other chamber the possibly chemotactic stimulus is introduced. After a defined incubation time, the amount of migrated cells was evaluated manually from takes images assisted by a Cell Counter plugin for the optical analysis software ImageJ.

## 2.4. Statistical analysis

In the context of descriptive statistics, all data sets from the different stimulation experiments were each tested for normal distribution using the Lilliefors-corrected Kolmogorov-Smirnov test. Normally distributed data sets were analyzed with a paired Student's t-test to detect significant changes compared with negative controls. Data sets that were not normally distributed were tested for significance using the nonparametric Mann-Whitney U test. Because only one statistical test was performed for each data set, a Bonferroni-Holms-corrected p value of  $0.05/1 = 0.05$  was considered significant. Due to the low risk of a multiple comparison problem, no additional post-hoc tests were performed. Since high standard deviations are to be expected due to the work with human native samples and the associated donor variability, a Grubbs outlier test was performed on all data sets to minimize errors of the second kind.

The correlation of the optically determined cell vitality with the fluorometrically quantified results of the metabolic vitality measurement was performed individually for each donor using the two tailed Pearson test for correlation analyses

For the establishment of the osteochondral thin-section tissue cultures an a priori case number calculation was performed. Based on the existing studies on the high efficacy of anabolic and

catabolic signaling proteins on osteochondral tissue in conjunction with the effect uncertainties in the reestablishment of this particular tissue culture, a moderate coefficient of determination of the model of  $R=0.6$  was applied(52)(45). Thus, the required number of cases was calculated to be  $n=15$  donors with a target power of 0.8 and a fixed alpha error of 0.05. Since each stimulation time point and test concentration requires 15 biological replicates, a total of 390 tissue cultures from 15 different tissue donors were examined.

## 3. Results

### 3.1. Bioprinting and analysis of osteoid constructs from native human bone cells

#### *3.1.1. Different bone entities have different cell out-growth kinetics and cell yields*

The tissue from the different sampling sites each showed very different behavior in the outgrowth culture. While the periosteal cells and bone marrow cells reached first confluence after 14 days, it took up to 28 days for the solid bone parts to reach the first passage. Even after the first passages, the cancellous bone MPCs took 10 - 11 days to reach the next passage, while the bone marrow- and periost derived cell sources took about 4 - 5 days. To produce the required quantity of cells per sampling site, a total of 40-50 days were required.

#### *3.1.2. Stereolithography is suited to print highly viable cell laden 3D scaffolds*

To print cell-laden constructs with a cell density of  $20 \times 10^6$  cells per  $\text{mm}^3$ , a total of 30 million cells per donor were required. After Printing of the constructs, they were cultured in an osteogenic medium for 28 days and examined microscopically at day 0 and day 28. The microscopic images from day 0 showed a homogenous cell distribution in the cell-loaded constructs. Subsequently, the cell-free bioprints maintained their size and disc-like shape throughout the cultivation period, whereas shrinkage and central retractions were observable in the cell-loaded constructs. During cultivation, the periosteal cell-loaded constructs became progressively less translucent. All other constructs maintained translucency throughout. Propidium fluoride/fluorescein diacetate live-dead staining showed cell viability of  $>90\%$  for all cell-loaded printed constructs during the 28-day. dead (Fig. 4 (a)). To assess the kinetics of metabolic activity of the cells, a resazurin-based metabolic viability assay was also performed. All different cell types showed an increase in metabolic activity relative to baseline values at day 10, which also fell back to approximately baseline levels in cell types at day 28. The increase was most pronounced in periosteal cells (1.7-fold increase), followed by bone marrow (1.4-fold increase) extracted and bone-derived cells (1.2-fold increase) (Fig. 4 (b)).

#### *3.1.3. Periosteal cells show the strongest osteogenic potential*

The two-step process of bone matrix formation consists of collagen-I based formation of the osteoid and its subsequent calcification by osteoblast incorporation of small calcium phosphate crystals. These intercalations were investigated using the OsteoImage™ mineralization assay, which stains the hydroxyapatite components of the minerals. Analogous to the metabolic activity, constructs loaded with periosteal cells also showed a uniform signal on day 28. Constructs containing bone marrow-derived MPCs showed incipient ossification in the form of the formation of nodule-like structures. Constructs containing cells isolated from whole bone showed no signal at all in the majority (Fig. 4 (c)). To assess osteogenic differentiation of the printed constructs

at the level of gene expression, RT-qPCR normalized to the housekeeping gene TATA box binding protein (*TBP*) was performed. The markers of early osteogenic differentiation alkaline phosphatase (*ALPL*) and collagen I (*COL1A1*), the osteogenic regulatory marker runt-related-transcription factor 2 (*RUNX2*), and the markers of late osteogenic differentiation osteonectin (*SPARC*) and osteopontin (*SPP1*) were measured. All of the above genes were detectable in the differently loaded constructs, but with widely varying expression: The marker gene of early osteogenic differentiation *ALPL* showed a significant increase over the 28 days of cultivation only in B-MPCs. The also early mentioned osteogenic marker gene *COL1A1* displayed a significant increase in constructs with B-MPCs and for BM-MPCs. In contrast, a significant decrease in *COL1A1* expression was observed in constructs with periosteal cells within the first 7 days and remained at a lower level at day 28. Furthermore, a stable expression of the marker genes of late osteogenic differentiation *SPARC* and *SPP1* could be detected.

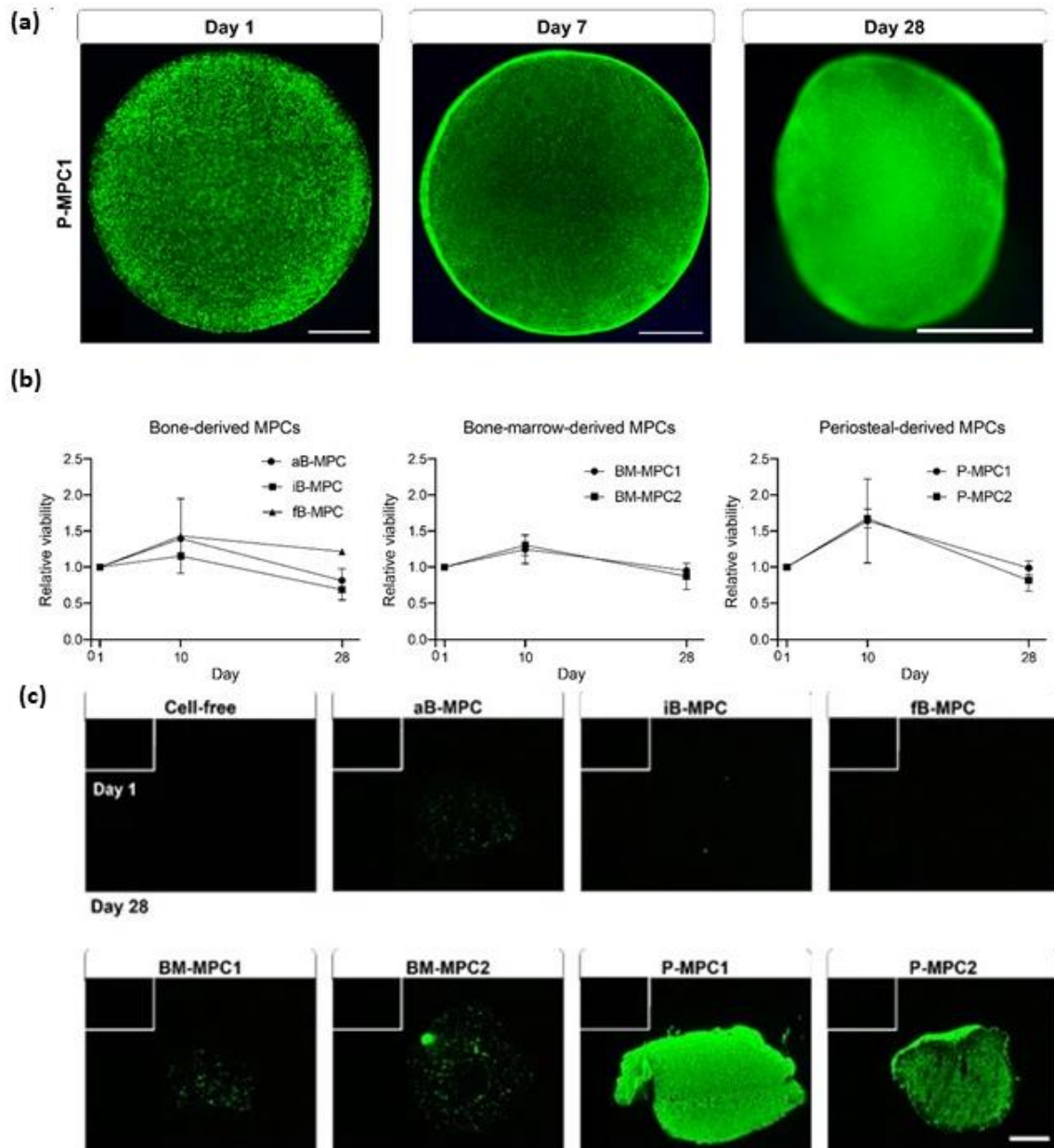


**Figure 4. Viability of cells and mineralization in bioprints.** (a) Fluorescence microscopy images of propidium iodide/fluorescein diacetate stained constructs showing living cells in green and dead cells in red on days 1, 7, and 28. Representative images shown for P-MPC1. Scale bar = 1000  $\mu$ m. (b) Results of alamarBlue™ assay on days 1, 10, and 28 of cultivation. Viability was normalized to the respective value for each cell type on day 1,  $n = 2$ . (c) Mineralization of printed constructs. Histological staining on day 1 (white bordered rectangle) and day 28, using OsteoImage™ Mineralization Assay. Scale bar = 500  $\mu$ m. Alveolar bone (aB-MPC), fibula bone (fB-MPC), iliac crest bone (iB-MPC), iliac crest bone marrow (BM-MPC), periosteum of the mastoid (P-MPC)

Figure adapted from co-authored publication in *International Journal of molecular science*:

Amler A-K, Dinkelborg PH, Schlauch D, Spinnen J, Stich S, Lauster R, Sittinger M, Nahles S, Heiland M, Kloke L, Rendenbach C, Beck-Broichsitter B, Dehne T. Comparison of the Translational Potential of Human Mesenchymal Progenitor Cells from Different Bone Entities for Autologous 3D Bioprinted Bone Grafts. *Int J Mol Sci.* 2021 Jan 14;22(2):796, (47).

## 3.2. Establishment of osteochondral thin section cultures

### 3.2.1. Tissue slice cultures can be obtained in large quantities from single samples and exhibit stable histologic and gene expression long-term behavior

Tissue of 23/25 donors was suitable for the preparation of slice preparations. The extent of subchondral sclerosis of the bone proved to be a decisive factor for the suitability for the preparation of slice cultures. The brittleness of the bone increases noticeable with the degree of sclerosis, resulting in the subchondral cancellous bone being crushed rather than cut smoothly by the impact of the blade. Three punched cylinders were obtained from all other donors, from each of which 30 - 36 slice cultures could be safely prepared. For reasons of logistical feasibility, we cultivated the slice cultures from only one punch cylinder each - from a technical point of view, cultivation of 90-100 slice cultures per donor could have been archived.

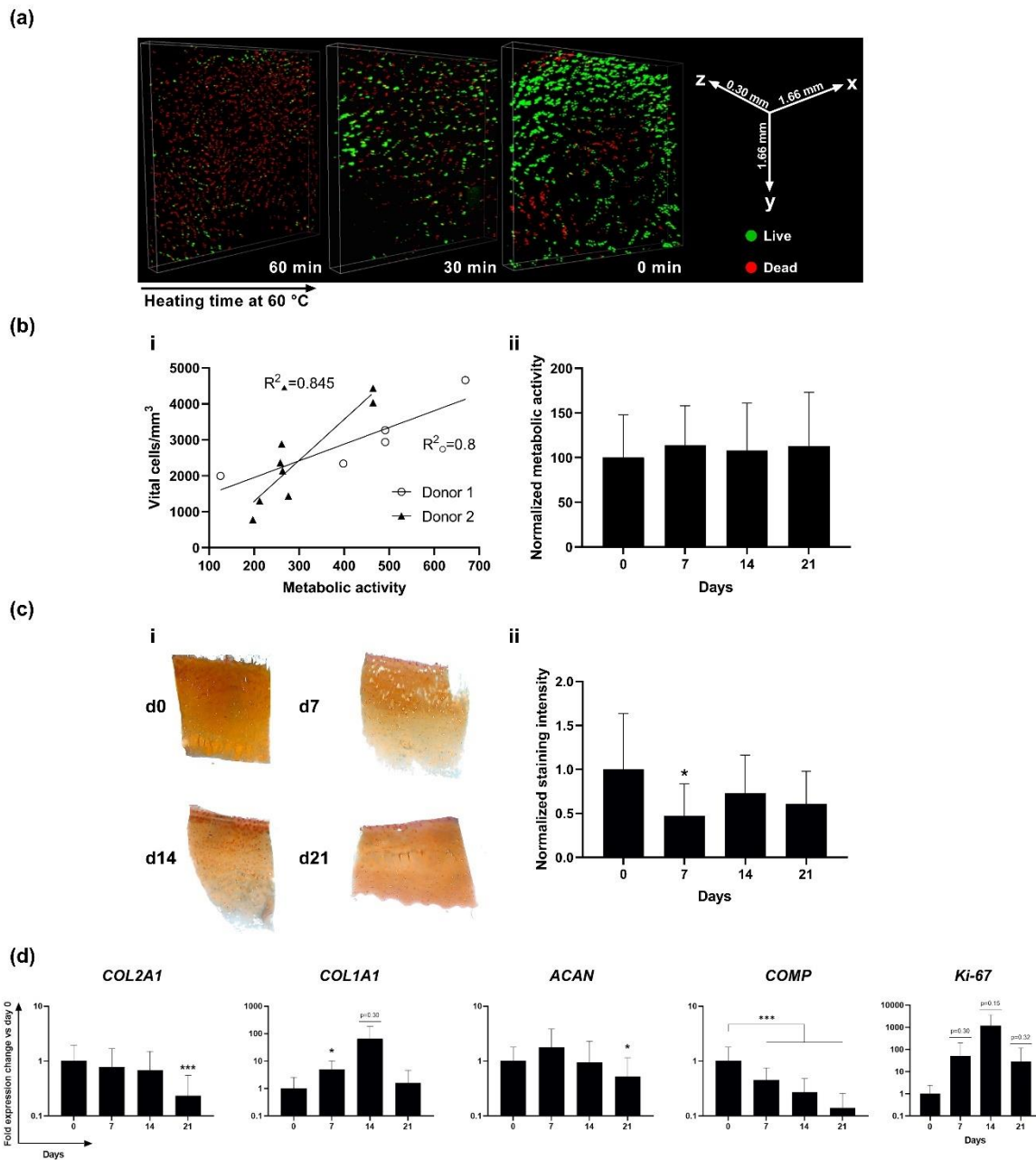
The section thickness of 500µm proved to be optimal in order to allow for sufficient laser penetration and thus perform a three-dimensional optical analysis of cell distribution and viability by confocal laser microscopy. The analysis revealed a highly preserved spatial distribution and of chondrocytes in the cartilage tissue with completely preserved stratification of the different cartilage zones (columnar deep zone; pearl cord-like structure in the middle zone; densely packed cells in the superficial zone) without signs of diffusion-induced cell outgrowth (Fig 5(a)).

Quantification of cell vitality in fluorescence microscopy staining showed a value above 90% after a culture period of 21 days. To ensure that the further performed metabolic resazurin assay also adequately reflected viability and was not hindered by the dense osteochondral ECM, the results of the optical analysis were compared with the fluoroscopic measurements of the resazurin assay. A regressive correlation analysis showed a correlation coefficient of  $R^2 = 80 - 84.5\%$  of the optically determined cell viability with the metabolic resazurin assay (Fig. 5(b - i)). Therefore, in the further course, continuous resazurin measurements were performed to assess long-term viability. These showed long-term viability of  $<95\%$  at all measured time points (Fig. 5(b - ii)).

To analyze whether native slice cultures retained their tissue-specific histological composition, the proteoglycan content of the long-term cultures was quantified by Safranin-O staining. Although a statistically significant decrease in proteoglycan content ( $p < 0.05$ ) was observed at day 7, in the long-term experiment compared to day 0 the overall mean proteoglycan content not significantly different from day 0 at days 14 and 21 (Fig. 5(c)).

Expression of the cartilage-related genes *COL2A1* and *ACAN* remained stable for 14 days compared with their levels at day 0 and decreased significantly by day 21 in unstimulated. The cartilage remodelling marker *COL1A1* briefly increased at 7 days but returned to day 0 levels by 21 days. *COMP* expression decreased more rapidly and significantly at 7 days and further decreased to  $27 \pm 21\%$  and  $14 \pm 12\%$  at 14 and 21 days, respectively (Fig. 5(d)).





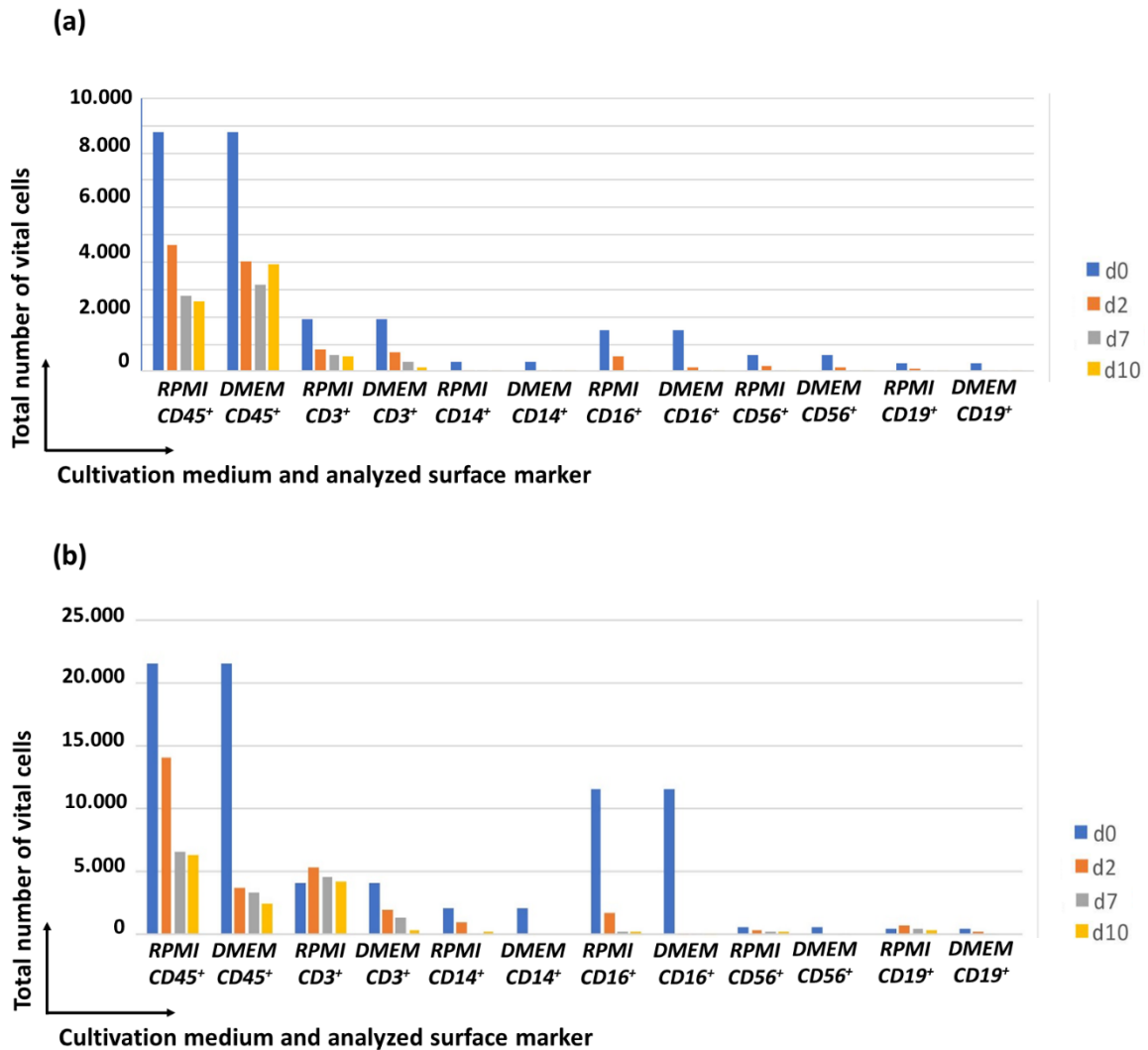
**Figure 5. Long term behaviour of osteochondral slice cultures.** (a) Confocal laser scanning microscopy of slices at three weeks of culture following heating at 60 °C for 0, 30 or 60 min and live/dead staining with PI/FDA. Vital cells appear green, while dead cells appear red. (b) i: Correlation analysis of vital cell count as determined by CLSM and metabolic activity as determined by AlamarBlue resazurin assay. Two donors and a total of 13 slices with varying viability were analyzed and revealed correlation coefficients of 0.8 and 0.845..ii: Viability of slices without FBS or other stimulating factors over 21 days, relative to day 0. (c) Safranin O-stained slices of one donor (i) and histomorphometrical analysis (ii) over three weeks (d) Gene expression analysis of live slice explants via RT-qPCR analysing cartilage-typical markers COL2A1, COL1A1, ACAN and COMP and proliferation Marker Ki-67 in serum-free cultured slices over three weeks (n = 12) relative to the day 0 value.

Figure adapted from own publication in *International Journal of Molecular Science*:

Spinnen J, Shopperly LK, Rendenbach C, Kühl AA, Sentürk U, Kendoff D, Hemmati-Sadeghi S, Sittinger M, Dehne T. A Novel Method Facilitating the Simple and Low-Cost Preparation of Human Osteochondral Slice Explants for Large-Scale Native Tissue Analysis. *Int J Mol Sci.* 2021 Jun 15;22(12):6394, (48).

### 3.2.2. Immune cells from synovial fluid and whole blood show low viability in tissue culture medium

To evaluate the possibility of tissue and synovial immune cell co-culture, immune cells were extracted from autologous synovial fluid of tissue donors, placed in the possible tissue culture condition (DMEM with 5% HEPES, 1% Penicillin/Streptomycin or RPMI with 5% HEPES, 1% Penicillin/Streptomycin), and analyzed for viability by flow cytometry after 1, 3, 7, and 10 days. The results were compared with leukocyte extracts from whole blood. The analysis showed that while 50% of the CD45<sup>+</sup> cells from synovial fluid survive until day 10, the viability of the subpopulations (CD3<sup>+</sup>, CD14<sup>+</sup>, CD16<sup>+</sup>, CD56<sup>+</sup>, CD19<sup>+</sup>) are reduced by an average of 90% at day two in culture and is no longer detectable by day seven at the latest (Fig. 6(a)). Immune cell populations from whole blood showed a similar result as cells from synovial fluid with already completely avital subpopulations in both media after 7 days (Fig. 6(b)).



**Figure 6. Vitality analysis of different immune cell subsets in low-stimulus environment** (a) Flow cytometric viability measurement of immune cells isolated from synovial fluid after days 0, 2, 7, and 10 in either DMEM or RPMI medium. Immune cells are plotted according to specific surface markers: T-cells CD3<sup>+</sup>; Monocytes CD14<sup>+</sup>; Neutrophil Granulocytes CD16<sup>+</sup>; Natural Killer Cells CD56<sup>+</sup>; B-cells CD19<sup>+</sup>. (b) Flow cytometric viability measurement of immune cells isolated from whole blood after days 0, 2, 7, and 10 in either DMEM or RPMI medium. Immune cells are plotted according to specific surface markers: T cells CD3<sup>+</sup>; Monocytes CD14<sup>+</sup>; Neutrophil Granulocytes CD16<sup>+</sup>; Natural Killer Cells CD56<sup>+</sup>; B cells CD19<sup>+</sup>. DMEM: Dulbeccos Modified Eagle Medium; RPMI: Roswell Park Memorial Institute Medium

### 3.2.3. Osteochondral live slice cultures stayed highly reactive towards anabolic and catabolic stimuli without additional serum

To test the reactivity of cells to external stimuli, we intended to induce measurable changes in tissue behavior of the cultures by the addition of the catabolic/anabolic stimuli TNF- $\alpha$  and TGF- $\beta$ 3; respectively, with and without the addition of FBS. Stimulation with TNF- $\alpha$  and TGF- $\beta$ 3 had no measurable effect on cell viability; however, FBS added to the culture medium resulted in significantly increased viability levels in all stimulated groups and in the control group (Fig 7. (a)). To analyze whether native slice cultures can respond to molecular stimuli with remodeling of the ECM, the slices of TNF- $\alpha$ -stimulated cultures (and their negative controls) were stained with Safranin-O, because TNF- $\alpha$  is an important trigger of matrix degeneration processes in cartilage. The proteoglycan content of the stimulated cultures and their negative controls were quantified histomorphometrically at days 0 and 7. The proteoglycan content in the TNF- $\alpha$ -treated group was significantly reduced by 32% compared to the untreated control group on day 7. Consistent with the changes in gene expression, TNF- $\alpha$ -stimulated slices exhibited altered histomorphology. Intra-cartilage fibers appeared less dense, while chondrocyte diameter and apparent volume increased (Fig. 7(b)).

Transcriptomic analysis showed different results in the stimulation groups with and without FCS addition. In the serum-free group, stimulation with TNF- $\alpha$  resulted in a significant and dose-dependent decrease in the expression of *COL2A1*, *ACAN*, and *COMP*. Compared with control at day 7, *COL2A1* expression was 11% and 5% at low and high TNF- $\alpha$  doses, respectively. *ACAN* expression was also significantly lower at 42% and 15%, whereas *COMP* expression decreased to 44% and 10%. Stimulation with TGF- $\beta$ 3 resulted in a 19-fold increase in *COL1A1* expression and a 9-fold increase in *COMP* expression. *MMP13* expression did not change significantly after incubation with TNF- $\alpha$  but was markedly decreased to 6% after stimulation with TGF- $\beta$ 3. In the serum-stimulated group, however, the responses were all significantly reduced. Stimulation with TNF- $\alpha$  resulted in reduced *COL2A1* expression of 33% at the low concentration and 11% at the high concentration compared with the control. The mean expression levels of *ACAN* and *COMP* in FBS<sup>+</sup> groups also decreased after TNF- $\alpha$  exposure, although no coherently dose-dependent or significant effects were observed. TGF- $\beta$ 3 stimulation resulted in a 29-fold increase in *COMP* expression and a 2.4-fold increase in *COL1A1* expression, as well as a decrease in *MMP13* expression to 42% (Fig. 7(c)).

On average, *Ki-67* expression increased considerably from day 0 to 7, but, presumably due to the the low initial absolute expression of *Ki-67* at day 0, very high inter-donor variability was observed, leading to statistically non-significant results. Stimulation with low-concentration TNF- $\alpha$  resulted in  $31 \pm 65\%$  expression at day 7 in the FBS<sup>+</sup> groups, whereas unexpectedly higher-concentration TNF- $\alpha$  resulted in a  $50 \pm 112$ -fold increase. TGF- $\beta$ 3 stimulation resulted in a  $37 \pm 60$ -fold increase in expression at 7 days compared with control at day 0 ( $p = 0.06$ ). However, in the FBS<sup>+</sup> group, all 3 stimulation groups and the control had statistically significant changes between days 0 and 7, achieving fold-changes of  $12,045 \pm 17,483$  (TNF- $\alpha$  low),  $1686 \pm 2180$  (TNF- $\alpha$  high), and  $4889 \pm 9110$  (TGF- $\beta$ 3) compared with day 0. No statistically significant differences were observed between the FBS<sup>+</sup> cultured stimulation groups or between any of the groups and the negative control at day 7 (Fig. 7 (d)). Because of this very pronounced, nonspecific overlay reaction of serum on *Ki-67*, the following stimulation experiments with CCL25 were performed without serum for higher sensitivity.

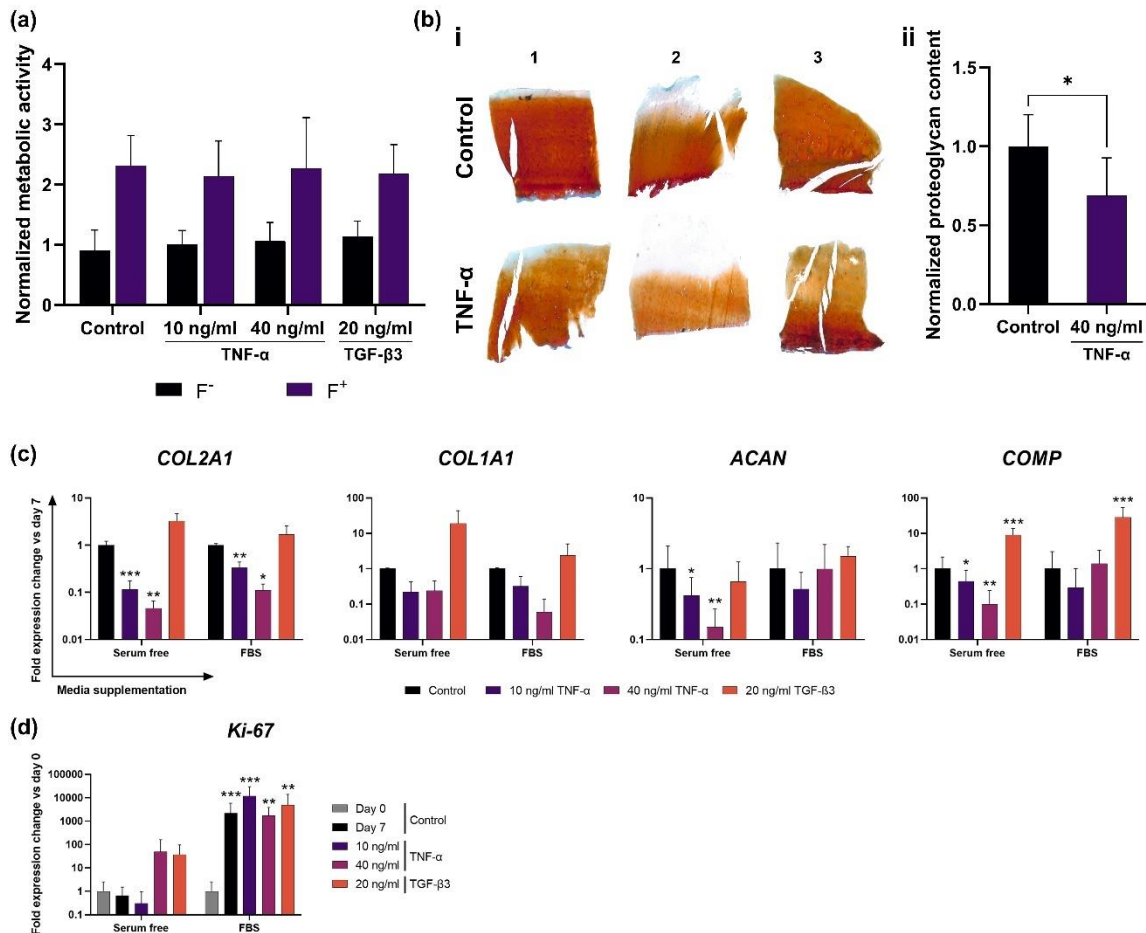


**Figure 7. Reactivity analysis towards TNF- $\alpha$  and TGF- $\beta$**  (a) Viability of slices with- and without FBS after stimulation with either TNF- $\alpha$  or TGF- $\beta$  over 21 days, relative to day 0 (b) Comparison of staining intensity in TNF- $\alpha$ -stimulated and non-stimulated slices. Stimulated slices (three exemplary donors shown in (i)) show a mean reduction in red intensity of 32% (ii, n = 6). (c) Gene expression of cartilage-typical markers after 7 days of stimulation with TNF- $\alpha$  or TGF- $\beta$ 3 and with or without FBS (n = 6) relative to the control on day 7 (d) expression of proliferation marker Ki-67 after 7 days of stimulation with TNF- $\alpha$  or TGF- $\beta$ 3 and with or without FBS (n = 6), relative to the day 0 control to show the larger increase in the F<sup>+</sup> group. Statistically significant differences denoted as \*p < 0.05, \*\*p < 0.01, \*\*\*p < 0.001. **Figure is adapted from own publication in International Journal of Molecular Science: Spinnen J, Shopperly LK, Rendenbach C, Kühl AA, Sentürk U, Kendoff D, Hemmati-Sadeghi S, Sittinger M, Dehne T. A Novel Method Facilitating the Simple and Low-Cost Preparation of Human Osteochondral Slice Explants for Large-Scale Native Tissue Analysis. Int J Mol Sci. 2021 Jun 15;22(12):6394, (48).**

### 3.3. Stimulation of osteochondral explant cultures with CCL25

#### 3.3.1. CCL25 shows no cell-toxic effects on osteochondral cells

To investigate the response of joint tissues to stimulation with CCL25, 26 individual thin section cultures were prepared from the knee joint tissues of each of 15 tissue donors, stimulated with either 1, 5 or 50 nM CCL25 and cultured for 21 days. Every 7 days, a sample from the corresponding stimulation group was taken for histological and gene expression analysis, respectively. Viability analysis of the cultures by resazurin assay showed no statistically significant deviation from the viability measured at day zero for any of the doses of CCL25 tested. The average viability at day 21 was 107% (1 nM CCL25), 128% (5 nM CCL25), and 104% (50 nM) (Fig. 8 (a)).

### 3.3.2. *Histology shows CCR9 receptor in superficial cartilage layers but no catabolic or anabolic reactions towards CCL25 stimulation*

First, the explant cultures were examined immunohistologically for expression of the CCL25-specific receptor CCR9. The receptor was strongly expressed on all samples examined. Strikingly, expression was only evident in the superficial cartilage zone, where chondrocytes typically resemble mesenchymal stromal cells in their phenotype or genotype than chondrocytes in the deeper cartilage layers (Fig 8 (b)). To detect possible anabolic or catabolic processes induced by CCL25, the samples were stained with Safranin-O and the color intensity was quantified by histomorphometry analogous to the establishment of the slice cultures. There was no statistically significant deviation of red intensity from the negative control detectable in any of the stimulation groups (Fig. 8 (c)).

### 3.3.3. *Low doses of CCL25 cause proliferation marker spikes in chondrocytes while high doses result in a mild catabolic reaction*

Quantitative analysis of key marker genes of cartilaginous matrix production revealed a CCL25 dose-dependent reduction in collagen II expressions that reached statistical significance at a stimulation concentration of 50 nM after 14 days. Collagen I expression decreased after stimulation with CCL25 on day 14 for all three CCL25 stimulation concentrations – but only statistically significant in the 5nM stimulation group. Afterwards, the expression increased again to no statistically detectable difference from the control group. Aggrecan gene expression after stimulation with CCL25 did not significantly deviate from the control groups (Fig 8(d)), which remained stable for 14 days and then dropped slightly after 21 days (Fig. 5 (d)). Similarly, the expression of *COMP* did not show any statistically significant change towards all concentrations of CCL25 (Fig. 8 (d)) and behaved similarly to the preliminary experiments with a continuous decrease in expression with no detectable anabolic or catabolic effect from CCL25 stimulation (Fig. 5 (d)). The expression of the proliferation marker *Ki-67* showed a steep increase at a concentration of 1 nM and statistically significant increase at a concentration of 5 nM after 7 days of stimulation, which then dropped significantly below the initial level in the next measurement after 14 days. After stimulation with 50 nM CCL25, *Ki-67* showed a tendency to increase but without reaching statistical significance (Fig. 8 (d)).

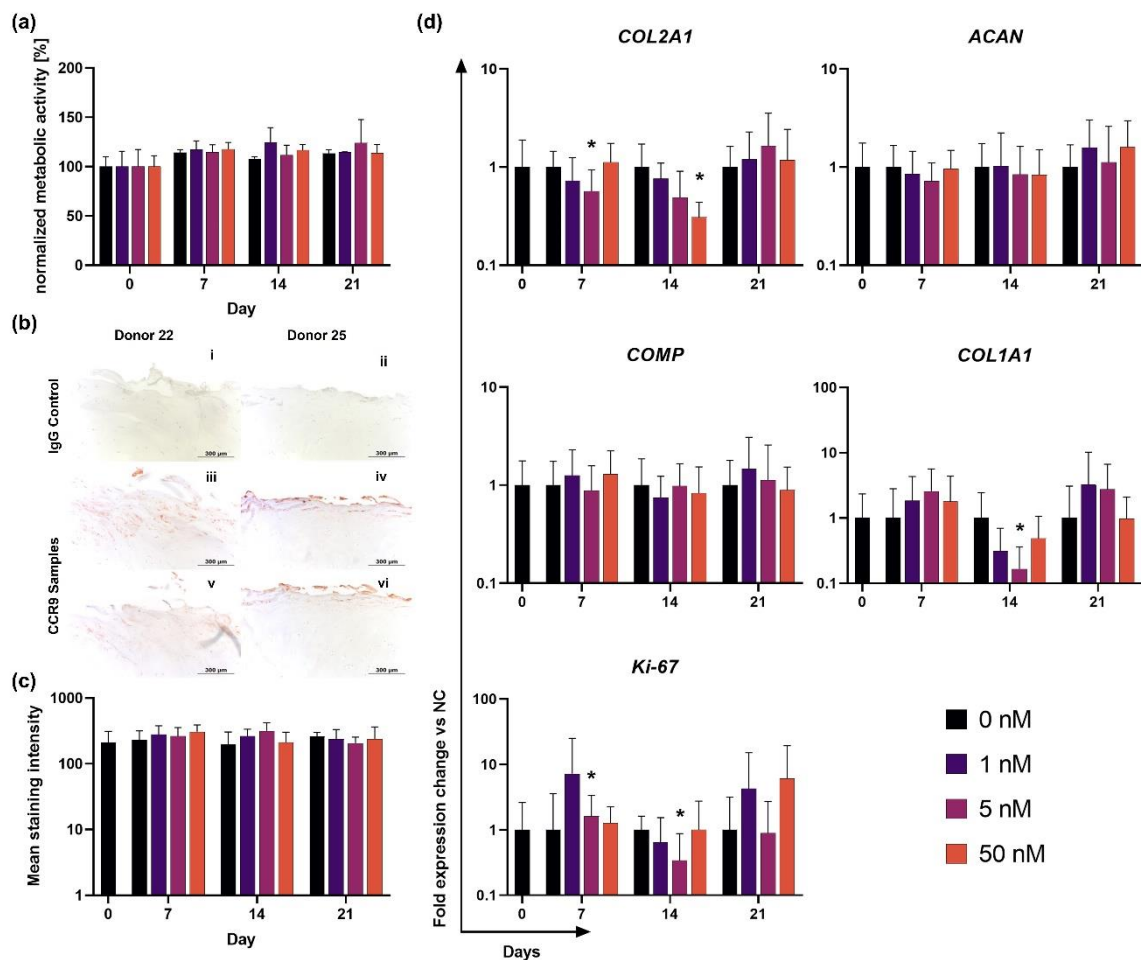


**Figure 8. Stimulation of osteochondral tissue cultures with CCL25** (a) Viability of slices after stimulation with 1 nM, 5 nM or 50 nM CCL25 over 21 days, relative to day 0 (b) Immunohistochemical staining of native human cartilage for CCR9 surface receptor (c) Histomorphometric analysis of Safranin-O-stained osteochondral thin section cultures after stimulation with 1nM, 5nM and 50nM CCL25 on day 7, 14 and 21. (d) gene expression of cartilage-typical markers and proliferation marker after stimulation with 1 nM, 5 nM and 50nM CCL25 on day 7, 14 and 21. Statistically significant differences denoted as \*  $p < 0.05$ ,

### 3.4. Analysis regarding inflammatory potential of CCL25

To assess the inflammatory potential of CCL25, different immune cell subclasses were isolated from human whole blood, stimulated with CCL25 and the components of its PLGA based delivery device, and subsequently analyzed for the extent of any inflammatory response. First, the different subpopulations were flow cytometrically analyzed for expression of the CCL25-specific receptor CCR9. Analysis showed that CCR9 was expressed proportionately in each subpopulation: PBMCs, monocytes, and CD4<sup>+</sup> showed CCR9 expression of 31%, 45%, and 34%, respectively. The lowest expression was on CD8<sup>+</sup> T cells at 21%; the highest expression was on M1 polarized macrophage genes at 78%. Of the M0 polarized macrophages, a significantly lower proportion expressed the CCR9 receptor at 34%.

#### 3.4.1. Direct CCL25 stimulation causes unspecific inflammatory activation and migration of different leukocyte subsets

To investigate the direct response of immune cell subclasses to CCL25, PBMCs and differently polarized macrophages were inoculated with solutions of 10, 100 and 750 nM CCL25 for 5 days. LEGENDplex immunoassay analysis of their supernatant revealed a dose-dependent increase in

the secretion of pro-inflammatory cytokines, which was different in the different subpopulations: PBMCs responded with a pronounced and dose-dependent secretion of the pro-inflammatory chemokines and cytokines IL-8, MCP-1, TNF- $\alpha$ , IL-1 $\beta$ , interleukin-6 (IL-6) and IFN- $\gamma$ . In terms of stimulation dose, a concise difference was seen between the response to high and low doses: whereas only moderate increases were seen for most cytokines/chemokines in the 10 nM and 100 nM CCL25 stimulation groups, PBMCs responded with a strong increase in all mediators tested in the 750 nM stimulation group. When testing different macrophage subsets, M0 macrophages responded strongly and dose-dependently to CCL25 stimulation with up to a tenfold increase in IL-8 secretion in the 750 nM group ( $p = 0.08$ ), whereas M1 macrophages showed a small increase regardless of the dose used (Fig. 9 (A) and (B)).

Furthermore, analysis of the expression of the leukocyte activation marker HLA-DR was performed on PBMCs by flow cytometry. Here, PBMCs showed very significant HLA-DR upregulation when exposed to all three CCL25 concentrations. The strongest upregulation was seen in CD45+CD3-negative cells (all mononuclear leukocytes except T cells) - with a dose-dependent increase up to a 1.8-fold change compared with the negative control. Furthermore, CD4+ cells also responded to CCL25 stimulation in a dose-dependent manner with significant HLA-DR upregulation. The changes in HLA-DR expression levels in CD8+ cytotoxic T cells was significantly weaker - showing lesser changes in expression levels and did not reach statistical significance. M0 and M1 macrophages also showed no statistically significant changes in their expression patterns (Fig. 10 (A) and (C)).

Analysis of chemoattractive potential by Boyden-Chamber migration assay revealed a strong increase in migration in T-cells at CCL25 concentrations in the range of 500 – 1000 nM, more pronounced in CD8+ than in CD4+ positive cells (Fig. 10 (B)).

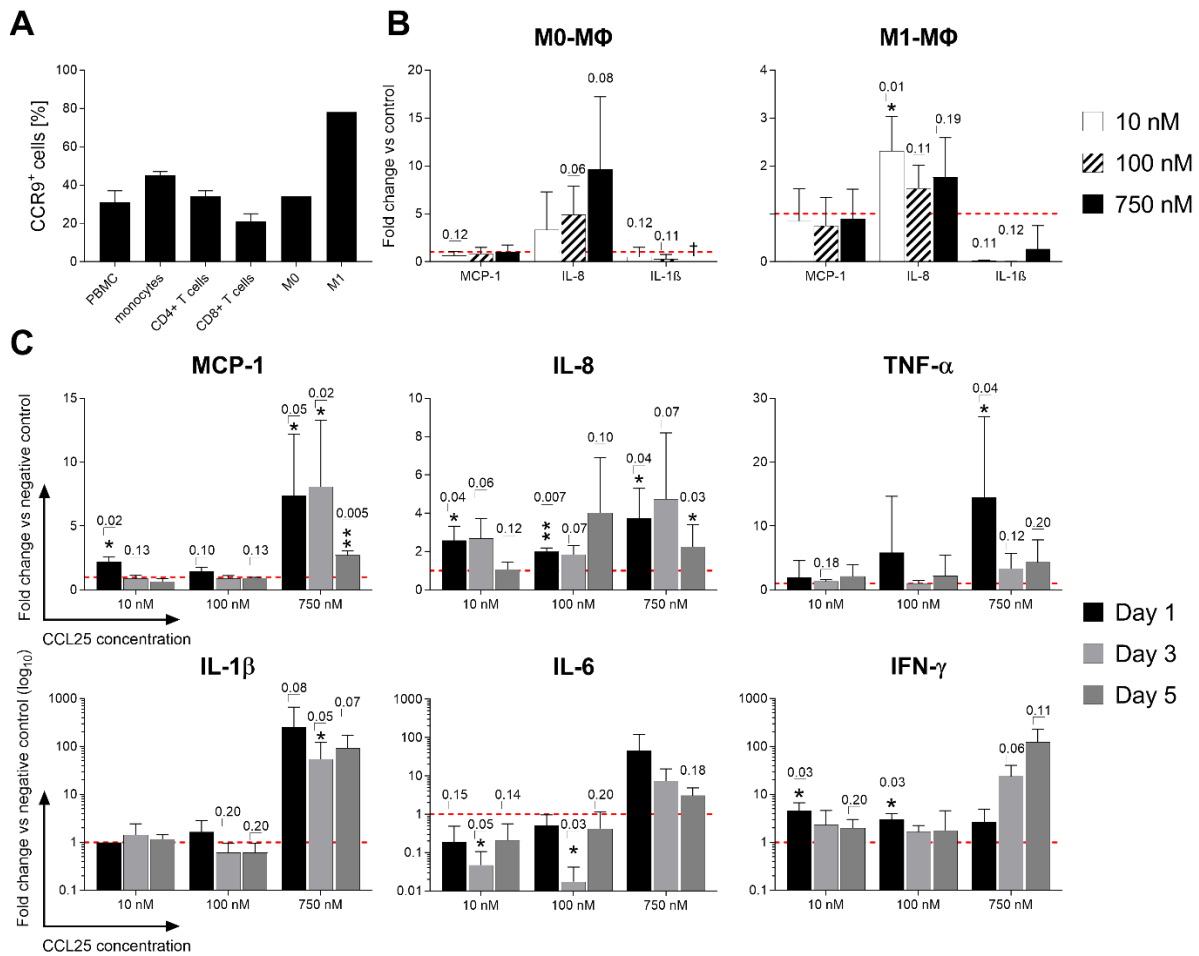


**Figure 9. CCR9 expression and secretion profile of immune cell subsets after stimulation with CCL25.** PBMCs, unpolarized (M0) and polarized macrophages (M1) were stained with a CCR9-specific antibody and analyzed by flow cytometry. PBMCs and macrophages were stimulated with different dosages of CCL25 or left unstimulated as a negative control. A LEGENDplex cytokine array was performed using the culture supernatants after day 1, day 3 and day 5. **a** The expression of the CCL25-receptor CCR9 on different immune cell subsets is shown as mean of the percentage of marker positive cells + SD ( $n = 1-4$ ). **b** Shown are the cytokine/chemokine release data for M0 and M1 macrophages after one-day stimulation with 10, 100 and 750 nM CCL25 as the mean fold change + SD compared to the negative control (red dotted line) ( $n = 4$ ). **c** The cytokine/chemokine release data for PBMCs stimulated with 10, 100 and 750 nM CCL25 over three days are displayed as the mean fold change + SD normalized to the negative control (red dotted line) ( $n = 3$ ). Significance was analyzed using either a student's *T*-test or the Mann-Whitney-*U* test depending on whether data followed normal distribution. Individual *p*-values are given above the bars if lower than  $p = 0.20$ . PBMCs: peripheral blood mononuclear cells, MΦ Macrophages

Figure is adapted from own publication in *Journal of Nanobiotechnology*:

Spinnen J, Fröhlich K, Sinner N, Stolk M, Ringe J, Shopperly L, Sittinger M, Dehne T, Seifert M. Therapies with CCL25 require controlled release via microparticles to avoid strong inflammatory reactions. *J Nanobiotechnology*. 2021 Dec 25;19(1):83, (51).



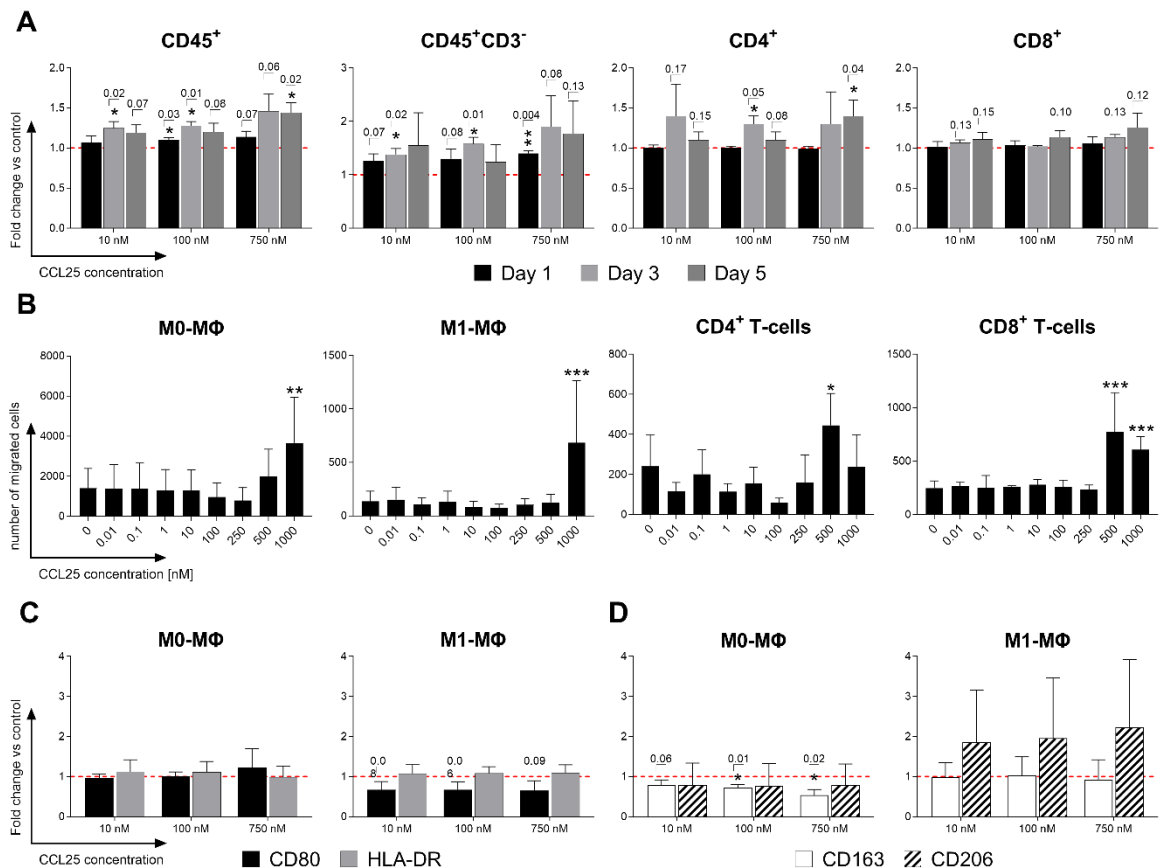


**Figure 10. Surface marker changes and migration behavior of immune cell subsets after CCL25 stimulation.** After stimulation with different dosages of CCL25 (10, 100, 750 nM), immunofluorescence staining with antibody panels and subsequent flow cytometry was performed to detect leukocyte activation and macrophage polarization based on surface marker expression. Additionally, a Boyden-Chamber migration assay was performed with a CCL25 dilution series (0.01–1000 nM). **a** HLA-DR expression levels of different immune cell subsets stimulated with 10, 100 and 750 nM CCL25 over three days are shown as the mean of the percentage of marker positive cells + SD normalized to the negative control (red dotted line);  $n = 3$ . **b** The migration of immune cell subsets towards a dilution series of CCL25 is displayed as the mean + SD of the number of migrated cells ( $n = 4$ ). Macrophage polarization through CCL25 stimulation was analyzed by immunofluorescence antibody staining and flow cytometric analysis of M0 and M1 macrophages against either **c** M1 polarization markers CD80 and HLA-DR or **d** M2 polarization markers CD163 and CD206 ( $n = 4$ ). Surface marker expression levels are shown as the mean + SD of normalized values compared to the negative control (red dotted line). Statistical significance was analyzed using either a student's T-test or the Mann-Whitney-U test depending on whether data followed a normal distribution. Individual  $p$  values are given above the bars if lower than  $p = 0.20$ . MΦ MacrophagesResponse to CCL25 loaded and unloaded PLGA particles

Figure is adapted from own publication in *Journal of Nanobiotechnology*:

Spinnen J, Fröhlich K, Sinner N, Stolk M, Ringe J, Shopperly L, Sittinger M, Dehne T, Seifert M. Therapies with CCL25 require controlled release via microparticles to avoid strong inflammatory reactions. *J Nanobiotechnology*. 2021 Dec 25;19(1):83, (51).

### 3.4.2. Neither CCL25 loaded- nor unloaded PLGA microparticles show strong inflammatory potential.

To exclude the possibility that the PLGA particles have their own inflammatory potential or that the encapsulation of CCL25 does not function sufficiently, the same immune cell subclasses were stimulated with both CCL25-loaded (CL) and unloaded PLGA microparticles (NL) and also examined for secretome, surface marker expression and migration. Secretome analysis of

PBMCs showed a slight increase in secretion of the cytokines IL-8 and MCP-1, with no significant difference between loaded and unloaded particles. Macrophages also reacted with an increase in IL-8 secretion, which was significantly more pronounced in the M0 group than in the M1 group (Fig. 11 (A) and (B)).

Analysis of surface markers revealed no statistically significant changes in PBMCs, but a significant reduction in CD80 expression, a typical M1 marker, by 1.5-fold in M1 macrophages in both loaded and unloaded particles. However, the second M1 marker studied, HLA-DR, showed no significant changes in expression level. At the same time, expression of the characteristic M2 surface marker CD206 tended to increase in co-cultures of already polarized M1 macrophages with the particles. Expression of the M2 marker CD163 tended to decrease by 1.20 in both groups with the 0.5 % w/v particles. Unpolarized M0 macrophages also showed a slight decrease in CD80 and CD163 but no increase in CD206 after particle incubation. No significant differences were observed between the loaded and unloaded particles (Fig. 11 (C)). No induction of migration by either loaded - or unloaded PLGA particles was detected.

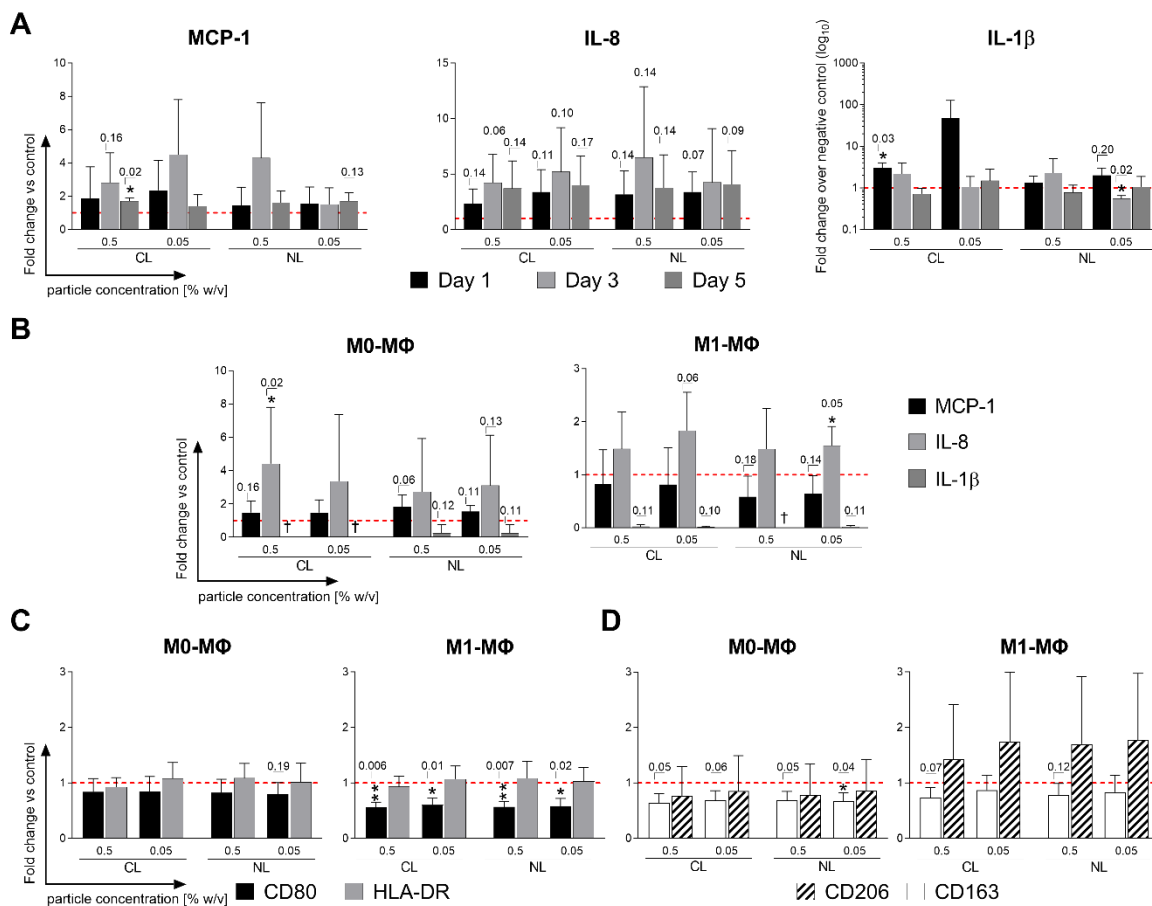


**Figure 11. Response profile of immune cell subsets after stimulation with CCL25-loaded/unloaded PLGA particles.** PBMCs and macrophages were stimulated with CCL25-loaded (CL) and unloaded (NL) PLGA particles at two different concentrations (0.5% w/v and 0.05% w/v). Induced changes in the cytokine/chemokine secretion profiles of PBMCs and macrophages were analyzed with a LEGENDplex cytokine array. In addition, unpolarized M0 macrophages and polarized M1 macrophages were stained for characteristic surface markers with fluorescently labeled antibodies and measured by flow cytometry to analyze their polarization status. **a** Cytokine release data (IL-8, MCP-1, IL-1) of PBMCs stimulated with 0.5% w/v and 0.05% w/v of CL and NL PLGA particles over 5 days are shown as mean fold change + SD normalized to the negative control (red dotted line) (n = 3). **b** Cytokine release data (IL-8, MCP-1, IL-1) of M0/M1 macrophages stimulated with 0.5% w/v and 0.05% w/v of CL and NL PLGA particles over 1 day are shown as the mean fold change + SD normalized to the negative control (red dotted line) (n = 4). Surface expression levels of M0

(left) and M1 (right) macrophages for the characteristic M1 polarization markers CD80 and HLA-DR (c) and for M2 polarization markers CD206 and CD163 (d) after stimulation with 0.5% w/v and 0.05% w/v of CL and NL PLGA particles over 1 day are displayed as mean of the fold change + SD normalized to the control (red dotted line), (n = 4). Statistical analysis was performed using either a student's T-test or the Mann-Whitney-U test depending on whether data showed normal distribution. Individual p-values are given above the bars if they are lower than  $p = 0.20$ . CL CCL25-loaded, NL non-loaded, PC Particle concentration., w/v weight per volume, MΦ MacrophagesResponse to the supernatants of degraded CCL25 loaded and unloaded PLGA particles.

**Figure is adapted from own publication in Journal of Nanobiotechnology:**

**Spinnen J, Fröhlich K, Sinner N, Stolk M, Ringe J, Shopperly L, Sittinger M, Dehne T, Seifert M.** Therapies with CCL25 require controlled release via microparticles to avoid strong inflammatory reactions. *J Nanobiotechnology*. 2021 Dec 25;19(1):83, (51).

### 3.4.3. Degradation products from CCL25 loaded- and unloaded PLGA microparticles cause a mild inflammatory reaction

To determine the inflammatory potential of the complete particle degradation mass and additionally to distinguish between the effects of particle fragments and the released CCL25 on leukocytes, both loaded and unloaded particles were allowed to degrade for periods of either 21 or 63 days. The supernatants of the degraded particles were then added to the immune cell cultures. Subsequently, secretome, surface marker expression, and migration of the immune cells thus stimulated were examined in a manner analogous to the previous experiments. PBMC cultures treated with particle supernatants showed higher secretion levels of IL-8, MCP-1, and IL-1 $\beta$  compared with controls. The supernatants of non-loaded particles induced an increase in IL-8 levels, which did not reach statistical significance. IL-1 $\beta$  secretion increased in a statistically non-significant manner in both CCL25 loaded- and unloaded particle groups to approximately the same extent after three days. However, after five days, IL-1 $\beta$  secretion increased in a statistically significant manner in PBMCs stimulated with the 21-day CCL25-loaded supernatant, whereas IL-1 $\beta$  secretion tended to decrease to the negative control level in the corresponding NL particle supernatants. The same dynamics were observable for the cytokine MCP-1, with a sharp increase after three days in all groups and with high levels maintained on the fifth day in the CCL25 loaded particle supernatant group. At the same time, MCP-1 secretion decreased in the non loaded particle supernatant group. Macrophages were also analyzed in the same manner but showed higher secretion levels for IL-8 only. Interestingly, IL-1 $\beta$  secretion from M1-polarized macrophages was significantly lower in all supernatant groups (Fig. 12 (A) and (B)).

While no change in surface marker expression was detected in PBMCs, M1-polarized macrophages responded to exposure of both CCL25-containing and empty PLGA degradation supernatant with the significant increase of HLA-DR, while the M1 marker CD80 significantly decreased. M0 macrophages showed a similar tendency - but the changes did not reach statistical significance (Fig 12 (D)). Analysis of migration behavior in the Boyden-Chamber migration assay showed no chemoattractant potential of either CCL25-loaded or unloaded particle degradation products on the different immune cell subclasses. Stimulation was performed in a 1000-fold dilution series to distinguish between the effects of CCL25 and PLGA fragments. When CD4+ T cells were tested, the undiluted supernatants of both groups of particles decreased migration by 10-fold, representing a statistically significant decrease. M1 macrophages also showed a statistically significant decrease in migration when the particle supernatants were diluted 1:10 and 1:100, but only in the unloaded group. All other immune cell subclasses showed no change in migratory behavior in response to contact with the supernatants (Fig 12(C)).

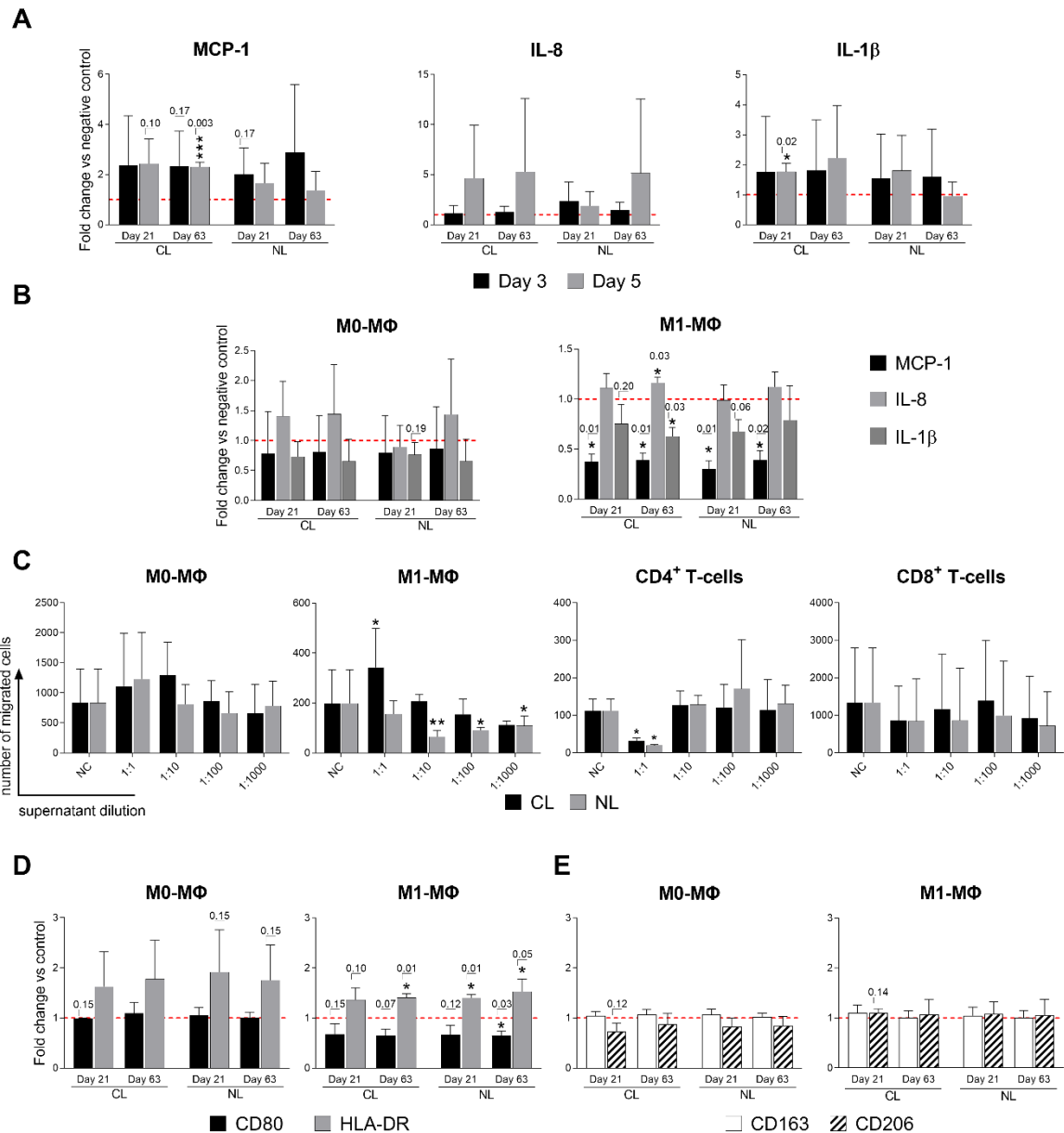


**Figure 12. Immune cell subsets reaction after stimulation with supernatant from degraded CCL25-loaded/unloaded PLGA particles.** CCL25-loaded (CL) and unloaded (NL) PLGA particles were allowed to degrade for either 21 or 63 days and particle supernatant was collected and used for *in vitro* stimulation assays with human PBMCs and macrophages. Changes in the cytokine/chemokine release pattern of PBMCs and macrophages were analyzed with a LEGENDplex cytokine array. Additionally, macrophages were analyzed by immunofluorescence staining and flow cytometry for the expression of surface markers indicating activation or polarization. **a** Cytokine array of PBMCs stimulated over 5 days with 21 and 63-day CL and NL PLGA particle supernatants. Cytokines with detectable differences in fold change are IL-8, MCP-1 and IL-1β. Data are shown as the mean fold change + SD normalized to the negative control (red dotted line) ( $n = 3$ ). **b** Cytokine array of M0/M1 macrophages stimulated over 1 day with 21- and 63-day CL and NL PLGA particle supernatants. Cytokines with detectable differences in fold change are IL-8 and MCP-1. Data is shown as mean fold change + SD normalized to the negative control (red dotted line) ( $n = 4$ ). **c** The migration of immune cell subsets towards a dilution series of particle degradation supernatant is displayed as the mean + SD of the number of migrated cells ( $n = 4$ ). **d/e** Flow cytometric analysis of M0/M1 macrophage polarization surface markers after 1 day of stimulation with 21- and 63-day CL and NL PLGA particle supernatants. Increased CD80 and HLA-DR indicates M1 polarization (d), while increased CD163 and CD206 indicates M2 polarization (e). Results are displayed as the mean of the fold change + SD normalized to the control (red dotted line), ( $n = 4$ ). Statistical analysis was performed using either a student's *T*-test or the Mann-Whitney-*U* test depending on whether data followed normal distribution. Individual *p*-values are given above the bars if lower than  $p = 0.20$ . CL CCL25-loaded, NL non-loaded, NC negative control, MΦ Macrophage

Figure is adapted from own publication in Journal of Nanobiotechnology:

Spinnen J, Fröhlich K, Sinner N, Stolk M, Ringe J, Shopperly L, Sittinger M, Dehne T, Seifert M. Therapies with CCL25 require controlled release via microparticles to avoid strong inflammatory reactions. *J Nanobiotechnology*. 2021 Dec 25;19(1):83,(51).

## 4. Discussion

### 4.1. Bioprinting is a promising method for the development of tissue grafts but of limited use for manufacturing high numbers of pharmacological screening tissue cultures

The additive manufacturing of the osseous tissue culture proved to be successful in principle. The stereolithographic printing process based on methacrylated gelatin was found to be very beneficial for cell viability- and scaffold colonizing behavior. The digital light projection process and printing conditions at 37° C proved to be a non-toxic environment with post-print cell viability rates of >95%. Cell viability is one of the major limitations of bioprinting, as most processes involve either shear forces, high temperatures, or extreme pH levels that negatively affect cell viability in bioinks(53,54). The high long-term cell viability suggests that both the spheroid shape and the composition of the construct provide optimal diffusion conditions. Histological analysis revealed a clear discrepancy between the different cell sources in terms of osteoid potency. While cells grown from different bone sources displayed hardly any mineralization, both MSCs from bone marrow and especially periosteal cells could produce a clear mineralization of the ECM they formed which was further validated by gene expression analysis. The periosteal cells showed significantly higher expression patterns of marker genes of late osteogenic differentiation such as *SPARC* and *SPP-1* than the MPCs isolated from cancellous bone(55,56). These observations suggest that periosteal cells already provide a considerably more osteogenic pattern of activity and, in contrast to quiescent cells in bone, require substantially less stimulation to undergo osteoid differentiation. Concerning, the prospective use of this method for the production of autologous bone grafts, this is a very practical finding, since periosteal cells are by far the easiest of the analyzed sources to obtain autologously from the patient(47).

Regarding the usability for pharmacological screening of osteo(chondral) tissue, however, the benefit of this technology must be considered rather low for the time being due to the following factors: First, analysis has shown that, in particular, periosteal cells are very suitable for culturing osseous tissue. While there are advantages for bone-graft research, as they can easily be autologously harvested from the patient via periosteal shaving, the downlights in regards to pharmacological research are considerable. Periosteal cells are not easily accessible on a large scale and more difficult to isolate from surgical remains due to their high metabolic activity, as they tolerate lower ischemia times compared to intraosseous bone cells. As previously shown by our group, it would be possible to cultivate the periosteal cells permanently in a bioreactor - but this is not available everywhere and is associated with considerable know-how and resource requirements(57).

Furthermore, the cultures are very complex to produce and maintain. First, cells have to be brought into culture and expanded sufficiently. Since a cell density of 20 million cells per milliliter of bioink requires 30 million cells in this setup, a cell culture time of 40-50 days is necessary to

grow the required quantity of cells. This number naturally increases in a pharmacological assay setup with the amount of drug or concentration to be assayed. Secondly, the subsequently printed constructs require 28 days to show basic mineralization. During these 28 days, the media must be changed several times a week, the constructs must be analyzed for cell vitality and mineralization and regularly checked microscopically for spatial integrity. This involves considerable laboratory work and expensive resources that increase exponentially with the size of the analysis.

Although the additive manufacturing process allows high numbers of highly reproducible cultures to be produced in a short time, it still takes a total of 80 days for the cultures to be usable and another 20-30 days depending on the subsequent analysis time. In our case, this amounts to a total of 110 days including labour intensive wet-lab work for only 70 culture replicates. In addition, commercially available GelMA is still relatively expensive. To establish an economic workflow in large-scale dose-finding and toxicity studies in the long term, one would additionally have to establish an in-house methacrylation of gelatin, which represents additional labor and cost factor.

Based on these findings, we have decided that due to the extent of the upcoming measurements, for which almost 400 individual tissue cultures are required, 3D printed osseous and chondral cultures are not suitable and have therefore focused on the optimization of osteochondral explant cultures.

#### 4.2. Thin sectioned osteochondral explant cultures prove to be highly feasible as pharmacological testing device

The combination of lateral tissue punching and subsequent thin preparation under sterile conditions using 3D-printed microtome insert proved to be very reliable for producing at least 30 to a maximum of 100 individual tissue cultures from a single donor in a short time, - even from small tissue samples. The limiting factor for successful tissue preparation proved to be the extent of subchondral sclerosis of the bone(58). The degree of sclerosis causes a gradual increase in bone brittleness, which significantly complicates the cutting process and usually results in crushing the cancellous bone during cutting. Therefore, the removal site of the punch cylinder must be thoroughly checked for the condition of the subchondral bone before punching. Overall, 92% of the tissue specimens were suitable for culture preparation. Although the tissue is exposed to high thermal and mechanical stress due to the cutting procedure as well as higher oxygen concentrations and thus oxidative stress due to the thin preparation, the cell viability and native tissue configuration remained stable in the long term.

Fluoroscopic live/dead staining by confocal laser microscopy showed > 90% cell viability down to the deeper tissue layers of the cartilage. Therefore, the layer thickness of 500 µm seems to ensure adequate nutrient perfusion by motion-assisted diffusion while providing sufficient protection of intra-tissue cells. Furthermore, the cartilage-specific cell architecture was preserved throughout the analysis period. The hyaline cartilage of the joint is divided into three distinct cellular zones: The superficial zone (densely packed with spindle-shaped cells), the middle zone (pearl cord-like alignment), and the deep zone (columnar chondrocyte alignment). Maintenance of the cellular zones depend on nutrient supply and physiological cartilage infrastructure, suggesting minimal cellular stress from malnutrition and/or hypoxia(59).

The previously determined high correlation of the actual cell viability of the samples with the viability values determined by the resazurin assay allowed precise multipoint analyses in this culture form using this inexpensive and easy-to-use method. These also yielded stable viability values over 21 days. Furthermore, no addition of serum was required to maintain cell viability, which

clearly distinguishes it from tissue engineered cultures or most other explant models (most authors use serum mixtures in concentrations of 2 - 10%)(60–62). This further suggests that nutrient and signaling protein diffusion at a tissue thickness of 500  $\mu\text{m}$  is sufficient to maintain the native metabolic configuration of the cells. From the pharmacological analysis point of view, this is a major advantage compared to cultured tissue cultures or conventional explant cultures, since serum as an unstandardized mixture of proteins is an incalculable confounding factor in the study of protein-tissue interactions.

In terms of tissue stability over long-term culturing, the thin-section cultures behaved very similarly to conventional explant cultures, which usually remain stable in their tissue phenotypes for about three weeks under static conditions(63). Histomorphometric examination of the proteoglycans showed a significant decrease in Safranin-O staining intensity on day 7, but this stabilized again on days 14 and 21. We attribute this initial mainly to the relative size of the cut edges, which overall account for a higher proportion of the total cartilage volume than conventional explants and increase the risk of initial proteoglycan efflux.

Gene expression analysis was also similar to previously published results of conventional explants(61,64). *COL2A1* and *ACAN* remained stable over 14 days until a slight reduction was seen after 21 days, *COL1A1* increased over 14 days and fell back to baseline after 21 days, and *COMP* decreased in an approximately linear response at each measurement time point. All in all, the thin-section cultures show the behavior of a semi-static osteochondral tissue culture, which regularly reduces matrix synthesis after 2-3 weeks due to the lack of physiological tissue pressure.

Analysis of tissue reactivity revealed an adequate response to biological stimuli. The catabolic cytokine TNF- $\alpha$  led to a significant reduction of proteoglycans in cartilage tissue and a dose-dependent reduction of ECM gene expression to less than 10% of the control group within only 7 days. Anabolic stimuli also elicited adequate responses without serum supplementation: Growth-stimulating TGF- $\beta$ 3 resulted in an increase of *COL2A1*, *COL1A1*, and *COMP* expression, as well as in the almost complete silencing of MMP-13 expression. Here, the short diffusion distance under pharmacological processes may prove to be very favorable; conventional explant cultures, for example, required significantly longer and/or more potent catabolic agents to achieve a similar catabolic response(45,65,66). Furthermore, the possibility of co-culturing joint tissue and resident synovial immune cells was considered to also elicit the inflammatory potential of a potential therapeutic candidate. However, analysis of the viability of synovial leukocytes in the stimulation-poor medium of tissue culture revealed that this approach is probably poorly feasible. The total amount of vital leukocytes dropped to half of the initial value over 10 days. This drop might have been acceptable for co-cultivation, but it also showed that the concentration of e.g. vital T cells (CD3+) had already dropped below 10% of the initial value after 10 days. A similar response was also observed for cells with the surface markers CD16+ (neutrophil granulocytes), CD19+ (B cells) and CD56+ (NK cells). Since different immune cell subclasses have different contributions to the inflammatory processes in the joint (e.g. in OA), such a reduced immune cell diversity would reflect the physiological inflammatory response to a very limited extent and probably generate false-negative results in a pharmacological analysis(67–70). Therefore, in a pre-clinical study of a compound, the inflammatory potential should be investigated in a separate immune cell culture to ensure sufficient sensitivity.

#### 4.3. Presence of CCR9 receptor and paradox effect of different CCL25 dosages on osteochondral tissue suggest an alternative/new/different mode of action

The initial immunohistochemical staining of the osteochondral tissue showed a highly consistent expression of the CCR9 receptor exclusively in the superficial cartilage layer. Recently, the cells of this layer are increasingly often described in the literature, consistent with the preliminary results of the study group, as MSC-like cells with still relatively high differentiation capacity(71,72). The presence of the receptor in the target tissue provides an impetus to reconsider the previously assumed mechanism of action of CCL25 (MSC chemoattraction) and to investigate a direct effect on cartilaginous cells. The stimulation of tissue cultures with CCL25 itself did not show a reduction of cell viability in any concentration - a direct cytotoxic and/or apoptotic effect on osteochondral tissue of the chemokine can therefore not be assumed in therapeutic doses (1 nM) and fiftyfold (50 nM). The analysis of the tissue reaction also showed no statistically significant deviation of the proteoglycan concentration in the cartilage layer of the cultures. This suggests that CCL25 does not exert a direct anabolic or catabolic effect on osteochondral tissue. This assumption is supported by the gene expression analysis, in which no statistically significant change was shown in the ECM genes *ACAN*, *COMP*, and *COL 1A1* by CCL25 stimulation. Only the high concentration of CCL25 (50 nM) resulted in an increase initially after 7 days and then in a slight but statistically significant reduced expression of *COL2A1* after 14 days. This is in agreement with similar results obtained by our group on cartilage micromasses, where an incipient tendency towards catabolic metabolism was also observed from 50 nM(52). However, the response is much weaker than e.g. established catabolic cytokines such as TNF- $\alpha$  and does not follow linear dynamics. Thus, the effect may be due to a more complex signaling pathway rather than direct induction or suppression of the corresponding genes.

In the analysis of the proliferation marker *Ki-67*, the therapeutic concentration 1 nM showed a non-significant increase- and concentrations of 5 nM showed a significant increase in its expression after 7 days, which dropped below the initial level after 14 days. This pro-proliferative tendency follows no clear trend but it is one of a series of observations suggesting that low concentrations of CCL25 trigger proliferative processes via a not yet understood mechanism, whereas high concentrations of CCL25 rather trigger a catabolic situation(73,74). In any case, more research is needed to further elucidate this mechanism. Possibly, chemokines could become a new substance class of interest in tissue regeneration, as they are able to influence cell cycle and matrix synthesis independently of classical anabolic stimuli.

#### 4.4. Encapsulation of CCL25 in PLGA microparticles prevents strong inflammatory activation of different immunecell subsets

Initially, the proportional presence of the CCR9 receptor of each immune cell subclass studied, as determined by FACS, underscores the need for a separate investigation of the inflammatory potentials of CCL25 in a controlled culture. Stimulation of immune cells with unencapsulated suspensions of CCL25 resulted in a massive inflammatory response starting at concentrations of 100 nM CCL25. The protein assay of the supernatants showed immense increases of all measured pro-inflammatory cytokines, including the highly inflammatory and tissue catabolic cytokines TNF- $\alpha$  and IL-1 $\beta$ (75,76). Even significantly lower concentrations of 10 nM CCL25 were sufficient to cause significant upregulation of the activation marker HLA-DR on monocytes and CD4+ positive T cells(77). Again, a dose-dependence of the effect size was shown. Furthermore, CCL25 showed the worrying property of exerting a high chemoattractive potential on CD4+ and CD8+ T cells as well as M0 and M1 polarized macrophages in dose ranges of 500-1000nM. Given



that CCL25 was initially discovered in the context of T-cell homing and its chemoattractive potential on leukocytes *in vivo* has already been described, these results are not surprising - but in the overall picture, they underline the pronounced pro-inflammatory potential of CCL25, especially in concentration ranges of 250 – 500 nM(78–81).

Particle stimulation results were less pronounced. Cytokine measurement showed only a moderate increase in IL-8 and MCP-1 in PBMCs and macrophages, which was minimally higher in the group stimulated with loaded particles. The increase in IL-8 may be due to acidic degradation of PLGA, which also triggered similar response patterns in other cell types(82,83). Analysis of surface markers showed no change in PBMCs, but a decrease in CD80, and an increase in CD206 expression in macrophages. This pattern indicates a polarization shift toward the pro-regenerative M2 macrophage type. The M2 shift by PLGA is also reported elsewhere in the literature and highlights the suitability of this polymer as a delivery device in tissue engineering applications(84,85). Overall, these results are consistent with existing findings on the tissue compatibility of PLGA; the small differences in the loaded and unloaded particles indicate the sufficiency or tightness of CCL25 encapsulation, as leaking concentrations of 10nM CCL25 would have already been visible in the HLA-DR expression levels of PBMCs. However, stimulation of immune cells with the supernatants of degraded particles showed a much stronger response than to the intact particles themselves. In PBMCs, the supernatants triggered secretion of MPC-1, IL-8, and (unlike the intact particles) IL-1 $\beta$ . The secretion response was significantly more pronounced and prolonged in CCL25-containing degradation products than in blank controls, suggesting that the response was not solely due to the PLGA fragments. IL-1 $\beta$  is considered a major signaling protein in the maintenance of the pro-inflammatory milieu in OA and would be associated with adverse side effects, if indeed induced by CCL25 after intra-articular injection(66).

However, in an *in vivo* situation, the released CCL25 would be degraded not only hydrolytically, as in the *in vitro* setup, but also enzymatically. Based on the encapsulated amount of CCL25, the 0.5% w/v supernatants released 352 nM and the 0.05%w/V supernatants released a total of 35.2 nM CCL25, respectively, - the *in vivo* continuously biologically active CCL25 concentration being significantly lower than those used here. Furthermore, the supernatants did not induce changes in HLA-DR expression levels or migration behavior and therefore probably did not contain active concentrations of more than 100 nM CCL25 at any time. Furthermore, the distribution volume in the knee joint at synovial fluid volumes of 5 - 10 ml is significantly higher than in the assay and therefore a lower potency can be assumed there as well.

Overall, it can be concluded from these experiments that high concentration peaks of CCL25 have an extremely potent pro-inflammatory potential, which, when injected into an already inflammatory tissue, could cause more damage via the induction of pro-inflammatory cytokines and recruitment of further immune cells than is achieved via the recruitment and activation of MSCs. However, the stimulation experiments with the PLGA microparticles or their degradation products show that encapsulation into this biopolymer causes a sufficient reduction or regulation of the active CCL25 concentration. Despite a particle loading above the determined threshold of at least 100 nM CCL25, only mild inflammatory effects are shown, which are significantly below the level of direct stimulation. However, in practice this means that any delivery devices must be subject to rigid quality controls with regards to high safety against spontaneous degradation or rupture. The spontaneous release of large amounts of CCL25 could reverse the therapeutic effect into a harmful opposite.

## 5. Conclusion

This study has succeeded in establishing a tissue-based osteochondral *in vitro* culture model that can be produced in large quantities and requires low maintenance, so that it can be used to

perform larger pharmacological studies for dose finding. Furthermore, the data from this model, in conjunction with the collected immune cell culture measurements, allow us to propose a safe therapeutic range for the chemokine CCL25 as a potential treatment for OA and to prepare the necessary vigilance regarding possible inflammatory side effects for a clinical trial.

In terms of a platform for larger-scale pharmacological analyses of new therapeutics for joint diseases, bioprinting does not yet seem particularly suitable. The low availability of the required cells, high culture time and high materials costs make the method too laborious for analyses where high amounts of cultures are needed due to analysis time points and different assay concentrations of the agent. In contrast, the method established during the thesis for thin-section preparation of osteochondral explants has proven to be better suited for the rapid, simple and cost-effective preparation of large quantities of up to 100 cultures from individual joint tissue samples. Despite the high mechanical stress caused by the preparation process and the tissue thickness of only 500  $\mu\text{m}$ , the thin-section cultures, despite serum-free cultivation, exhibit the same biological properties with regard to cell viability and chondrocyte genotypes as conventional thick punched explant cultures and respond significantly faster to biological stimuli in comparison. In terms of the 3R principles, thin-sectioned osteochondral explants represent a useful and important complement or possible alternative to animal models in the field of preclinical musculoskeletal pharmaceutical research. Based on the findings of this study, pharmacological studies with an immunological focus should additionally take place in a separate setting, as co-cultivation of the tissue with autologous resident leukocytes has not proven useful due to the high discrepancy in nutrient requirements between tissue-residing osteochondral cells and immune cells.

Stimulation of osteochondral tissue cultures with CCL25 showed no toxic and no clear catabolic or anabolic effects on the tissue. However, it repeated the observation already made in other contexts that low levels of CCL25 appear to provide a growth stimulus to tissue, whereas higher levels of CCL25 limit anabolic processes. In addition, immunohistochemical evidence of the CCL25-specific CCR9 reporter in the superficial cartilage layer was obtained for the first time. This picture suggests that the beneficial effect of CCL25 on cartilage tissue demonstrated *in vivo* may be subject to other mechanisms than exclusively the recruitment of neighboring MSCs into the articular cavity. In the future, more detailed analyses on possible additional mechanisms of action of this chemokine on tissues should be performed, on the one hand to better understand the drug class and, on the other hand, to explore new possibilities for tissue manipulation and regeneration.

In contrast to tissue culture, human leukocyte cultures showed a pronounced pro-inflammatory response at doses around 50 - 100 nM. In the context of the planned application into an inflammatory tissue, this is probably the most relevant source of side effects and should be included in any consideration of a possible therapeutic application. However, these effects could be very effectively prevented by encapsulation in PLGA microparticles. Both loaded microparticles and their degraded supernatants elicited only very marginal inflammatory responses, suggesting that there may well be a therapeutic range of CCL25 concentration in which the inflammatory side effects are very limited. However, it is imperative that this delivery device be characterized by the highest reliability, since spontaneous degradation or another opening of the particles could result in the release of actually harmful concentrations of CCL25, especially in the first 7 - 14 days after application.

## 6. References

1. **Vina ER, Kwoh CK.** Epidemiology of osteoarthritis: literature update. *Curr Opin Rheumatol.* 2018 Mar;30(2):160–7.
2. **Robert Koch Institut.** Gesundheit in Deutschland. Gesundheitsbericht 2015. *Gesundheitsberichterstattung des Bundes Gem getragen von RKI und Destatis.* 2015;
3. **Jevsevar DS.** Treatment of Osteoarthritis of the Knee: Evidence-Based Guideline, 2nd Edition. *J Am Acad Orthop Surg.* 2013 Sep 1;21(9):571–6.
4. **Giwner U, Rubin G, Orbach H, Rozen N.** Treatment for Osteoarthritis of the Knee. Vol. 155, Harefuah. 2016. p. 403–6.
5. **Kan H, Chan P, Chiu K, Yan C, Yeung S, Ng Y, Shiu K, Ho T.** Non-surgical treatment of knee osteoarthritis. *Hong Kong Med J.* 2019 Mar 28;25(2):127–33.
6. **Rabenberg M.** Gesundheitsberichterstattung des Bundes ; 54 , Arthrose. *Robert Koch Inst.* 2013;36.
7. **Ossendorf C, Kaps C, Kreuz PC, Burmester GR, Sittinger M, Erggelet C.** Treatment of posttraumatic and focal osteoarthritic cartilage defects of the knee with autologous polymer-based three-dimensional chondrocyte grafts: 2-year clinical results. *Arthritis Res Ther.* 2007;9(2):R41.
8. **Foldager CB indzu.** Advances in autologous chondrocyte implantation and related techniques for cartilage repair. *Dan Med J.* 2013;60(4):B4600.
9. **Chow YY, Chin K-Y.** The Role of Inflammation in the Pathogenesis of Osteoarthritis. *Mediators Inflamm.* 2020 Mar 3;2020:1–19.
10. **Ansari MY, Ahmad N, Haqqi TM.** Oxidative stress and inflammation in osteoarthritis pathogenesis: Role of polyphenols. *Biomed Pharmacother.* 2020 Sep;129:110452.
11. **Goldring MB, Otero M.** Inflammation in osteoarthritis. *Curr Opin Rheumatol.* 2011 Sep;23(5):471–8.
12. **Deng ZH, Li YS, Gao X, Lei GH, Huard J.** Bone morphogenetic proteins for articular cartilage regeneration. *Osteoarthr Cartil.* 2018 Sep;26(9):1153–61.
13. **Liu Q, Jia Z, Duan L, Xiong J, Wang D, Ding Y.** Functional peptides for cartilage repair and regeneration. *Am J Transl Res.* 2018;10(2):501–10.
14. **Le H, Xu W, Zhuang X, Chang F, Wang Y, Ding J.** Mesenchymal stem cells for cartilage regeneration. *J Tissue Eng.* 2020 Jan 26;11:204173142094383.
15. **Sakata R, Iwakura T, Reddi AH.** Regeneration of Articular Cartilage Surface: Morphogens, Cells, and Extracellular Matrix Scaffolds. *Tissue Eng Part B Rev.* 2015 Oct;21(5):461–73.
16. **Seon J-K, Choi I-S, Ko J-W.** Current Update of Cartilage Regeneration Using Stem Cells in Osteoarthritis. *J Korean Orthop Assoc.* 2019;54(6):478.
17. **Graham AD, Olof SN, Burke MJ, Armstrong JPK, Mikhailova EA, Nicholson JG, Box**

- SJ, Szele FG, Perriman AW, Bayley H.** High-Resolution Patterned Cellular Constructs by Droplet-Based 3D Printing. *Sci Rep.* 2017 Dec 1;7(1):7004.
18. **Andreas K, Sittinger M, Ringe J.** Toward in situ tissue engineering: chemokine-guided stem cell recruitment. *Trends Biotechnol.* 2014 Sep;32(9):483–92.
  19. **Binger T, Stich S, Andreas K, Kaps C, Sezer O, Notter M, Sittinger M, Ringe J.** Migration potential and gene expression profile of human mesenchymal stem cells induced by CCL25. *Exp Cell Res.* 2009 May;315(8):1468–79.
  20. **Ringe J, Hemmati-Sadeghi S, Fröhlich K, Engels A, Reiter K, Dehne T, Sittinger M.** CCL25-Supplemented Hyaluronic Acid Attenuates Cartilage Degeneration in a Guinea Pig Model of Knee Osteoarthritis. *J Orthop Res.* 2019 Aug 29;37(8):1723–9.
  21. **Fröhlich K, Hartzke D, Schmidt F, Eucker J, Gurlo A, Sittinger M, Ringe J.** Delayed release of chemokine CCL25 with bioresorbable microparticles for mobilization of human mesenchymal stem cells. *Acta Biomater.* 2018 Mar;69:290–300.
  22. **Andreas K, Zehbe R, Kazubek M, Grzeschik K, Sternberg N, Bäuml H, Schubert H, Sittinger M, Ringe J.** Biodegradable insulin-loaded PLGA microspheres fabricated by three different emulsification techniques: Investigation for cartilage tissue engineering. *Acta Biomater.* 2011 Apr;7(4):1485–95.
  23. **Wouters OJ, McKee M, Luyten J.** Estimated Research and Development Investment Needed to Bring a New Medicine to Market, 2009-2018. *JAMA.* 2020 Mar 3;323(9):844.
  24. **Spinnen J, Ringe J, Sittinger M.** CCL25 chemokine-guided stem cell attraction: an assessment of possible benefits and risks. *Regen Med.* 2018;13(7):833–44.
  25. **Xu B, Deng C, Wu X, Ji T, Zhao L, Han Y, Yang W, Qi Y, Wang Z, Yang Z, Yang Y.** CCR9 and CCL25: A review of their roles in tumor promotion. *J Cell Physiol.* 2020 Dec 13;235(12):9121–32.
  26. **Heinrich EL, Arrington AK, Ko ME, Luu C, Lee W, Lu J, Kim J.** Paracrine Activation of Chemokine Receptor CCR9 Enhances The Invasiveness of Pancreatic Cancer Cells. *Cancer Microenviron.* 2013 Dec 1;6(3):241–5.
  27. **Niu Y, Tang D, Fan L, Gao W, Lin H.** CCL25 promotes the migration and invasion of non-small cell lung cancer cells by regulating VEGF and MMPs in a CCR9-dependent manner. *Exp Ther Med.* 2020 Apr 2;
  28. **Sharma PK, Singh R, Novakovic KR, Eaton JW, Grizzle WE, Singh S.** CCR9 mediates PI3K/AKT-dependent antiapoptotic signals in prostate cancer cells and inhibition of CCR9-CCL25 interaction enhances the cytotoxic effects of etoposide. *Int J Cancer.* 2010;127(9):2020–30.
  29. **Borrelli GM, Carvalho KI, Kallas EG, Mechsner S, Baracat EC, Abrão MS.** Chemokines in the pathogenesis of endometriosis and infertility. *J Reprod Immunol.* 2013 Jun;98(1–2):1–9.
  30. **Žigon-Branc S, Barlič A, Jeras M.** In vitro Cell-Based Assays for Potency Testing of Anti-TNF- $\alpha$  Biological Drugs. In: Cytokines. IntechOpen; 2020.
  31. **Kuyinu EL, Narayanan G, Nair LS, Laurencin CT.** Animal models of osteoarthritis: classification, update, and measurement of outcomes. *J Orthop Surg Res.* 2016 Dec 2;11(1):19.
  32. **Serra CI, Soler C.** Animal Models of Osteoarthritis in Small Mammals. *Vet Clin North Am Exot Anim Pract.* 2019 May;22(2):211–21.

33. **Žigon-Branc S, Jeras M, Blejec A, Barlič A.** Applicability of human osteoarthritic chondrocytes for in vitro efficacy testing of anti-TNF $\alpha$  drugs. *Biologicals*. 2017 Jan;45:96–101.
34. **Cope PJ, Ourradi K, Li Y, Sharif M.** Models of osteoarthritis: the good, the bad and the promising. *Osteoarthr Cartil*. 2019 Feb;27(2):230–9.
35. **Bapat S, Hubbard D, Munjal A, Hunter M, Fulzele S.** Pros and cons of mouse models for studying osteoarthritis. *Clin Transl Med*. 2018 Dec 21;7(1).
36. **Aske KC, Waugh CA.** Expanding the 3R principles. *EMBO Rep*. 2017 Sep 25;18(9):1490–2.
37. **Jorgensen C, Simon M.** In Vitro Human Joint Models Combining Advanced 3D Cell Culture and Cutting-Edge 3D Bioprinting Technologies. *Cells*. 2021 Mar 8;10(3):596.
38. **Rothbauer M, Schobesberger S, Byrne R, Kiener HP, Tögel S, Ertl P.** A human joint-on-a-chip as alternative to animal models in osteoarthritis. *Osteoarthr Cartil*. 2020;28:S89.
39. **Arrigoni C, Lopa S, Candrian C, Moretti M.** Organs-on-a-chip as model systems for multifactorial musculoskeletal diseases. *Curr Opin Biotechnol*. 2020 Jun;63:79–88.
40. **Mandrycky C, Wang Z, Kim K, Kim D-H.** 3D bioprinting for engineering complex tissues. *Biotechnol Adv*. 2016 Jul;34(4):422–34.
41. **Galarraga JH, Kwon MY, Burdick JA.** 3D bioprinting via an in situ crosslinking technique towards engineering cartilage tissue. *Sci Rep*. 2019;9(1).
42. **Lam T, Dehne T, Krüger JP, Hondke S, Endres M, Thomas A, Lauster R, Sittinger M, Kloke L.** Photopolymerizable gelatin and hyaluronic acid for stereolithographic 3D bioprinting of tissue-engineered cartilage. *J Biomed Mater Res Part B Appl Biomater*. 2019 Nov 12;107(8):2649–57.
43. **Salvador Vergés À, Yildirim M, Salvador B, Garcia Cuyas F.** Trends in Scientific Reports on Cartilage Bioprinting: Scoping Review. *JMIR Form Res*. 2019 Aug 28;3(3):e15017.
44. **Houtman E, van Hoolwerff M, Lakenberg N, Suchiman EHD, van der Linden-van der Zwaag E, Nelissen RGHH, Ramos YFM, Meulenbelt I.** Human Osteochondral Explants: Reliable Biomimetic Models to Investigate Disease Mechanisms and Develop Personalized Treatments for Osteoarthritis. *Rheumatol Ther*. 2021 Mar 20;8(1):499–515.
45. **Pretzel D, Pohlert D, Weinert S, Kinne RW.** In vitro model for the analysis of synovial fibroblast-mediated degradation of intact cartilage. *Arthritis Res Ther*. 2009;11(1):R25.
46. **Haltmayer E, Ribitsch I, Gabner S, Rosser J, Gueltekin S, Peham J, Giese U, Dolezal M, Egerbacher M, Jenner F.** Co-culture of osteochondral explants and synovial membrane as in vitro model for osteoarthritis. Ahmad R, editor. *PLoS One*. 2019 Apr 2;14(4):e0214709.
47. **Amler A-K, Dinkelborg PH, Schlauch D, Spinnen J, Stich S, Lauster R, Sittinger M, Nahles S, Heiland M, Kloke L, Rendenbach C, Beck-Broichsitter B, Dehne T.** Comparison of the Translational Potential of Human Mesenchymal Progenitor Cells from Different Bone Entities for Autologous 3D Bioprinted Bone Grafts. *Int J Mol Sci*. 2021 Jan 14;22(2):796.
48. **Spinnen J, Shopperly LK, Rendenbach C, Kühl AA, Sentürk U, Kendoff D, Hemmati-Sadeghi S, Sittinger M, Dehne T.** A Novel Method Facilitating the Simple and Low-Cost

- Preparation of Human Osteochondral Slice Explants for Large-Scale Native Tissue Analysis. *Int J Mol Sci*. 2021 Jun 15;22(12):6394.
49. **van den Berg WB**. Osteoarthritis year 2010 in review: pathomechanisms. *Osteoarthr Cartil*. 2011 Apr;19(4):338–41.
  50. **Cook JL, Kuroki K, Visco D, Pelletier J-P, Schulz L, Lafebber FPJG**. The OARSI histopathology initiative – recommendations for histological assessments of osteoarthritis in the dog. *Osteoarthr Cartil*. 2010 Oct;18(SUPPL. 3):S66–79.
  51. **Spinnen J, Fröhlich K, Sinner N, Stolk M, Ringe J, Shopperly L, Sittinger M, Dehne T, Seifert M**. Therapies with CCL25 require controlled release via microparticles to avoid strong inflammatory reactions. *J Nanobiotechnology*. 2021 Dec 25;19(1):83.
  52. **Lüderitz L, Dehne T, Sittinger M, Ringe J**. Dose-Dependent Effect of Mesenchymal Stromal Cell Recruiting Chemokine CCL25 on Porcine Tissue-Engineered Healthy and Osteoarthritic Cartilage. *Int J Mol Sci*. 2018 Dec 23;20(1):52.
  53. **Nair K, Gandhi M, Khalil S, Yan KC, Marcolongo M, Barbee K, Sun W**. Characterization of cell viability during bioprinting processes. *Biotechnol J*. 2009 Aug;4(8):1168–77.
  54. **Memic A, Navaei A, Mirani B, Cordova JAV, Aldahri M, Dolatshahi-Pirouz A, Akbari M, Nikkhah M**. Bioprinting technologies for disease modeling. *Biotechnol Lett*. 2017 Sep 26;39(9):1279–90.
  55. **Miron RJ, Zhang YF**. Osteoinduction. *J Dent Res*. 2012 Aug 8;91(8):736–44.
  56. **Long F**. Building strong bones: molecular regulation of the osteoblast lineage. *Nat Rev Mol Cell Biol*. 2012 Jan 22;13(1):27–38.
  57. **Ringe J, Leinase I, Stich S, Loch A, Neumann K, Haisch A, Häup T, Manz R, Kaps C, Sittinger M**. Human mastoid periosteum-derived stem cells: promising candidates for skeletal tissue engineering. *J Tissue Eng Regen Med*. 2008 Mar;2(2–3):136–46.
  58. **Lajeunesse D, Massicotte F, Pelletier J-P, Martel-Pelletier J**. Subchondral bone sclerosis in osteoarthritis: not just an innocent bystander. *Mod Rheumatol*. 2003 Mar 2;13(1):0007–14.
  59. **Poole AR, Kojima T, Yasuda T, Mwale F, Kobayashi M, Laverty S**. Composition and structure of articular cartilage: A template for tissue repair. In: *Clinical Orthopaedics and Related Research*. 2001.
  60. **Secretan C, Bagnall KM, Jomha NM**. Effects of introducing cultured human chondrocytes into a human articular cartilage explant model. *Cell Tissue Res*. 2010 Feb 12;339(2):421–7.
  61. **Gavénis K, Andereya S, Schmidt-Rohlfing B, Mueller-Rath R, Silny J, Schneider U**. Millicurrent stimulation of human articular chondrocytes cultivated in a collagen type-I gel and of human osteochondral explants. *BMC Complement Altern Med*. 2010 Dec 6;10(1):43.
  62. **Lyman JR, Chappell JD, Morales TI, Kelley SS, Lee GM**. Response of Chondrocytes to Local Mechanical Injury in an Ex Vivo Model. *Cartilage*. 2012 Jan 13;3(1):58–69.
  63. **Bian L, Lima EG, Angione SL, Ng KW, Williams DY, Xu D, Stoker AM, Cook JL, Ateshian GA, Hung CT**. Mechanical and biochemical characterization of cartilage explants in serum-free culture. *J Biomech*. 2008;41(6):1153–9.

64. **Ragan PM, Badger AM, Cook M, Chin VI, Gowen M, Grodzinsky AJ, Lark MW.** Down-regulation of Chondrocyte Aggrecan and Type-II Collagen Gene Expression Correlates with Increases in Static Compression Magnitude and Duration. *J Bone Jt Surgery-American Vol.* 2000 Apr;82(4):32.
65. **Thudium CS, Engstrom A, Groen SS, Karsdal MA, Bay-Jensen AC, Bioscience N.** An ex vivo tissue culture model of cartilage remodeling in bovine knee explants. *J Vis Exp.* 2019;2019(153).
66. **Clutterbuck AL, Mobasheri A, Shakibaei M, Allaway D, Harris P.** Interleukin-1 $\beta$ -Induced Extracellular Matrix Degradation and Glycosaminoglycan Release Is Inhibited by Curcumin in an Explant Model of Cartilage Inflammation. *Ann N Y Acad Sci.* 2009 Aug;1171(1):428–35.
67. **Yang D, Zhang Z.** The role of helper T cell in the pathogenesis of osteoarthritis. *Zhongguo Xiu Fu Chong Jian Wai Ke Za Zhi.* 2020;34(7):932–8.
68. **Sakkas LI, Platsoucas CD.** The role of T cells in the pathogenesis of osteoarthritis. *Arthritis Rheum.* 2007 Feb;56(2):409–24.
69. **Chen Y, Jiang W, Yong H, He M, Yang Y, Deng Z, Li Y.** Macrophages in osteoarthritis: Pathophysiology and therapeutics. *Am J Transl Res.* 2020;12(1):261–8.
70. **Griffin TM, Scanzello CR.** Innate inflammation and synovial macrophages in osteoarthritis pathophysiology. Vol. 37, *Clinical and experimental rheumatology.* 2019. p. 57–63.
71. **Li L, Newton PT, Boudierlique T, Sejnohova M, Zikmund T, Kozhemyakina E, Xie M, Krivanek J, Kaiser J, Qian H, Dyachuk V, Lassar AB, Warman ML, Barenus B, Adameyko I, Chagin AS.** Superficial cells are self-renewing chondrocyte progenitors, which form the articular cartilage in juvenile mice. *FASEB J.* 2017 Mar 13;31(3):1067–84.
72. **Jiang Y, Tuan RS.** Origin and function of cartilage stem/progenitor cells in osteoarthritis. Vol. 11, *Nature Reviews Rheumatology.* 2015. p. 206–12.
73. **Chen HJ, Edwards R, Tucci S, Bu P, Milsom J, Lee S, Edelmann W, Gümüş ZH, Shen X, Lipkin S.** Chemokine 25 - Induced signaling suppresses colon cancer invasion and metastasis. *J Clin Invest.* 2012;
74. **Chen H, Cong X, Wu C, Wu X, Wang J, Mao K, Li J, Zhu G, Liu F, Meng X, Song J, Sun X, Wang X, Liu S, Zhang S, Yang X, Song Y, Yang Y-G, Sun T.** Intratumoral delivery of CCL25 enhances immunotherapy against triple-negative breast cancer by recruiting CCR9 + T cells. *Sci Adv.* 2020 Jan 31;6(5):eaax4690.
75. **Ren K, Torres R.** Role of interleukin-1 $\beta$  during pain and inflammation. *Brain Res Rev.* 2009 Apr;60(1):57–64.
76. **Zwerina J, Redlich K, Polzer K, Joosten L, Krönke G, Distler J, Hess A, Pundt N, Pap T, Hoffmann O, Gasser J, Scheinecker C, Smolen JS, van den Berg W, Schett G.** TNF-induced structural joint damage is mediated by IL-1. *Proc Natl Acad Sci.* 2007 Jul 10;104(28):11742–7.
77. **Salgado FJ, Lojo J, Fernández-Alonso CM, Viñuela JE, Cordero OJ, Nogueira M.** Interleukin-dependent modulation of HLA-DR expression on CD4 and CD8 activated T cells. *Immunol Cell Biol.* 2002 Apr;80(2):138–47.
78. **Pabst O, Ohl L, Wendland M, Wurbel M-A, Kremmer E, Malissen B, Förster R.** Chemokine Receptor CCR9 Contributes to the Localization of Plasma Cells to the Small Intestine. *J Exp Med.* 2004 Feb 2;199(3):411–6.

79. **Onai N.** Pivotal role of CCL25 (TECK)-CCR9 in the formation of gut cryptopatches and consequent appearance of intestinal intraepithelial T lymphocytes. *Int Immunol.* 2002 Jul 1;14(7):687–94.
80. **Meurens F, Whale J, Brownlie R, Dybvig T, Thompson DR, Gerdt V.** Expression of mucosal chemokines TECK/CCL25 and MEC/CCL28 during fetal development of the ovine mucosal immune system. *Immunology.* 2007 Apr;120(4):544–55.
81. **Uehara S, Song K, Farber JM, Love PE.** Characterization of CCR9 Expression and CCL25/Thymus-Expressed Chemokine Responsiveness During T Cell Development: CD3 high CD69 + Thymocytes and  $\gamma\delta$ TCR + Thymocytes Preferentially Respond to CCL25. *J Immunol.* 2002 Jan 1;168(1):134–42.
82. **Xu L, Fidler IJ.** Acidic pH-induced elevation in interleukin 8 expression by human ovarian carcinoma cells. *Cancer Res.* 2000;60(16):4610–6.
83. **Shan J, Oshima T, Fukui H, Watari J, Miwa H.** Acidic deoxycholic acid and chenodeoxycholic acid induce interleukin-8 production through p38 mitogen-activated protein kinase and protein kinase A in a squamous epithelial model. *J Gastroenterol Hepatol.* 2013 May;28(5):823–8.
84. **Chen X, Zhu X, Ma L, Lin A, Gong Y, Yuan G, Liu J.** A core-shell structure QRu-PLGA-RES-DS NP nanocomposite with photothermal response-induced M2 macrophage polarization for rheumatoid arthritis therapy. *Nanoscale.* 2019;11(39):18209–23.
85. **Huang J, Zhou X, Shen Y, Li H, Zhou G, Zhang W, Zhang Y, Liu W.** Asiaticoside loading into polylactic-co-glycolic acid electrospun nanofibers attenuates host inflammatory response and promotes M2 macrophage polarization. *J Biomed Mater Res Part A.* 2020 Jan 12;108(1):69–80.

## 7. Affidavit

"I, Jacob Burkhard Spinnen affirm in lieu of an oath by my own handwritten signature that I have written the submitted dissertation with the topic: "In vitro pharmacological risk assessment of new therapeutic agents for osteoarthritis on osteochondral tissue cultures – a risk profile of CCL25/ In vitro pharmakologische Risikobewertung neuer therapeutischer Wirkstoffe gegen Osteoarthritis an osteochondralen Gewebekulturen - ein Risikoprofil von CCL25" independently and without the undisclosed help of third parties and have not used any sources or aids other than those indicated.

All passages that are literally or in spirit based on publications or lectures of other authors are marked as such in correct citation. I am responsible for the sections on methodology (especially practical work, laboratory determinations, statistical processing) and results (especially figures, graphs and tables). I further assure that I have correctly identified the data, data analysis and conclusions generated in cooperation with other persons and that I have correctly identified my own contribution as well as the contributions of other persons (see declaration of share). I have correctly identified texts or parts of texts that were created or used jointly with others. My shares in any publications on this dissertation correspond to those stated in the joint declaration with the first supervisor below. The ICMJE (International Committee of Medical Journal Editors; [www.icmje.org](http://www.icmje.org)) guidelines on authorship have been followed for all publications arising from this dissertation. I declare further that I commit myself to comply with the statutes of the Charité - Universitätsmedizin Berlin to ensure good scientific practice.



Furthermore, I affirm that I have not already submitted this dissertation in the same or similar form to another faculty. I am aware of the significance of this affidavit and the criminal consequences of an untrue affidavit (§§156, 161 of the Criminal Code)."

Berlin, 04.11.2021

Signature

I, the doctoral student Jacob Burkhard Spinnen had the following share in the following publications:

**Publication 1:**

**Spinnen J, Shopperly LK, Rendenbach C, Kühl AA, Sentürk U, Kendoff D, Hemmati-Sadeghi S, Sittinger M, Dehne T.** A Novel Method Facilitating the Simple and Low-Cost Preparation of Human Osteochondral Slice Explants for Large-Scale Native Tissue Analysis. *Int J Mol Sci.* 2021 Jun 15;22(12):6394.

Contribution to the project: The entire conception (project planning, ethical application, theoretical preparatory work), laboratory work (tissue processing, tissue culture, histological and gene expression examinations), the analysis of the data as well as the writing of the manuscript were carried out by me independently. The project was supported by the Charité Core Facilities iPATH, AMBIO and Werkstatt Charité, which provided know-how and infrastructure for special analytical methods as internal service providers.

Contribution to the publication:

I have independently and primarily authored and composed the entire written publication. This includes all illustrations and text sections of this publication.

**Publication 2:**

**Amler A-K, Dinkelborg PH, Schlauch D, Spinnen J, Stich S, Lauster R, Sittinger M, Nahles S, Heiland M, Kloke L, Rendenbach C, Beck-Broichsitter B, Dehne T** (2021).

Comparison of the Translational Potential of Human Mesenchymal Progenitor Cells from Different Bone Entities for Autologous 3D Bioprinted Bone Grafts *Int J Mol Sci.* 2021 Jan 14;22(2):796.

Contribution in to the project:

I was significantly involved in the conception of the study (detailed experimental design, measurement times, analysis methods) and in the execution of the laboratory work (cell culture, measurements on the printed tissue cultures) as well as in editing of the manuscript. The 3D printing and the data analysis of the gene expression as well as the main manuscript conception were performed by the project partners of the Oral and Maxillofacial Surgery and the company

CellBricks GmbH.

Contribution to the publication:

I co-authored the text section of the introduction, the text section of Results-“ Bioprinting and Cultivation of Printed Construct” and “Viability and Metabolic Activity” as well as the Discussion of the publication.

Publication 3:

**Spinnen J, Fröhlich K, Sinner N, Stolk M, Ringe J, Shopperly L, Sittinger M, Dehne T, Seifert M.** Therapies with CCL25 require controlled release via microparticles to avoid strong inflammatory reactions. *J Nanobiotechnology*. 2021 Dec 25;19(1):83.

Contribution to the project:

In the analysis of the inflammatory potential of CCL25, I was significantly involved in the conception of the study and developed the evaluation strategy of the migration, protein and flow cytometry assays in his own work. On this basis, I performed the complete data analysis, presentation and writing of the manuscript. The laboratory experiments were mainly performed in the facilities of our cooperation partners of the research group of Prof. Dr. Martina Seifert, since the know-how and infra-structure with an immunological focus was required for this work.

Contribution to the publication:

I have independently and primarily authored and composed the entire written publication and designed the figures 1, 2, 3 and 4. The method-related figures 5 and 6 were designed by Lennard K. Shopperly.

---

Signature, date and stamp of the first supervising university teacher

---

Signature of the doctoral student

## 8. Publications

- 8.1. **Spinnen J, Shopperly LK, Rendenbach C, Kühl AA, Sentürk U, Kendoff D, Hemmati-Sadeghi S, Sittinger M, Dehne T.**  
A Novel Method Facilitating the Simple and Low-Cost Preparation of Human Osteochondral Slice Explants for Large-Scale Native Tissue Analysis.  
*Int J Mol Sci.* 2021 Jun 15;22(12):6394.

Journal Data Filtered By: **Selected JCR Year: 2019** Selected Editions: SCIE,SSCI  
 Selected Categories: **"BIOCHEMISTRY and MOLECULAR BIOLOGY"** Selected  
 Category Scheme: WoS

**Gesamtanzahl: 297 Journale**

Rank	Full Journal Title	Total Cites	Journal Impact Factor	Eigenfactor Score
1	CELL	258,178	38.637	0.564970
2	NATURE MEDICINE	85,220	36.130	0.168730
3	Annual Review of Biochemistry	20,499	25.787	0.024820
4	MOLECULAR CELL	69,148	15.584	0.166260
5	Molecular Cancer	15,448	15.302	0.023990
6	PROGRESS IN LIPID RESEARCH	6,139	15.083	0.005730
7	TRENDS IN BIOCHEMICAL SCIENCES	18,416	14.732	0.032060
8	TRENDS IN MICROBIOLOGY	13,604	13.546	0.022780
9	Signal Transduction and Targeted Therapy	1,182	13.493	0.003380
10	Nature Chemical Biology	22,084	12.587	0.060130
11	MOLECULAR PSYCHIATRY	22,227	12.384	0.054730
12	Molecular Plant	11,432	12.084	0.028530
13	NATURAL PRODUCT REPORTS	11,239	12.000	0.013610
14	NATURE STRUCTURAL & MOLECULAR BIOLOGY	27,178	11.980	0.056800
15	NUCLEIC ACIDS RESEARCH	201,649	11.501	0.403470
16	TRENDS IN MOLECULAR MEDICINE	10,618	11.099	0.018720
17	GENOME RESEARCH	41,755	11.093	0.076940
18	MOLECULAR BIOLOGY AND EVOLUTION	50,486	11.062	0.084810
19	CELL DEATH AND DIFFERENTIATION	21,095	10.717	0.029600
20	Redox Biology	10,157	9.986	0.023810

Rank	Full Journal Title	Total Cites	Journal Impact Factor	Eigenfactor Score
21	EMBO JOURNAL	64,724	9.889	0.059690
22	CURRENT OPINION IN CHEMICAL BIOLOGY	10,968	9.689	0.017770
23	PLANT CELL	54,927	9.618	0.048640
24	CURRENT BIOLOGY	63,256	9.601	0.133170
25	MOLECULAR ASPECTS OF MEDICINE	6,207	9.577	0.005750
26	Molecular Systems Biology	8,914	8.991	0.017390
27	Cell Systems	3,822	8.673	0.029290
28	MATRIX BIOLOGY	6,878	8.572	0.011920
29	ONCOGENE	66,303	7.971	0.068320
30	Cell Chemical Biology	3,326	7.739	0.015770
31	CRITICAL REVIEWS IN BIOCHEMISTRY AND MOLECULAR BIOLOGY	3,675	7.634	0.006380
32	EMBO REPORTS	14,976	7.497	0.030290
33	BIOCHIMICA ET BIOPHYSICA ACTA-REVIEWS ON CANCER	5,650	7.365	0.007800
34	PLOS BIOLOGY	31,650	7.076	0.060300
35	Essays in Biochemistry	2,383	6.966	0.005060
36	CURRENT OPINION IN STRUCTURAL BIOLOGY	11,035	6.908	0.021890
37	CELLULAR AND MOLECULAR LIFE SCIENCES	26,128	6.496	0.037010
38	Science Signaling	12,736	6.467	0.026590
39	ANTIOXIDANTS & REDOX SIGNALING	21,119	6.323	0.024660
40	Molecular Ecology Resources	10,868	6.286	0.019630
41	FREE RADICAL BIOLOGY AND MEDICINE	42,665	6.170	0.036960
42	BIOMACROMOLECULES	38,863	6.092	0.031320

Selected JCR Year: 2019; Selected Categories: "BIOCHEMISTRY and MOLECULAR BIOLOGY"

Rank	Full Journal Title	Total Cites	Journal Impact Factor	Eigenfactor Score
43	Computational and Structural Biotechnology Journal	1,954	6.018	0.004980
44	CYTOKINE & GROWTH FACTOR REVIEWS	5,935	5.982	0.007380
45	Advances in Carbohydrate Chemistry and Biochemistry	634	5.800	0.000340
46	EXPERIMENTAL AND MOLECULAR MEDICINE	5,536	5.418	0.010300
47	AMERICAN JOURNAL OF RESPIRATORY CELL AND MOLECULAR BIOLOGY	12,243	5.373	0.016040
48	RNA Biology	6,589	5.350	0.015820
49	Acta Crystallographica Section D-Structural Biology	21,750	5.266	0.018220
50	MOLECULAR ECOLOGY	38,951	5.163	0.050800
51	INTERNATIONAL JOURNAL OF BIOLOGICAL MACROMOLECULES	47,121	5.162	0.057240
52	BIOCHEMICAL SOCIETY TRANSACTIONS	12,651	5.160	0.016140
53	HUMAN MOLECULAR GENETICS	39,652	5.100	0.064170
54	Journal of Genetics and Genomics	2,271	5.065	0.004310
55	Cell and Bioscience	1,898	5.026	0.004210
56	Antioxidants	2,568	5.014	0.004170
57	FASEB JOURNAL	43,126	4.966	0.043730
58	International Review of Cell and Molecular Biology	2,167	4.934	0.004350
59	Open Biology	2,886	4.931	0.009590
60	Journal of Integrative Plant Biology	5,005	4.885	0.006830
61	Advances in Microbial Physiology	1,227	4.875	0.000960
61	Nucleic Acid Therapeutics	1,030	4.875	0.003610

Rank	Full Journal Title	Total Cites	Journal Impact Factor	Eigenfactor Score
63	JOURNAL OF NUTRITIONAL BIOCHEMISTRY	11,460	4.873	0.011150
64	STRUCTURE	15,145	4.862	0.026940
65	International Journal of Biological Sciences	6,262	4.858	0.009710
66	BIOORGANIC CHEMISTRY	5,712	4.831	0.006730
67	Genes & Diseases	1,081	4.803	0.003310
68	JOURNAL OF MOLECULAR BIOLOGY	56,952	4.760	0.040330
69	BIOFACTORS	3,769	4.734	0.002930
70	BIOELECTROCHEMISTRY	4,944	4.722	0.004950
71	Reviews of Physiology Biochemistry and Pharmacology	805	4.700	0.000670
72	JOURNAL OF ENZYME INHIBITION AND MEDICINAL CHEMISTRY	5,415	4.673	0.005420
73	BIOESSAYS	10,189	4.627	0.016560
74	INTERNATIONAL JOURNAL OF MOLECULAR SCIENCES	77,286	4.556	0.143760
75	APOPTOSIS	6,539	4.543	0.005880
76	BIOCHIMICA ET BIOPHYSICA ACTA- MOLECULAR AND CELL BIOLOGY OF LIPIDS	10,266	4.519	0.016350
77	ACS Chemical Neuroscience	6,881	4.486	0.015300
78	JOURNAL OF LIPID RESEARCH	24,223	4.483	0.022420
79	ACS Chemical Biology	12,884	4.434	0.035490
80	FEBS Journal	18,845	4.392	0.025250
81	JOURNAL OF PHOTOCHEMISTRY AND PHOTOBIOLOGY B- BIOLOGY	12,794	4.383	0.013640
82	BIOCHIMICA ET BIOPHYSICA ACTA- MOLECULAR BASIS OF DISEASE	15,965	4.352	0.024200



Selected JCR Year: 2019; Selected Categories: "BIOCHEMISTRY and MOLECULAR BIOLOGY"

4



Article

# A Novel Method Facilitating the Simple and Low-Cost Preparation of Human Osteochondral Slice Explants for Large-Scale Native Tissue Analysis

Jacob Spinnen <sup>1,\*</sup> , Lennard K. Shopperly <sup>1</sup>, Carsten Rendenbach <sup>2</sup>, Anja A. Kühl <sup>3</sup>, Ufuk Sentürk <sup>4</sup>, Daniel Kendoff <sup>5</sup>, Shabnam Hemmati-Sadeghi <sup>1</sup>, Michael Sittinger <sup>1</sup> and Tilo Dehne <sup>1</sup> 

- <sup>1</sup> Department of Rheumatology, Charité-Universitätsmedizin Berlin, Corporate Member of Freie Universität Berlin, Humboldt Universität zu Berlin, and Berlin Institute of Health, 10117 Berlin, Germany; lennard.shopperly@charite.de (L.K.S.); shabnam.hemmati-sadeghi@charite.de (S.H.-S.); michael.sittinger@charite.de (M.S.); tilo.dehne@charite.de (T.D.)
  - <sup>2</sup> Department of Oral and Maxillofacial Surgery, Charité-Universitätsmedizin Berlin, Corporate Member of Freie Universität Berlin, Humboldt Universität zu Berlin, and Berlin Institute of Health, 13353 Berlin, Germany; carsten.rendenbach@charite.de
  - <sup>3</sup> iPATH Histopathology Core Unit, Charité-Universitätsmedizin Berlin, Corporate Member of Freie Universität Berlin, Humboldt Universität zu Berlin, and Berlin Institute of Health, 13353 Berlin, Germany; anja.kuehl@charite.de
  - <sup>4</sup> Department of Orthopedics, Charité-Universitätsmedizin Berlin, Corporate Member of Freie Universität Berlin, Humboldt Universität zu Berlin, and Berlin Institute of Health, 13353 Berlin, Germany; ufuk.sentuerk@charite.de
  - <sup>5</sup> Department of Orthopaedic Surgery, Helios Klinikum Berlin-Buch, 13125 Berlin, Germany; daniel.kendoff@helios-gesundheit.de
- \* Correspondence: jacob.spinnen@charite.de



**Citation:** Spinnen, J.; Shopperly, L.K.; Rendenbach, C.; Kühl, A.A.; Sentürk, U.; Kendoff, D.; Hemmati-Sadeghi, S.; Sittinger, M.; Dehne, T. A Novel Method Facilitating the Simple and Low-Cost Preparation of Human Osteochondral Slice Explants for Large-Scale Native Tissue Analysis. *Int. J. Mol. Sci.* **2021**, *22*, 6394. <https://doi.org/10.3390/ijms22126394>

Academic Editor: Lih Kuo

Received: 25 May 2021

Accepted: 9 June 2021

Published: 15 June 2021

**Publisher's Note:** MDPI stays neutral with regard to jurisdictional claims in published maps and institutional affiliations.



**Copyright:** © 2021 by the authors. Licensee MDPI, Basel, Switzerland. This article is an open access article distributed under the terms and conditions of the Creative Commons Attribution (CC BY) license (<https://creativecommons.org/licenses/by/4.0/>).

**Abstract:** For in vitro modeling of human joints, osteochondral explants represent an acceptable compromise between conventional cell culture and animal models. However, the scarcity of native human joint tissue poses a challenge for experiments requiring high numbers of samples and makes the method rather unsuitable for toxicity analyses and dosing studies. To scale their application, we developed a novel method that allows the preparation of up to 100 explant cultures from a single human sample with a simple setup. Explants were cultured for 21 days, stimulated with TNF- $\alpha$  or TGF- $\beta$ 3, and analyzed for cell viability, gene expression and histological changes. Tissue cell viability remained stable at >90% for three weeks. Proteoglycan levels and gene expression of *COL2A1*, *ACAN* and *COMP* were maintained for 14 days before decreasing. TNF- $\alpha$  and TGF- $\beta$ 3 caused dose-dependent changes in cartilage marker gene expression as early as 7 days. Histologically, cultures under TNF- $\alpha$  stimulation showed a 32% reduction in proteoglycans, detachment of collagen fibers and cell swelling after 7 days. In conclusion, thin osteochondral slice cultures behaved analogously to conventional punch explants despite cell stress exerted during fabrication. In pharmacological testing, both the shorter diffusion distance and the lack of need for serum in the culture suggest a positive effect on sensitivity. The ease of fabrication and the scalability of the sample number make this manufacturing method a promising platform for large-scale preclinical testing in joint research.

**Keywords:** osteoarthritis; osteochondral explant culture; joint modelling; pharmacological assay; native tissue analysis

## 1. Introduction

Osteoarthritis (OA) is a condition involving the degeneration of articular cartilage, sclerosis of subchondral bone and chronic inflammation of the synovial membrane. To date, it is the main cause of physical disability worldwide [1,2]. Both the underlying pathomechanisms of OA as well as the mechanisms of physiological reorganization of cartilage tissue are poorly understood. Due to this lack of understanding, the treatment of such defects



remains challenging. However, research in recent years has provided increasing evidence that cartilage cells have the general ability to regenerate if stimulated correctly. Limited traumatic cartilage defects can now be successfully treated and regenerated by autologous chondrocyte transplantation and specific cell-modulating substances. The emergence of growth factors as therapeutic agents is expected to further enable the regeneration of osteochondral tissue [3–5], increasing the need for an adequate platform to assess cartilage (repair) treatment strategies.

Traditionally, two-dimensional chondrocyte cultures in monolayer and OA animal models have been the main tools available for preclinical testing of the efficacy and side effects (ADME (absorption, distribution, metabolism, excretion) screening) of such substances. Unfortunately, the former often leads to limited insights due to the lack of representation of the complex tissue composition of the joint, while the latter, in addition to ethical aspects, entails high costs and time expenditure and is therefore usually only applied when a basic efficacy already seems very likely [6,7]. Recently, this spectrum has been expanded to include sophisticated 3D cultures and organ-on-chip applications. However, 3D cultures are either effortful to maintain or, in the case of joint-on-a-chip, not yet commercially available. Therefore, rapid, agile research and development of regenerative therapeutics for cartilage regeneration is limited to a certain extent [8–10].

A sustainable middle ground in joint modelling is the use of tissue explants. Explants are living, native and functional parts from organs, which are obtained from donor tissues or cadavers. Explants can accurately represent part of the tissue composition and architecture. Specifically, the tissue cells remain in their native extracellular matrix (ECM) configuration and questions regarding their response to biological stimuli can be answered much more reliably in the native situation than, for example, with monolayer cultures of only one cell type [11–13]. However, this modelling technique is severely limited by the availability of donor tissue. Employing the frequently used technique of vertical punching of the tissue and subsequent production of osteochondral punchings with diameters of at least 3 mm, only a very small number of explants can be produced from a tissue sample, depending on the tissue properties. Furthermore, the diffusion of nutrients and potentially interacting proteins is severely impeded by the amount of glycosaminoglycans in the tissue [14]. Hence, the explant thickness negatively correlates with information that can be obtained about the behavior of cells located deeper in the tissue.

To address this issue, we have developed a low-cost and uncomplex method to produce explant cultures using a thin-section approach. Similar to the live-slice technology known from neurophysiology, the method allows the production of vital tissue slices with a thickness of 500–800  $\mu\text{m}$  [15]. This allows the production of up to 100 slice cultures from a single tissue sample for subsequent analysis of many different substances and concentrations. Furthermore, the thin tissue architecture is suitable for easy-to-maintain semi-static culture conditions, as the perfusion distance is sufficiently short to reliably guide both nutrients and any therapeutic agents through the tissue to the target cells.

This study aimed to analyze the suitability of osteochondral slices for osteochondral tissue modelling and pharmacological screening of biologically active substances. For this purpose, we obtained a large number of human slice cultures from surgically explanted tibial plateaus and analyzed the behavior of the tissue over 21 days at the histological, metabolic and transcriptional levels. Furthermore, we examined the reactivity of the embedded chondrocytes to the factors TNF- $\alpha$  and TGF- $\beta$ 3, known to affect cartilage matrix synthesis, to determine whether the tissue is in a sufficiently close state to that of the native situation to be used as a testing device [16,17].

## 2. Results

To develop a physiological model for osteochondral tissue which allows for quick handling and high-throughput applications with limited donor material at hand, we developed a method for the manufacturing of native osteochondral live slice cultures from human joint tissue. 500–800  $\mu\text{m}$  thick osteochondral slice cultures were prepared

from 23 different surgically explanted tibial plateaus using a custom-made microtome insert and then cultured in hanging inserts of 24-well plates. In this study, we assessed whether the explanted live slice cultures maintain their physiological properties such as long-term cell viability, gene expression, extracellular matrix and responsiveness towards biological stimuli.

### 2.1. Suitability for Slicing Varies with the Degree of Subchondral Bone Sclerosis

23 of 25 donors were suitable for the production of slice explants. The extent of subchondral sclerosis of the bone proved to be a decisive factor for the suitability of slice culture production. The brittleness of the bone increases sharply with the degree of sclerosis, leading to the subchondral cancellous bone not being cut smoothly by the impact of the blade but instead being crushed. Three punch cylinders were easily obtained from all other donors, from each of which 30–36 slice cultures could be safely produced. For reasons of logistical feasibility, we only cultivated the slice cultures from one punch at a time—from a technical perspective, the cultivation of 90–100 slice cultures per donor would have been possible.

### 2.2. Confocal Laser Scanning Microscopy Shows Highly Conserved Spatial Cell Order

To validate the use of the resazurin assay and to evaluate the spatial distribution of living and dead cells, additional live/dead determination via CLSM was performed on 13 slices of two donors (7 and 8) after three weeks of culture. The slice explant cultures were thin enough to penetrate deep into the tissue layers with confocal laser microscopy and produce a three-dimensional image of the cell distribution- and vitality (3D rendered video in supplemental files). The analysis revealed >90% viability in non-heated slices, roughly 50% viability in slices that were heated for 30 min at 60 °C, and <10% chondrocyte viability after 60 min of heating (Figure 1a). Chondrocytes remained localized in their cartilage-typical, spatial alignment (column-like deep zone; pearl-bead structure in the mid-zone; tightly packed cells in the superficial zone, Figure 1a). No cell culture effects due to nutrition gradients were observed (e.g., no elongated cells in the peripheral tissue).

### 2.3. Resazurin Assay Correlates with Optically Determined Viability

To ensure that the resazurin assay sufficiently reflects viability and is not obstructed by the dense osteochondral ECM, samples of varying viability (obtained by heating at 60 °C) were analyzed with the resazurin metabolic assay and by live/dead determination via PI/FDA staining and CLSM analysis. The results of both methods were correlated, as shown by the correlation coefficient of  $R^2 = 80\text{--}84.5\%$  (Figure 1b). We regarded this as sufficient to assess the general viability state of the tissue culture. Further viability analyses of tissue cultures were therefore performed using the resazurin assay since it allows for progredient viability analysis of the same tissue slice in a non-destructible manner.

### 2.4. Cell Viability Is Maintained in $F^-$ and Increased in $F^+$ Groups over 21 Days

After 7 days,  $F^-$  cultured slices of the cytokine-stimulated groups exhibited either a slight increase or maintenance of viability as determined by the resazurin assay. Stimulation with TNF- $\alpha$  resulted in  $101 \pm 23\%$  (10 ng/mL) and  $106 \pm 31\%$  (40 ng/mL) compared to control, while TGF- $\beta$ 3 stimulated slices exhibited an increase to  $113 \pm 26\%$ . Unstimulated slices showed a slight decrease to  $91 \pm 34\%$ . No significant differences in viability from day 0 to day 7 as well as between the four different cytokine stimulation groups were observed. Addition of FBS to the culture medium resulted in significantly increased viability values in all stimulated groups (TNF- $\alpha$ :  $214 \pm 58\%$  (low),  $227 \pm 84\%$  (high); TGF- $\beta$ 3:  $218 \pm 48\%$ ) and the control ( $231 \pm 50\%$ ) (Figure 1c(i)). During three-week culture without FBS viability values of  $114 \pm 43$ ,  $108 \pm 52\%$  and  $113 \pm 55\%$  were observed after 7, 14 and 21 days, respectively. Statistical analysis revealed no significant differences in viability between the timepoints (Figure 1c(ii)).

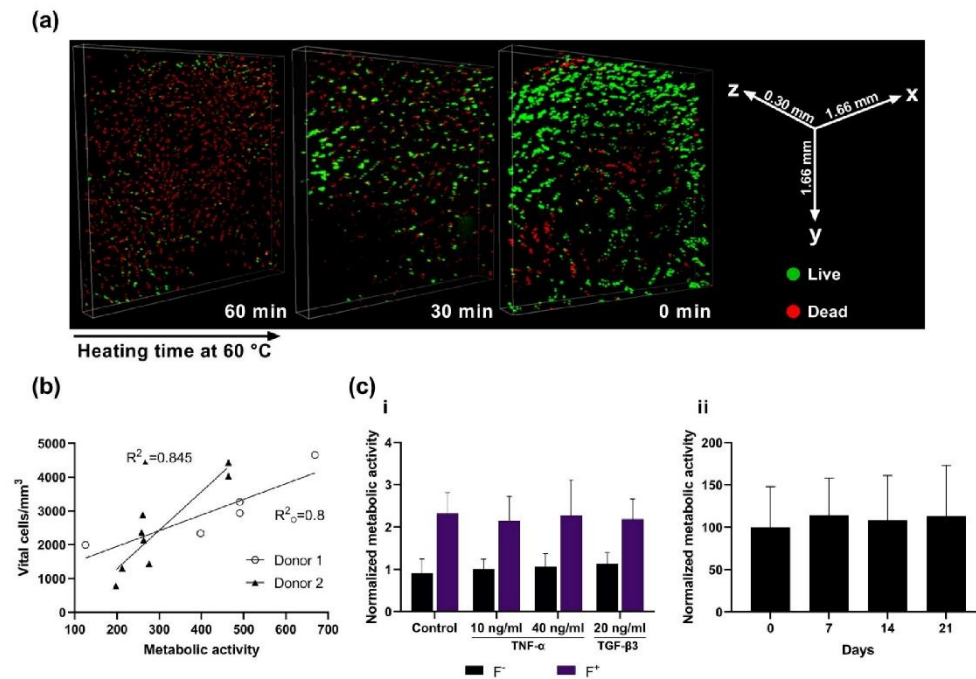


**Figure 1.** Viability analysis of osteochondral live slices. (a) Confocal laser scanning microscopy of slices at three weeks of culture following heating at 60 °C for 0, 30 or 60 min and live/dead staining with PI/FDA. Vital cells appear green, while dead cells appear red. (b) Correlation analysis of vital cell count as determined by CLSM and metabolic activity as determined by AlamarBlue resazurin assay. Two donors and a total of 13 slices with varying viability were analyzed and revealed correlation coefficients of 0.8 and 0.845. (c) Resazurin assay results with and without additional stimulation. i: Viability of slices on day 7 relative to day 0. Slices were stimulated with 10 or 40 ng/mL TNF- $\alpha$  or with 20 ng/mL TGF- $\beta$ 3, and either with or without FBS. ii: Viability of slices without FBS or other stimulating factors over 21 days, relative to day 0.

### 2.5. Expression of Cartilage-Typical Markers ACAN and COL2A1 Is Maintained for 14 Days in Unstimulated Slice Culture

Expression of cartilage-relevant genes *COL2A1* and *ACAN* remained stable relative to their day 0 value for 14 days and declined significantly by day 21 in unstimulated slice cultures (no stimulating factors, no FBS) (*COL2A1*:  $32 \pm 23\%$ ,  $p < 0.001$ ; *ACAN*:  $51 \pm 64\%$ ,  $p < 0.05$ ; Figure 2a). Cartilage remodeling marker *COL1A1* showed a short increase after 7 days but returned to levels comparable to day 0 by day 21. Expression of *COMP* decreased sooner and significantly to  $45 \pm 30\%$  after 7 days and further to  $27 \pm 21\%$  and  $14 \pm 12\%$  after 14 and 21 days (all  $p$ -values  $< 0.001$ ).



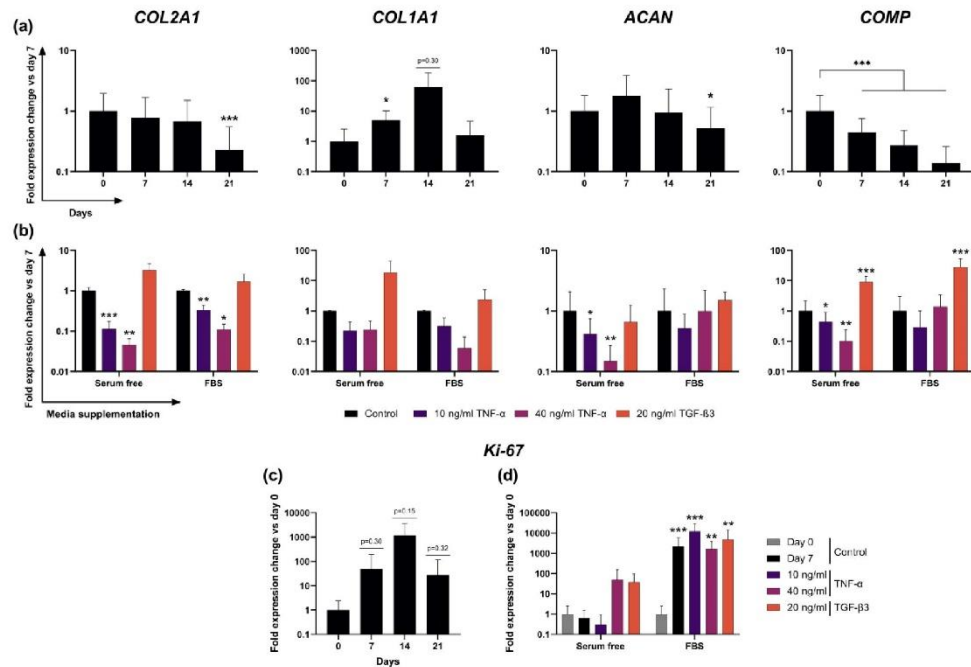


**Figure 2.** Gene expression analysis of live slice explants via RT-qPCR. (a) Gene expression of cartilage-typical markers *COL2A1*, *COL1A1*, *ACAN* and *COMP* in  $F^-$  cultured slices over three weeks ( $n = 12$ ) relative to the day 0 value. (b) Gene expression of the same cartilage-typical markers as in A, after 7 days of stimulation with TNF- $\alpha$  or TGF- $\beta$ 3 and with or without FBS ( $n = 6$ ) relative to the control on day 7. (c) Expression of proliferation marker *Ki-67* in  $F^-$  cultured slices over three weeks ( $n = 12$ ) relative to the day 0 value and (d) after 7 days of stimulation with TNF- $\alpha$  or TGF- $\beta$ 3 and with or without FBS ( $n = 6$ ), relative to the day 0 control to show the larger increase in the  $F^+$  group. Statistically significant differences denoted as \*  $p < 0.05$ , \*\*  $p < 0.01$ , \*\*\*  $p < 0.001$ .

### 2.6. Transcription of ECM Proteins Remains Highly Reactive to External Stimuli in $F^-$ Culture

To test cell reactivity to external stimuli, we intended to induce measurable changes in chondrocyte gene expression. Slices were stimulated with TNF- $\alpha$  and TGF- $\beta$ 3 to either suppress or induce the expression of cartilage-relevant gene markers. Gene expression analysis showed differing results in the  $F^-$  and  $F^+$  stimulation groups. In the  $F^-$  group, stimulation with TNF- $\alpha$  resulted in significant and dose-dependent reductions of *COL2A1*, *ACAN* and *COMP* expression. Compared to the day 7 control, *COL2A1* expression exhibited levels of  $11 \pm 7\%$  and  $5 \pm 5\%$  in low and high dose TNF- $\alpha$  stimulations, respectively. *ACAN* expression also was significantly lower at  $42 \pm 33\%$  and  $15 \pm 12\%$ , while *COMP* expression dropped to  $44 \pm 48\%$  and  $10 \pm 14\%$ . Stimulation with TGF- $\beta$ 3 resulted in a  $19 \pm 25$ -fold higher *COL1A1* expression and  $9 \pm 5$ -fold higher *COMP* expression (Figure 2b). Expression of *MMP13* did not change significantly after incubation with TNF- $\alpha$  but was significantly lower after stimulation with TGF- $\beta$ 3 ( $6 \pm 6\%$ , Supplemental Figure S1). In the  $F^+$  group, stimulation with TNF- $\alpha$  resulted in a reduced *COL2A1* expression of  $33 \pm 11\%$  in the lower concentration and  $11 \pm 4\%$  in the high concentration compared to the control. Mean expression levels of *ACAN* and *COMP* in  $F^+$  also decreased after TNF- $\alpha$  exposure, although no coherent dose-dependent or significant effects could be observed. TGF- $\beta$ 3 stimulation resulted in a  $29 \pm 25$ -fold higher expression of *COMP* and a  $2.4 \pm 2.7$ -fold

higher *COL1A1* expression (Figure 2b), as well as a decrease to  $42 \pm 40\%$  of *MMP13* expression (Supplemental Figure S1).

#### 2.7. Addition of FBS to Culture Media Causes Dominant Effects on Proliferation Marker *Ki-67* Expression

Expression of *Ki-67* as a marker for cell proliferation in serum-free culture varied strongly over three weeks and between donors, as shown by the very high standard deviations and surge to a >1000-fold increase on day 14 before it returned to a  $28 \pm 90$ -fold higher level compared to day 0 on day 21 (Figure 2c). Even though the average increase in *Ki-67* expression from day 0 to 7 was substantial, presumably because of the low absolute initial expression of *Ki-67* at day 0, very high variability between donors was observed and led to statistically insignificant results. Stimulation with low concentration TNF- $\alpha$  in F<sup>-</sup> groups led to  $31 \pm 65\%$  of day 0 expression, while unexpectedly higher concentrated TNF- $\alpha$  resulted in a  $50 \pm 112$ -fold increase. TGF- $\beta$ 3 stimulation revealed a  $37 \pm 60$ -fold increase in expression after 7 days compared to day 0 control ( $p = 0.06$ ). In the F<sup>+</sup> group, however, all 3 stimulation groups and the control exhibited statistically significant changes between day 0 and 7, reaching fold-changes compared to day 0 of  $12,045 \pm 17,483$  (TNF- $\alpha$  low),  $1686 \pm 2180$  (TNF- $\alpha$  high) and  $4889 \pm 9110$  (TGF- $\beta$ 3). No statistically significant differences were detected among the F<sup>+</sup> cultured stimulation groups or between either of the groups and the day 7 negative control (Figure 2d).

#### 2.8. Tissue Slices React to TNF- $\alpha$ Stimulation with Observable Remodeling of ECM and Cellular Swelling

To analyze whether native slice cultures retain their tissue-specific histological composition or whether they can respond to molecular stimuli with remodeling of the ECM, the slices of long-term culture and those of TNF- $\alpha$ -stimulated cultures were stained with Safranin-O, because TNF- $\alpha$  is an important inducer of matrix degeneration processes in cartilage. The proteoglycan contents of non-stimulated, F<sup>-</sup> cultured slices on days 0, 7, 14 and 21 (Figure 3a), as well as TNF- $\alpha$ -stimulated slices and negative controls on days 0 and 7 (Figure 3b), were quantified histomorphometrically. Even though a statistically significant decrease in proteoglycan content ( $p < 0.05$ ) compared to day 0 was observed on day 7 in the long-term setup (Figure 3a(ii)), the mean proteoglycan content overall was maintained, as on days 14 and 21 it did not significantly differ from day 0. Proteoglycan content in the TNF- $\alpha$ -treated group was significantly lower than in the untreated control on day 7 ( $68 \pm 24\%$ ;  $p < 0.05$ ; Figure 3b(ii)). Corresponding to the changes in gene expression, TNF- $\alpha$ -stimulated slices exhibited a strongly altered histomorphology. Intra-cartilage fibers appeared less dense, while chondrocyte diameter and apparent volume increased (Figure 3c).

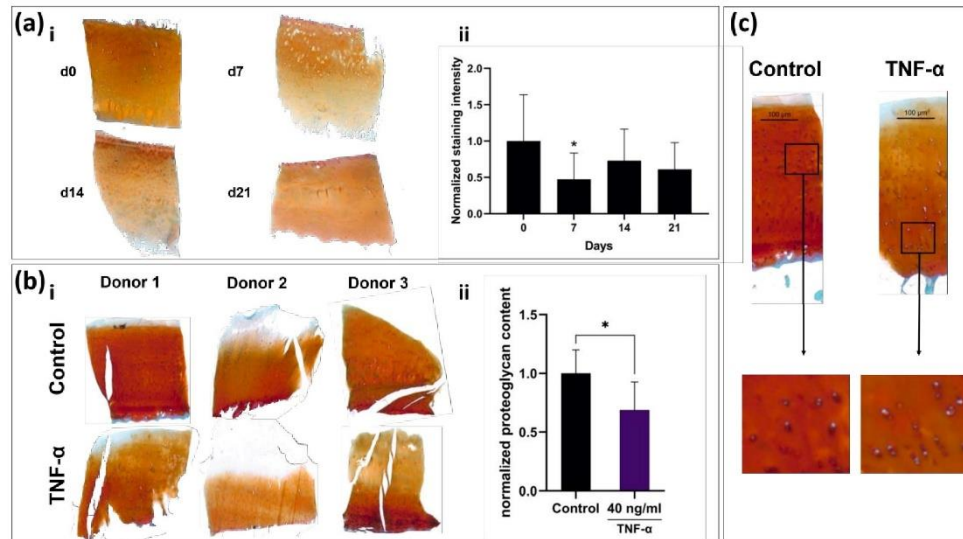


**Figure 3.** Histomorphometrical and histological analysis of live slices. (a) Safranin-O-stained slices of one donor (i) and histomorphometrical analysis (ii) over three weeks. (b) Comparison of staining intensity in TNF- $\alpha$ -stimulated and non-stimulated slices. Stimulated slices (three exemplary donors shown in (i)) show a mean reduction in red intensity of 32% (ii,  $n = 6$ ). (c) Representative picture of TNF- $\alpha$ -treated slice and control. TNF- $\alpha$ -treated slices show less intense Safranin-O staining, loosened matrix structure and swollen cells in the mid-zone of the cartilage. Statistically significant differences denoted as \*  $p < 0.05$ .

### 3. Discussion

The herein presented cost- and time-effective setup of surgical punch, 3D-printed microtome insert and rotary microtome is a reliable method to produce up to 100 explant cultures from a single human tissue sample. Critical to the usability of these thin osteochondral slice cultures is the long-term preservation of native tissue configuration and cell vitality despite thermal and mechanical stress development during preparation on the microtome and exposure of cells to atmospheric oxygen levels. CLSM analysis showed high cell vitality in both superficial and deeper tissue layers. Therefore, the slice thickness of 500  $\mu\text{m}$  appears to be sufficient for cell protection within the tissue while ensuring adequate nutrient perfusion through motion-assisted diffusion. Furthermore, CLSM shows preservation of cartilage-specific cell architecture within the tissue even after three weeks of culture. Cartilage is divided into three distinct cellular zones: The superficial zone (densely packed with spindle-shaped cells), the middle zone (pearl cord-like alignment) and the deep zone (columnar chondrocyte alignment). Maintenance of the cellular zones depended on nutrient supply and physiological cartilage infrastructure, suggesting minimal cellular stress from malnutrition and/or hypoxia. However, as Secretan et al., already mentioned in their explant model, the disadvantage of the standard optical live/dead analysis of explants is the exclusive possibility of endpoint analysis and the uncertainty about apoptotic cells that may have been cleared in the meantime [18]. Therefore, the high correlation between cell vitality as determined by CLSM and viability determined by resazurin assay enable the utilization of the inexpensive and easy-to-handle resazurin assay for multi-point analyses in this culture form. This is particularly advantageous for high sample quantities, which can be created by this cutting method. Long-term analysis of cell viability revealed very stable viability values over 21 days with only minor fluctuations from the baseline. Interestingly, this stability was achieved in a regular cell culture medium without serum



supplementation. Most explant cultures published to date use serum mixtures between 2–10% during cultivation [18–20]. While the addition of serum is a standard cell culture procedure, it is highly desirable, especially in light of pharmacological testing, if serum were not required as an undefined and potentially interacting, interfering or confounding factor for culture maintenance. This incentive is evident from the immense increase in absolute values and variation in viability values in the short-term culture with FBS addition, where toxicity effects would presumably not be visible due to the increased metabolic activity.

In terms of long-term stability, the slice explants provide similar characteristics to conventional punch explants. Bian et al. were able to demonstrate relative stability regarding the glycosaminoglycan content in serum-free cultivation of 3 mm thick explants over several weeks [21]. While we observed a significant decrease in the histomorphometrically determined Safranin-O staining intensity on day 7, it stabilized again on days 14 and 21. This could be due to an initial outflow of glycosaminoglycans at the cut edges of the cartilage, which account for a larger proportion of the total cartilage volume than in conventional punch explants. Regarding cartilage gene expression, the results are also similar to previously published analyses of explant gene expression. Different studies also described an initial increase of aggrecan followed by a decrease after 14 days and a decrease of the collagen type II expression of >50% after three weeks of cultivation following an initial stable phase [19,22]. *COMP* as a very sensitive marker for cartilage synthesis is the only gene in the analyzed panel to show a constant, almost linear decrease over time [23,24].

Stimulation of osteochondral slices with biological stimuli showed that chondrocytes in slice cultures responded adequately to external stimulation with catabolic molecules. TNF- $\alpha$  is known to be a proinflammatory cytokine in the joint and to induce cartilage matrix degradation both in vivo and in vitro [25,26], but other explant models either took significantly longer for a similarly strong reduction in matrix expression and degradation of proteoglycans or required additional catabolic stimuli such as oncostatin-M or interleukin-1 $\beta$  [11,27,28]. Here, the short perfusion distance between the medium and cells could be an advantage for pharmacological testing, since a shorter diffusion distance results in a higher and faster penetration by the corresponding factors than in thicker explant cultures. In addition to the decrease in anabolic biomarkers such as *COL2A1*, catabolic biomarkers such as *MMP13* also responded to external stimuli. Stimulation of the cultures with TGF- $\beta$ 3 resulted in close to complete suppression of *MMP13* expression more clearly observed in the serum free culture. Meanwhile, stimulation with TNF- $\alpha$  did not significantly increase *MMP13* expression. This suggests that due to the osteoarthritic damage and semi-static nature of the culture, only decreases catabolic marker genes are suitable as indicators of efficacy in pharmacological studies.

In studies aimed at analyzing pathological processes in cartilage or the long-term effects of an external stimulus rather than large-scale screening, it would also be beneficial to examine the distribution of the different collagen subtypes histologically, as these provide the most accurate information on cartilaginous remodeling processes.

Analogous to the viability measurement, it was also shown that when serum was added to the culture, the influences of the stimuli on the chondrocytes were significantly lower. In the serum-containing group, only the decrease of *COL2A1* expression following higher-dose TNF- $\alpha$  stimulation and the TGF- $\beta$ 3-dependent increase of *COMP* on day seven reached statistical significance compared to the control. Furthermore, analysis of the proliferation marker *Ki-67* showed that in the serum-containing group, all stimulated groups including the negative control showed a huge increase, whereas, in the F<sup>-</sup> group, only TGF- $\beta$ 3 stimulation resulted in higher expression of *Ki-67*. This is further evidence of nonspecific responses by serum addition masking the specific effects of other stimuli, rendering it neither necessary nor advisable for pharmacological testing.

The method is limited by donor variability, the increased effort in handling, the use of priorly diseased tissue and its static nature. In comparison to conventional explants, which are merely punched out of the tissue specimen, slice cultures require several processing steps until successfully produced. Since the chondrocyte phenotype is strongly related to

mechanical stimulation, several approaches are currently aiming to increase the dynamics and longevity of explant cultures by applying mechanical pressure [13,29–31]. This approach is more suitable for thicker, cylindrical explants and would, for the thin sections, be very difficult to implement. Therefore, the native tissue status is inherently limited to a window of 3 to 4 weeks using this preparation method. This also limits the model in particular to the analysis of toxic-catabolic processes. Anabolic stimuli such as TGF- $\beta$ 3, while showing an increase in matrix protein expression at the transcriptional level, are associated with the simultaneous presence of mechanical stimuli [32]. A prior induction of catabolism would most likely be required to study the effects of an anabolic stimulus as previously described by Schlichting et al. [8,33]. Furthermore, the exact reproduction of slice thickness can be impaired by different qualities of bone density. Stronger bone calcification can make it necessary to cut the slice 100–200  $\mu$ m thicker as the brittleness causes the bone to crush while being cut, resulting in unusable slices. Due to these slight variations in the cutting process, every donor must be related to itself when performing multipoint analysis. Therefore, the availability of a progredient analysis method like the resazurin assay is necessary to monitor individual slice viability. In accordance with this, a proteoglycan assay from the culture supernatants would also be conceivable for the analysis of the ECM. This could also provide continuous data from a slice culture instead of having to sacrifice the culture for histological endpoint analysis.

#### 4. Materials and Methods

##### 4.1. Sample Acquisition and Slice Production

Whole tibial plateaus (TPs;  $n = 23$ ; 13 female, 10 male, 61–89 years,  $\bar{x}$  72 years) were acquired from patients undergoing knee arthroplasty comprising TP removal. The specimens were transported in serum-free cell culture medium (Dulbecco's Modified Eagle Medium with 1 g/L glucose; 1% Penicillin/Streptomycin; 2% HEPES, Merck, Darmstadt Germany) to the laboratory with a maximum delay of 1 h. TPs were then immediately placed in Petri dishes filled with medium prewarmed to 37 °C under a laminar flow cabinet. After macroscopical inspection for an osteochondral site with a well-preserved cartilage-to-bone ratio (criteria: at least 1 mm high cartilage layer; no sclerosed subchondral bone below the cartilage), an orthopedic tissue punch (OATS<sup>®</sup>, Arthrex, Naples, FL, USA) press was used to create an osteochondral cylinder punch of 20  $\times$  10 mm (Figure 4a). The cylinder was inserted into a custom 3D-printed microtome insert (see Supplemental Figure S2 for exact insert dimensions) and then cut into eight disc-shaped cuts with a thickness of 500–800  $\mu$ m using a standard rotary microtome (Cut4060, MicroTec, Brixen, Italy). An 8 mm N35 microtome blade (FEATHER, Osaka, Japan) was used for cutting, which was exchanged after the preparation of 3 osteochondral cylinders. To produce a precise cut, the rotary handle was pulled downward at the point of maximum height in a powerful swing to exert maximum force on the cutting surface and thus prevent the bone from breaking. The cuts were then split into 3 cuboid-shaped slices using a scalpel, resulting in 24–36 individual slices per punch (Figure 4b). The remains of the cylinders were then discarded.

Two slices were immediately conserved either in 5% formaldehyde or in RNAlater<sup>®</sup> (Thermo Fisher, Waltham, MA, USA), posing as day 0 samples for histological analysis and real-time quantitative polymerase chain reaction (RT-qPCR). Slices in RNAlater were subsequently stored at  $-80$  °C. The remaining 22 slices were placed into hanging inserts (in a standing position with the cartilage facing up and leaning onto the upper rim of the inserts) of 24-well tissue culture plates with an 8  $\mu$ m pore diameter (Transwell<sup>®</sup>, Corning, New York, NY, USA) for optimal perfusion. All treatments of the tissue were performed with sterile surgical gloves and instruments. Tissue culture plates were cultured at 37 °C and 5% CO<sub>2</sub> on a horizontal shaker at 10 rpm (Figure 4c).



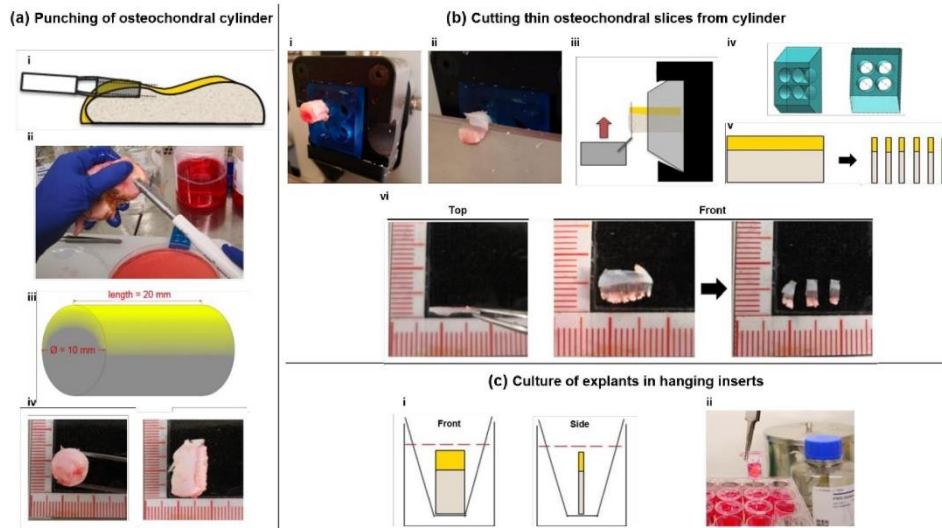


**Figure 4.** Fabrication and culture of osteochondral live slices. (a) Punching of Osteochondral cylinders. A  $2 \times 1 \times 1$  cm long osteochondral cylinder is punched out of the macroscopically unaffected area of a recently explanted human tibial plateau under sterile conditions using an orthopedic OATS<sup>®</sup> Tissue Punch (i,ii). The resulting cylinder is shown schematically in iii, cartilaginous areas are highlighted in yellow. Front and side views of the cylinder are shown in iv. (b) Cutting of osteochondral slices from cylinder. The cylinder is inserted into a 3D-printed microtome insert (iv) with no additional fixation (i), and 500–800  $\mu\text{m}$  thick cuts are cut out from the cylinder (ii). Fixation of the cylinder is shown schematically in iii. The resulting disc-shaped cuts (schematic: v) are cut into three parallelepipedal slices using a scalpel (vi). (c) Slices are immediately transferred to a hanging insert of a multi-well plate and covered in cell culture medium (i,ii). Plates are then placed on a horizontal shaker for culture at 37 °C and 5% CO<sub>2</sub>.

#### 4.2. Maintenance and Stimulation

Slices of donors 1–6 were divided into a serum-free (F<sup>-</sup>) culture group and a serum-containing group (F<sup>+</sup>). The F<sup>+</sup> group was cultured in the same medium as mentioned above with an additional 10% fetal bovine serum (FBS; Gibco, Thermo Fisher, Waltham, MA, USA). In both groups, four slices each were stimulated with either 0.3 nM (10 ng/mL) TNF- $\alpha$ , 1.2 nM (40 ng/mL) TNF- $\alpha$  or 0.8 nM (20 ng/mL) TGF- $\beta$ 3 (all Peprotech, Rocky Hill, NJ, USA) or no additives. Stimulating factors were pipetted with low-binding tips (Corning, New York, NY, USA) for minimal protein loss. Medium and stimulating factors were exchanged completely every three days. Analyses of slices for viability, gene expression and proteoglycan content were performed on days 0 and 7. Slices of the additional 17 donors were cultured without additional stimulating factors or FBS for 21 days in a large group viability and gene expression analysis (Figure 5). The medium was completely exchanged twice a week.

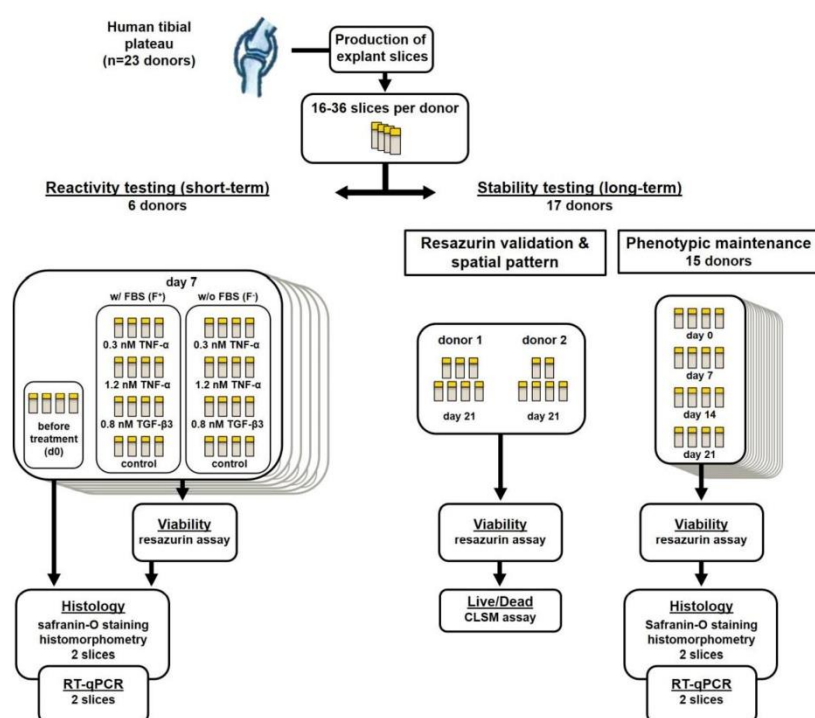


**Figure 5.** Flowchart depicting donor sample acquisition and distribution. Samples were obtained and then distributed for use in short-term (7 days, donors 1–6) stimulation experiments or long-term (21 days, donors 7–23) viability and gene expression experiments.

#### 4.3. Resazurin Viability Analysis

Resazurin stock solution (AlamarBlue<sup>®</sup>, Thermo Fisher, Waltham, MA, USA) was diluted 1:10 with serum-free cell culture medium. Slices were taken out of their hanging insert, washed once with phosphate-buffered saline (PBS) and transferred into a well of a 96-well plate filled with 300  $\mu$ L resazurin solution. Incubation of slices was performed for 2 h at 37  $^{\circ}$ C and 5% CO<sub>2</sub>. After the incubation period, duplicates of 100  $\mu$ L of the resazurin supernatant of each well were transferred to a fresh 96-well-plate. Fluorescence was determined on a plate reader (Synergy, BioTek, Winooski, VT, USA), applying excitation/emission wavelengths of 540/590 nm. Slices were placed back into their hanging inserts after viability determination.

#### 4.4. Confocal Laser Scanning Microscopy

To validate results from the resazurin assay and to evaluate the spatial distribution of living and dead cells, additional live/dead determination using confocal laser scanning microscopy (CLSM) was performed on 13 slices of two donors (7 and 8) after three weeks of culture. Prior to the resazurin assay, two slices were heated to 60  $^{\circ}$ C for 30 or 60 min to decrease intra-tissue cell viability to a minimum and obtain a portion of low-viability slices in comparison to the control. Subsequently, a resazurin assay was performed on all slices. Afterward, the slices were analyzed optically via live/dead staining with fluorescein diacetate (FDA) and propidium iodide (PI; both Sigma Aldrich, St. Louis, MO, USA). Slices were taken out of their hanging inserts, washed twice with PBS and incubated in 6

$\mu\text{g}/\text{mL}$  FDA in PBS solution (25 min), followed by a  $0.1 \text{ mg}/\text{mL}$  PI in PBS solution (3 min). After a washing step, slices were immediately transferred into the microscopes incubating chamber. Tissue imaging was carried out with a Nikon Scanning Confocal A1Rsi+ (Nikon, Tokyo, Japan) at  $37^\circ\text{C}$  in DMEM without phenol red (Thermo Fisher, Waltham, MA, USA). Excitation/Emission wavelengths were set at  $488/590 \text{ nm}$  for PI and  $485/514 \text{ nm}$  for FDA. The scanning area was set at  $2.82 \text{ mm}^2$ . Pictures were stitched with a 20% overlap and their corresponding volume was determined using Nikon Capture NX-D software (version 1.6.2, Nikon, Tokyo, Japan). Z-stacking was performed with  $10 \mu\text{m}$  spacing. Z-stacks were rendered into a 3D image with living cells depicted in green and dead cells in red. Living cells were counted using ImageJ software (version 1.8.0. [34]). For comparison of both methods, resazurin assay viability data was correlated to the number of living cells per  $\text{mm}^3$  sample using linear regression.

#### 4.5. RNA Extraction and Real-Time Quantitative PCR

For RNA isolation, cartilage was carefully dissected from bony tissue, the resulting slices were soaked in RNAlater (Thermo Fisher, Waltham, MA, USA) and then stored at  $-80^\circ\text{C}$  overnight. The following day, the frozen tissue was transferred into liquid nitrogen and pulverized using a Biopulverizer (BioSpec, Bartlesville, OK, USA). Pulverized samples were transferred into a 90% TriReagent<sup>®</sup>, 10% 4-Bromo-2-chlorophenol solution (both Sigma-Aldrich, St. Louis, MO, USA) followed by centrifugation for 45 min at  $13,000\times g$ . The aqueous phase was collected, and nucleic acids were precipitated by the addition of an equal volume of ice-cold 70% isopropanol. After 30 min of incubation, precipitated nucleic acids were collected and resolved in RNA isolation buffer RLT (Qiagen, Hilden, Germany). Further purification was performed using a PicoPure<sup>™</sup> Kit (Thermo Fisher, Waltham, MA, USA) according to the manufacturer's instructions. The integrity and purity of RNA were analyzed using an Agilent Bioanalyzer 2100 (Agilent, Palo Alto, CA, USA); RNA concentration was assessed with a NanoDrop 1000 spectrophotometer (Thermo Fisher, Waltham, MA, USA). RNA was reversely transcribed using a cDNA synthesis kit (iScript<sup>™</sup>, BioRad, Hercules, CA, USA). RT-qPCR was performed in triplicates in 96-well plates (Becton Dickinson, Franklin Lakes, NJ, USA) on a Mastercycler<sup>®</sup> ep gradient realplex (Eppendorf, Hamburg, Germany) using expression assays for TaqMan probes and primer sets (Thermo Fisher, Waltham, MA, USA; order no. in parentheses): collagen type II alpha 1 (*COL2A1*, Ss03373344\_g1), collagen type I alpha 1 (*COL1A1*, Ss003373341\_g1), aggrecan (*ACAN*, Ss03373387\_S1), *Ki-67* (*MKI67*, qHsaCID0011882) and cartilage oligomeric matrix protein (*COMP*, Hs01572837\_g1). Expression analysis for matrix metalloproteinase 13 (*MMP13*, Ss033733279\_m1) was only performed on short-term cultured slices. Succinate dehydrogenase complex, subunit A (*SDHA*, Hs00188166\_m1) was used as reference gene. Marker gene expression is given as fold change compared to *SHDA* or control sample expression applying the efficiency corrected  $\Delta\Delta\text{-Ct}$  method [35].

#### 4.6. Histological Analysis

Slices of each donor were fixated overnight in 5% formaldehyde solution and subsequently decalcified for 21 days in Osteosoft<sup>®</sup> solution (Merck, Darmstadt, Germany). Afterward, slices were frozen in liquid nitrogen and subsequently cut into  $4 \mu\text{m}$  thin sections using a CM19000 cryotome (Leica, Wetzlar, Germany). For Safranin-O staining, sections were stained for 30 min with 0.7% Safranin-O in 66% ethanol, counterstaining was performed with 0.2% Fast Green in 0.3% acetic acid (all Thermo Fisher, Waltham, MA, USA) for 1 min. To document ECM formation or loss, sections were mounted on glass slides; stainings were inspected using an AX 10 light microscope (Zeiss, Jena, Germany) and documented with a ProgRes<sup>®</sup> SpeedXT core 5 microscope-mounted camera system (JENOPTIK, Jena, Germany). The intensity of the Safranin-O staining is directly proportional to the glycosaminoglycan content of the tissue and was therefore analyzed employing a histomorphometrical approach as previously described [8]. Briefly, pictures were taken and all pixels in the areas of interest were valued in the RGB color mode with



a tool based on Xcode (Apple, Sunnyvale, CA, USA). When the red value (R) multiplied by 2 was higher than the sum of the green (G) and blue (B) values, the pixel was counted as red. The intensity of each red pixel was calculated as follows:  $\text{intensity} = 2 \times R\text{-value} - G\text{-value} - B\text{-value}$ . Values of the intensity ranged between 1 and 508, and reporting images depicting the intensity distribution were created (see Supplemental Figure S3). The mean intensity (sum of intensities/area of interest) was calculated from each image.

#### 4.7. Statistical Analysis

The significance level of log<sub>10</sub>-transformed data was determined with the independent two-sample *t*-test statistics of the Excel 2013 software package (Microsoft, Redmond, WA, USA). Normal distribution was checked applying the Anderson–Darling test, and equal variance of compared sample groups was tested applying the *f*-test. In all groups, signals were normally distributed. If the equal variance test was passed, student's *t*-test was used, if not Welch's *t*-test was applied. *p*-values < 0.05 were considered significant.

## 5. Conclusions

Native human osteochondral live slice explants represent a valid culture alternative to conventional punch explants. Its strengths lie in the greatly increased availability of tissue samples, as the thin nature of the slices allows for up to 50–100 pieces to be prepared from a single sample, the ease of fabrication and the simplicity of the culture in hanging inserts. This enables high-throughput screening of three-dimensional tissue processes and reactions in the native state that would otherwise require weeks of preparation in a tissue-based 3D culture or even in an animal model. Our results have shown that despite the stress of sharp dissection, the tissue fully retains its microarchitecture, and the cells retain their tissue-specific phenotype as well as their ability to properly respond to various stimuli. They also suggest that the short perfusion distance between cells and medium could also have a beneficial effect on the response strength of the cells to test stimuli, as the factors reliably reach cells embedded in the tissue. In addition, it was shown that the use of serum for cell expansion/survival is redundant in this culture form, which otherwise could mask adverse effects on tissue in the context of toxicity and degeneration analyses.

In summary, this production method is very well suited to produce native slice explants, which offer an interesting alternative to conventional explant cultures, especially in terms of pharmacological testing.

**Supplementary Materials:** The following are available online at <https://www.mdpi.com/article/10.3390/ijms22126394/s1>, Figure S1: *MMP13* gene expression analysis. Figure S2: technical details of custom-made microtome insert. Figure S3: examples of histomorphometrical analysis output.

**Author Contributions:** Conceptualization, J.S., T.D., L.K.S., U.S., A.A.K., C.R.; methodology, J.S., L.K.S. and T.D.; validation, J.S., L.K.S., A.A.K. and T.D.; formal analysis, T.D., S.H.-S. and C.R.; resources, C.R., U.S., D.K. and M.S.; data curation, J.S. and L.K.S.; writing—original draft preparation, J.S., L.K.S. and T.D.; writing—review and editing, J.S., L.K.S., T.D., C.R., A.A.K., S.H.-S., D.K. and M.S.; supervision, T.D., D.K. and M.S.; project administration, S.H.-S. and M.S. All authors have read and agreed to the published version of the manuscript.

**Funding:** This research was funded by the Einstein Centre for Regenerative Therapies and Elke-Kröner-Fresenius Stiftung (Grant Number FKZ 2018\_T12).

**Institutional Review Board Statement:** The study was conducted in accordance with the Declaration of Helsinki, and the protocol was approved by the Ethics Committee of Charité-Universitätsmedizin Berlin (EA4/072/18).

**Informed Consent Statement:** Informed consent was obtained from all subjects involved in the study.

**Data Availability Statement:** The data presented in this study are available on request from the corresponding author. The data are not publicly available due to the use of patient material and the protection of personal data.

**Acknowledgments:** We thank our colleagues from Charité Research Workshop for crafting special instruments for slice culture manufacturing. We thank Christoph Müller and Anja Fleischmann for their assistance with tissue culture maintenance. We would also like to show our gratitude to the core unit cell harvest for organizing the logistics of the live tissue transport. Furthermore, we thank Henrik Mei from DRFZ for his excellent advice in the field of immunology of arthritic diseases.

**Conflicts of Interest:** The authors declare no conflict of interest.

## References

- Puig-Junoy, J.; Ruiz Zamora, A. Socio-economic costs of osteoarthritis: A systematic review of cost-of-illness studies. *Semin. Arthritis Rheum.* **2015**, *44*, 531–541. [[CrossRef](#)] [[PubMed](#)]
- Vina, E.R.; Kwok, C.K. Epidemiology of osteoarthritis: Literature update. *Curr. Opin. Rheumatol.* **2018**, *30*, 160–167. [[CrossRef](#)]
- Knecht, S.; Erggelet, C.; Endres, M.; Sittlinger, M.; Kaps, C.; Stüssi, E. Mechanical testing of fixation techniques for scaffold-based tissue-engineered grafts. *J. Biomed. Mater. Res. Part B Appl. Biomater.* **2007**, *83B*, 50–57. [[CrossRef](#)] [[PubMed](#)]
- Deng, Z.H.; Li, Y.S.; Gao, X.; Lei, G.H.; Huard, J. Bone morphogenetic proteins for articular cartilage regeneration. *Osteoarthr. Cartil.* **2018**, *26*, 1153–1161. [[CrossRef](#)] [[PubMed](#)]
- Foldager, C.B. Advances in autologous chondrocyte implantation and related techniques for cartilage repair. *Dan. Med. J.* **2013**, *60*, B4600. [[PubMed](#)]
- Jimenez, P.A.; Glasson, S.S.; Trubetskoy, O.V.; Haimes, H.B. Spontaneous osteoarthritis in Dunkin Hartley guinea pigs: Histologic, radiologic, and biochemical changes. *Lab. Anim. Sci.* **1997**, *47*, 598–601.
- Kuyinu, E.L.; Narayanan, G.; Nair, L.S.; Laurencin, C.T. Animal models of osteoarthritis: Classification, update, and measurement of outcomes. *J. Orthop. Surg. Res.* **2016**, *11*, 1–27. [[CrossRef](#)]
- Schlichting, N.; Dehne, T.; Mans, K.; Endres, M.; Stuhlmüller, B.; Sittlinger, M.; Kaps, C.; Ringe, J. Suitability of Porcine Chondrocyte Micromass Culture To Model Osteoarthritis In Vitro. *Mol. Pharm.* **2014**, *11*, 2092–2105. [[CrossRef](#)]
- Jorgensen, C.; Simon, M. In Vitro Human Joint Models Combining Advanced 3D Cell Culture and Cutting-Edge 3D Bioprinting Technologies. *Cells* **2021**, *10*, 596. [[CrossRef](#)]
- Rothbauer, M.; Schobesberger, S.; Byrne, R.; Kiener, H.P.; Tögel, S.; Ertl, P. A human joint-on-a-chip as alternative to animal models in osteoarthritis. *Osteoarthr. Cartil.* **2020**, *28*, S89. [[CrossRef](#)]
- Pretzel, D.; Pohlers, D.; Weinert, S.; Kinne, R.W. In vitro model for the analysis of synovial fibroblast-mediated degradation of intact cartilage. *Arthritis Res. Ther.* **2009**, *11*, 1–20. [[CrossRef](#)]
- Haltmayer, E.; Ribitsch, I.; Gabner, S.; Rosser, J.; Gueltekin, S.; Peham, J.; Giese, U.; Dolezal, M.; Egerbacher, M.; Jenner, F. Co-culture of osteochondral explants and synovial membrane as in vitro model for osteoarthritis. *PLoS ONE* **2019**, *14*, e0214709. [[CrossRef](#)]
- Vainieri, M.L.; Wahl, D.; Alini, M.; Van Osch, G.; Grad, S. Mechanically stimulated osteochondral organ culture for evaluation of biomaterials in cartilage repair studies. *Acta Biomater.* **2018**, *81*, 256–266. [[CrossRef](#)]
- Maroudas, A. Transport of solutes through cartilage: Permeability to large molecules. *J. Anat.* **1976**, *122*, 335–347.
- Schwarz, N.; Uysal, B.; Welzer, M.; Bahr, J.C.; Layer, N.; Löffler, H.; Stanaitis, K.; Pa, H.; Weber, Y.G.; Hedrich, U.; et al. Long-term adult human brain slice cultures as a model system to study human CNS circuitry and disease. *eLife* **2019**, *8*, e48417. [[CrossRef](#)] [[PubMed](#)]
- Zwerina, J.; Redlich, K.; Polzer, K.; Joosten, L.; Krönke, G.; Distler, J.; Hess, A.; Pundt, N.; Pap, T.; Hoffmann, O.; et al. TNF-induced structural joint damage is mediated by IL-1. *Proc. Natl. Acad. Sci. USA* **2007**, *104*, 11742–11747. [[CrossRef](#)]
- Finsson, K.W.; Chi, Y.; Bou-Gharios, G.; Leask, A.; Philip, A. TGF- $\beta$  signaling in cartilage homeostasis and osteoarthritis. *Front. Biosci.* **2012**, *4*, 251–268. [[CrossRef](#)]
- Secretan, C.; Bagnall, K.M.; Jomha, N.M. Effects of introducing cultured human chondrocytes into a human articular cartilage explant model. *Cell Tissue Res.* **2010**, *339*, 421–427. [[CrossRef](#)] [[PubMed](#)]
- Gavénis, K.; Andereya, S.; Schmidt-Rohlfing, B.; Mueller-Rath, R.; Silny, J.; Schneider, U. Millicurrent stimulation of human articular chondrocytes cultivated in a collagen type-I gel and of human osteochondral explants. *BMC Complement. Altern. Med.* **2010**, *10*, 43. [[CrossRef](#)] [[PubMed](#)]
- Lyman, J.R.; Chappell, J.D.; Morales, T.I.; Kelley, S.S.; Lee, G.M. Response of Chondrocytes to Local Mechanical Injury in an Ex Vivo Model. *Cartilage* **2012**, *3*, 58–69. [[CrossRef](#)]
- Bian, L.; Lima, E.; Angione, S.; Ng, K.; Williams, D.; Xu, D.; Stoker, A.; Cook, J.; Ateshian, G.; Hung, C. Mechanical and biochemical characterization of cartilage explants in serum-free culture. *J. Biomech.* **2008**, *41*, 1153–1159. [[CrossRef](#)]
- Ragan, P.M.; Badger, A.M.; Cook, M.; Chin, V.I.; Gowen, M.; Grodzinsky, A.J.; Lark, M.W. Down-regulation of Chondrocyte Aggrecan and Type-II Collagen Gene Expression Correlates with Increases in Static Compression Magnitude and Duration. *J. Bone Jt. Surg.-Am. Vol.* **2000**, *82*, 32. [[CrossRef](#)]
- Zaucke, F.; Dinsler, R.; Maurer, P.; Paulsson, M. Cartilage oligomeric matrix protein (COMP) and collagen IX are sensitive markers for the differentiation state of articular primary chondrocytes. *Biochem. J.* **2001**, *358*, 17. [[CrossRef](#)] [[PubMed](#)]
- Sharma, A.; Jagga, S.; Lee, S.-S.; Nam, J.-S. Interplay between Cartilage and Subchondral Bone Contributing to Pathogenesis of Osteoarthritis. *Int. J. Mol. Sci.* **2013**, *14*, 19805–19830. [[CrossRef](#)] [[PubMed](#)]

25. Manicourt, D.-H.; Poilvache, P.; Van Egeren, A.; Devogelaer, J.-P.; Lenz, M.-E.; Thonar, E.J.-M.A. Synovial fluid levels of tumor necrosis factor  $\alpha$  and oncostatin M correlate with levels of markers of the degradation of crosslinked collagen and cartilage aggrecan in rheumatoid arthritis but not in osteoarthritis. *Arthritis Rheum.* **2000**, *43*, 281. [[CrossRef](#)]
26. Hui, W.; Rowan, A.D.; Richards, C.D.; Cawston, T.E. Oncostatin M in combination with tumor necrosis factor  $\alpha$  induces cartilage damage and matrix metalloproteinase expression in vitro and in vivo. *Arthritis Rheum.* **2003**, *48*, 3404–3418. [[CrossRef](#)] [[PubMed](#)]
27. Thudium, C.S.; Engstrom, A.; Groen, S.S.; Karsdal, M.A.; Bay-Jensen, A.-C. An Ex Vivo Tissue Culture Model of Cartilage Remodeling in Bovine Knee Explants. *J. Vis. Exp.* **2019**, e59467. [[CrossRef](#)]
28. Clutterbuck, A.L.; Mobasheri, A.; Shakibaei, M.; Allaway, D.; Harris, P. Interleukin-1 $\beta$ -Induced Extracellular Matrix Degradation and Glycosaminoglycan Release Is Inhibited by Curcumin in an Explant Model of Cartilage Inflammation. *Ann. N. Y. Acad. Sci.* **2009**, *1171*, 428–435. [[CrossRef](#)]
29. Theodoropoulos, J.S.; De Croos, A.J.N.; Petrera, M.; Park, S.; Kandel, R.A. Mechanical stimulation enhances integration in an in vitro model of cartilage repair. *Knee Surgery Sport. Traumatol. Arthrosc.* **2016**, *24*, 2055–2064. [[CrossRef](#)]
30. Spitters, T.W.; Leijten, J.C.; Deus, F.D.; Costa, I.B.; Van Apeldoorn, A.A.; Van Blitterswijk, C.A.; Karperien, M. A Dual Flow Bioreactor with Controlled Mechanical Stimulation for Cartilage Tissue Engineering. *Tissue Eng. Part C Methods* **2013**, *19*, 774–783. [[CrossRef](#)]
31. Qu, P.; Qi, J.; Han, Y.; Zhou, L.; Xie, D.; Song, H.; Geng, C.; Zhang, K.; Wang, G. Effects of Rolling-Sliding Mechanical Stimulation on Cartilage Preserved In Vitro. *Cell Mol. Bioeng.* **2019**, *12*, 301–310. [[CrossRef](#)] [[PubMed](#)]
32. Elder, B.D.; Athanasiou, K.A. Synergistic and Additive Effects of Hydrostatic Pressure and Growth Factors on Tissue Formation. *PLoS ONE* **2008**, *3*, e2341. [[CrossRef](#)] [[PubMed](#)]
33. Lüderitz, L.; Dehne, T.; Sittinger, M.; Ringe, J. Dose-Dependent Effect of Mesenchymal Stromal Cell Recruiting Chemokine CCL25 on Porcine Tissue-Engineered Healthy and Osteoarthritic Cartilage. *Int. J. Mol. Sci.* **2018**, *20*, 52. [[CrossRef](#)] [[PubMed](#)]
34. Schneider, C.A.; Rasband, W.S.; Eliceiri, K.W. NIH Image to ImageJ: 25 years of image analysis. *Nat. Methods* **2012**, *9*, 671–675. [[CrossRef](#)] [[PubMed](#)]
35. Pfaffl, M.W. A new mathematical model for relative quantification in real-time RT-PCR. *Nucleic Acids Res.* **2001**, *29*, e45. [[CrossRef](#)] [[PubMed](#)]

**8.2. Spinnen J, Fröhlich K, Sinner N, Stolk M, Ringe J, Shopperly L, Sittinger M, Dehne T, Seifert M.**

Therapies with CCL25 require controlled release via microparticles to avoid strong inflammatory reactions.

*J Nanobiotechnology*. 2021 Dec 25;19(1):83.



Journal Data Filtered By: **Selected JCR Year: 2019** Selected Editions: SCIE,SSCI  
 Selected Categories: **“BIOTECHNOLOGY and APPLIED MICROBIOLOGY”**  
 Selected Category Scheme: WoS  
**Gesamtanzahl: 156 Journale**

Rank	Full Journal Title	Total Cites	Journal Impact Factor	Eigenfactor Score
1	NATURE REVIEWS DRUG DISCOVERY	33,154	64.797	0.049170
2	NATURE BIOTECHNOLOGY	63,979	36.558	0.156640
3	TRENDS IN BIOTECHNOLOGY	17,028	14.343	0.018360
4	GENOME RESEARCH	41,755	11.093	0.076940
5	GENOME BIOLOGY	44,221	10.806	0.133970
6	BIOTECHNOLOGY ADVANCES	19,320	10.744	0.019250
7	BIOSENSORS & BIOELECTRONICS	62,284	10.257	0.085930
8	MOLECULAR THERAPY	17,977	8.986	0.030980
9	CURRENT OPINION IN BIOTECHNOLOGY	15,740	8.288	0.023620
10	PLANT BIOTECHNOLOGY JOURNAL	9,587	8.154	0.018450
11	CRITICAL REVIEWS IN BIOTECHNOLOGY	4,355	8.108	0.006090
12	BIORESOURCE TECHNOLOGY	131,781	7.539	0.108190
13	METABOLIC ENGINEERING	8,068	7.263	0.016040
14	npj Biofilms and Microbiomes	790	7.067	0.002840
15	JOURNAL OF NANOBIO TECHNOLOGY	4,376	6.518	0.005900
16	GENOMICS	9,595	6.205	0.005790
17	Annual Review of Animal Biosciences	955	6.091	0.002670
18	STEM CELLS	20,554	6.022	0.024110
19	MUTATION RESEARCH-REVIEWS IN MUTATION RESEARCH	3,621	5.803	0.003120
20	BIOINFORMATICS	122,242	5.610	0.218180

Selected JCR Year: 2019; Selected Categories: “BIOTECHNOOLOGY and APPLIED MICROBIOLOGY”



RESEARCH

Open Access

# Therapies with CCL25 require controlled release via microparticles to avoid strong inflammatory reactions



J. Spinnen<sup>1\*</sup> , K. Fröhlich<sup>1,†</sup>, N. Sinner<sup>1</sup>, M. Stolk<sup>1</sup>, J. Ringe<sup>1</sup>, L. Shopperly<sup>1</sup>, M. Sittinger<sup>1</sup>, T. Dehne<sup>1</sup> and M. Seifert<sup>2,3</sup>

## Abstract

**Background:** Chemokine therapy with C–C motif chemokine ligand 25 (CCL25) is currently under investigation as a promising approach to treat articular cartilage degeneration. We developed a delayed release mechanism based on Poly (lactic-co-glycolic acid) (PLGA) microparticle encapsulation for intraarticular injections to ensure prolonged release of therapeutic dosages. However, CCL25 plays an important role in immune cell regulation and inflammatory processes like T-cell homing and chronic tissue inflammation. Therefore, the potential of CCL25 to activate immune cells must be assessed more thoroughly before further translation into clinical practice. The aim of this study was to evaluate the reaction of different immune cell subsets upon stimulation with different dosages of CCL25 in comparison to CCL25 released from PLGA particles.

**Results:** Immune cell subsets were treated for up to 5 days with CCL25 and subsequently analyzed regarding their cytokine secretion, surface marker expression, polarization, and migratory behavior. The CCL25 receptor C–C chemokine receptor type 9 (CCR9) was expressed to a different extent on all immune cell subsets. Direct stimulation of peripheral blood mononuclear cells (PBMCs) with high dosages of CCL25 resulted in strong increases in the secretion of monocyte chemoattractant protein-1 (MCP-1), interleukin-8 (IL-8), interleukin-1 $\beta$  (IL-1 $\beta$ ), tumor-necrosis-factor- $\alpha$  (TNF- $\alpha$ ) and interferon- $\gamma$  (IFN- $\gamma$ ), upregulation of human leukocyte antigen-DR (HLA-DR) on monocytes and CD4<sup>+</sup> T-cells, as well as immune cell migration along a CCL25 gradient. Immune cell stimulation with the supernatants from CCL25 loaded PLGA microparticles caused moderate increases in MCP-1, IL-8, and IL-1 $\beta$  levels, but no changes in surface marker expression or migration. Both CCL25-loaded and unloaded PLGA microparticles induced an increase in IL-8 and MCP-1 release in PBMCs and macrophages, and a slight shift of the surface marker profile towards the direction of M2-macrophage polarization.

**Conclusions:** While supernatants of CCL25 loaded PLGA microparticles did not provoke strong inflammatory reactions, direct stimulation with CCL25 shows the critical potential to induce global inflammatory activation of human leukocytes at certain concentrations. These findings underline the importance of a safe and reliable release system

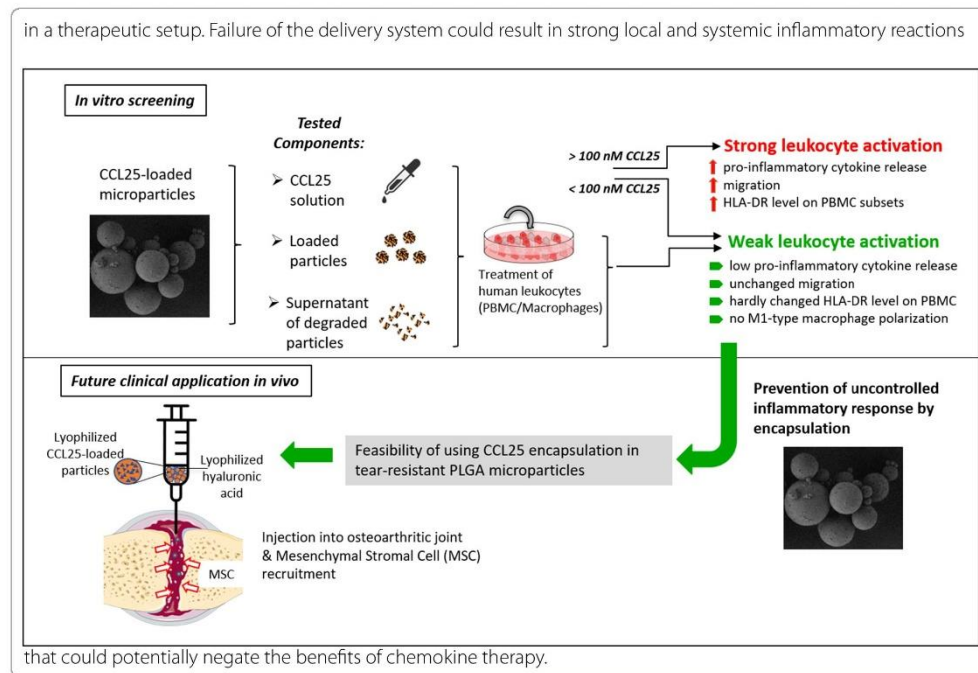
\*Correspondence: jacob.spinnen@charite.de

<sup>1</sup> Tissue Engineering Laboratory, BIH Center for Regenerative Therapies, Department for Rheumatology and Clinical Immunology & Berlin Institute of Health at Charité—Universitätsmedizin Berlin, BCRT, Charitéplatz 1, 10117 Berlin, Germany

Full list of author information is available at the end of the article  
K. Fröhlich—deceased



© The Author(s) 2021. This article is licensed under a Creative Commons Attribution 4.0 International License, which permits use, sharing, adaptation, distribution and reproduction in any medium or format, as long as you give appropriate credit to the original author(s) and the source, provide a link to the Creative Commons licence, and indicate if changes were made. The images or other third party material in this article are included in the article's Creative Commons licence, unless indicated otherwise in a credit line to the material. If material is not included in the article's Creative Commons licence and your intended use is not permitted by statutory regulation or exceeds the permitted use, you will need to obtain permission directly from the copyright holder. To view a copy of this licence, visit <http://creativecommons.org/licenses/by/4.0/>. The Creative Commons Public Domain Dedication waiver (<http://creativecommons.org/publicdomain/zero/1.0/>) applies to the data made available in this article, unless otherwise stated in a credit line to the data.



## Introduction

Research in the field of regenerative medicine is increasingly revealing the enormous potential of the human body's inherent self-healing powers. Chronic tissue damage, as seen in conditions such as osteoarthritis (OA) are not ignored by the body but mechanisms to repair damage are constantly being attempted. Unfortunately, these repair processes are often not perfectly synchronized with the underlying pathological conditions or are negatively affected by the inflammatory processes present. In OA, for example, chondrocytes in the deeper cartilage tissue respond to degeneration of the outer tissue layers with increased expression of cartilage-specific matrix proteins such as collagen II and aggrecan. However, these mechanisms are not sufficient to repair the tissue damage [1, 2].

Therefore, the tissue requires a general change in microenvironment to modulate chronic inflammation and provide pro-regenerative stimuli. Besides the injection of growth factors or instrument-based stimulation, multiple studies have shown that the intraarticular application of mesenchymal stromal cells (MSCs) can sway the microenvironment towards a pro-regenerative direction owing to their immune-regulatory and

proliferation-promoting secretome [3–5]. However, the efficacy of these treatments remains very limited and the results may not justify the cost of an ex vivo cell therapy. To enhance the cost-effectiveness and efficacy of MSC targeting therapies, the application of chemokines embedded in certain release devices are of growing interest. Chemokine enriched biopolymers enable both mechanical closure of the lesion as well as delayed release of their regenerative factors [6, 7]; an approach called in-situ tissue engineering [8]. Certain chemokines have been shown to both attract certain cells like MSCs to the site of application, as well as increase the tissue producing capacities of the resident cells. So far, multiple chemokine candidates are under investigation for their suitability, with C–X–C motif chemokine ligand 12 (CXCL12) and IL-8 being among the most popular [9, 10].

In previous work, we identified C–C motif chemokine ligand 25 (CCL25) as a potent candidate for therapeutic chemoattraction of MSCs through broad-based migration assays [11, 12]. Because the knee joint is thought to contain many loculated MSCs, and the knee as a pre-formed body cavity is well suited for injection therapy, the efficacy of CCL25 for osteoarthritis was investigated. In an in vivo OA model (Dunkin-Hartley guinea

Fig), one injection per week of CCL25 dissolved in hyaluronic acid (HA) into affected joints for four consecutive weeks resulted in up to 28% less cartilage damage (graded by the histopathological OARSI Score) in the CCL25-treated joint compared with the untreated joint and HA and sodium chloride (NaCl) control groups [13, 14]. After proof of concept, a release system based on poly (lactic-co-glycolic acid) (PLGA) microparticles was developed that allows a single injection followed by controlled, sustained release of CCL25 into the joint over several weeks. Importantly, microparticles with diameters of ~50–100  $\mu\text{m}$  allow for intraarticular injection using a syringe instead of arthroscopic implantation. On the one hand, this saves the patient a hypothetical invasive procedure, on the other hand, the PLGA degradation kinetics enable steady level of chemokines to recruit sufficient amounts of cells while avoiding potentially harmful peak concentrations that could result from multiple injections [15, 16]. PLGA was chosen because it is already successfully used as a microencapsulation material (also in the form of microparticles [17, 18]), encapsulation of proteins is well standardized and due to its biocompatibility and biodegradability is considered safe for use by international regulatory authorities—demonstrated by numerous approvals of PLGA-based drugs [19–21]. PLGA is degrading delayed due to the hydrolysis of its ester linkages in presence of water. The resulting carboxylic acid chain ends of the cleavage further may further accelerate the process and lead to autocatalysis [22]. As a result of internal diffusion, a pH gradient from the center to the surface of the particle is forming and degradation products and will diffuse and erode away from the entire volume of the particle (bulk erosion). As PLGA degradation is driven by hydrolysis and degradation products (glycolic and lactic acid) are non-toxic chemicals that can be metabolized by the body, it can be used as delivery system in physiological environments [23]. Furthermore, PLGA is commonly used in the knee cavity for autologous chondrocyte transplantation, suture material and not known to interact with the joint tissue in any harmful way. Since the expiration of first patents on PLGA microparticle systems, the development of generic products experiencing a revived interest in pharmaceutical research [24].

Advances in chemokine therapy are hampered by insufficient clinical biosafety data. Analysis of existing experimental data on CCL25 revealed strong involvement in adaptive immune system development, dysfunctional immunological processes in endometriosis, inflammatory bowel disease, and rheumatoid arthritis [25]. Hence, application of this chemokine could cause a significant inflammatory response and potentially cause more harm than good. Also, while the biocompatibility

of PLGA is well established [26], there is currently no approved treatment that uses free-floating PLGA particles in human joints. It is also conceivable that the bio-material itself could cause undesired inflammatory side effects related to its acidic properties.

To address these issues, we conducted an immunological study assessing the interaction of PLGA/CCL25 with different human immune cell subsets. The objective of this study was to assess the inflammatory potential of PLGA/CCL25 to induce typical changes that leukocytes show during an inflammatory response. In our analysis, we focused on the potential alteration of pro-inflammatory cytokine secretion, the regulation of cellular activation and polarization markers, and leukocyte migration induced by CCL25 or PLGA.

## Results

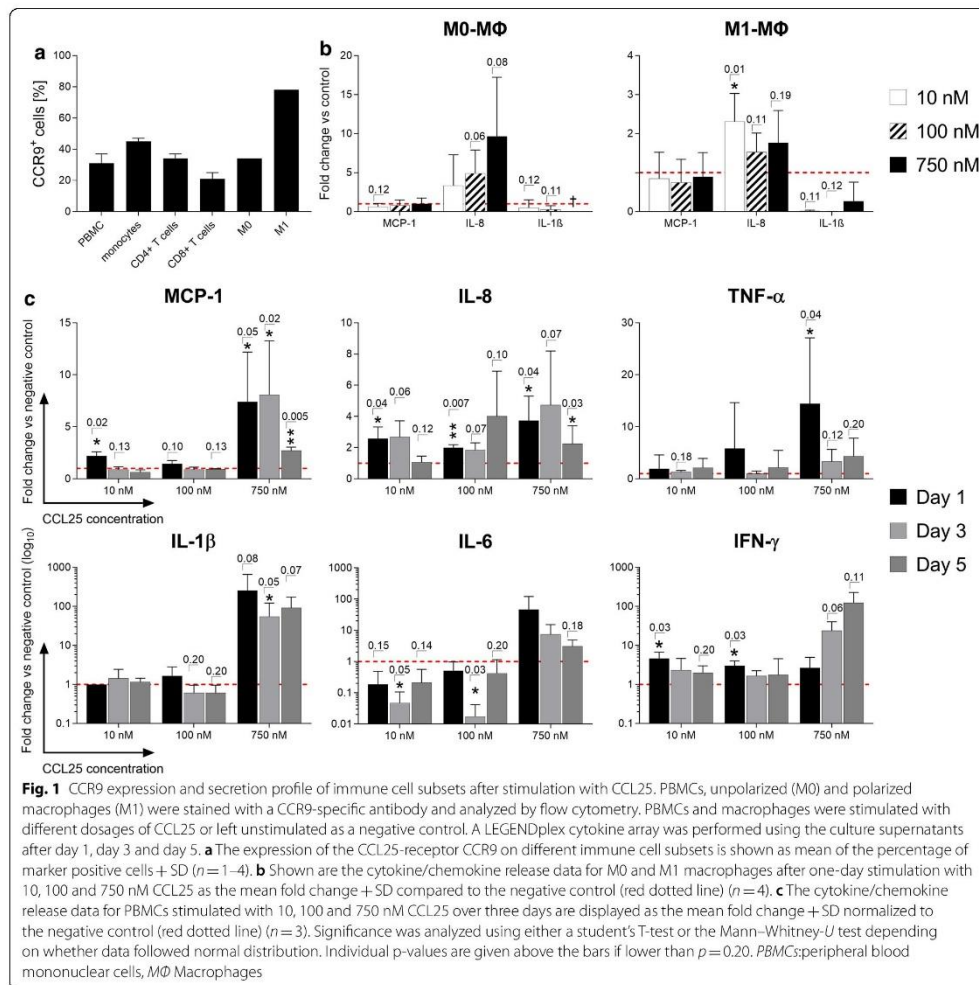
### Immune cell subsets exhibit differing expression levels of CCR9

The determination of CCR9 expression is an important prerequisite for enabling CCL25-induced cell migration and intracellular signaling as it is the receptor for the ligand CCL25. Thus, extracellular CCR9 expression was investigated using flow cytometry on different immune cell subsets by staining with a fluorescently labeled antibody (Fig. 1a). Peripheral blood mononuclear cells (PBMCs), monocytes and  $\text{CD4}^+$  T-cells exhibited a mean CCR9 expression of  $31 \pm 6\%$ ,  $45 \pm 2\%$  and  $34 \pm 3\%$ , respectively.  $\text{CD8}^+$  T-cells showed the lowest mean surface expression, with  $21 \pm 4\%$ . The strongest CCR9-expression was found on M1-type macrophages with around 78%. Unpolarized M0-type macrophages showed a seemingly lower CCR9 expression of about 34% (Fig. 1a).

### Stimulation with high dosages of CCL25 induces high secretion levels of pro-inflammatory cytokines in PBMCs

To assess the unmediated reaction of different leukocyte subsets to CCL25, PBMCs and differently polarized macrophages were stimulated over five days with dosages of 10, 100 and 750 nM CCL25 (Fig. 1b, c). Supernatants were collected on day one, three, and five, and the cytokines present were analyzed with the LEGENDplex immunoassay. When testing different macrophage subsets, unpolarized M0 macrophages reacted strongly and dose-dependently to CCL25 stimulation with an up to tenfold increase in IL-8 secretion in the 750 nM group ( $p=0.08$ ), while M1-polarized macrophages showed a small increase independent of the dose used (Fig. 1b). Direct stimulation of PBMCs with CCL25 leads to a very strong and dose-dependent secretion of the pro-inflammatory chemokines and cytokines IL-8, MCP-1, TNF- $\alpha$ , IL-1 $\beta$ , interleukin-6 (IL-6) and IFN- $\gamma$  (Fig. 1c). While





for most cytokines/chemokines there were only moderate increases in the 10 nM and 100 nM CCL25 stimulation groups, PBMCs reacted with a strong increase in all tested mediators for the 750 nM stimulation group. While IL-8 also showed a statistically significant increase in secretion after being triggered with lower CCL25 concentrations, the other cytokines increased exclusively after stimulation with the highest CCL25 concentration. On day 5 of stimulation, secretion of cytokines and chemokines seemed to decline. Apart from IFN- $\gamma$ , the

cytokines measured on the fifth day showed lower values than on day 1 after stimulation.

**CCL25 causes a dose-dependent upregulation of the activation marker human leukocyte antigen-DR (HLA-DR) on immune cells**

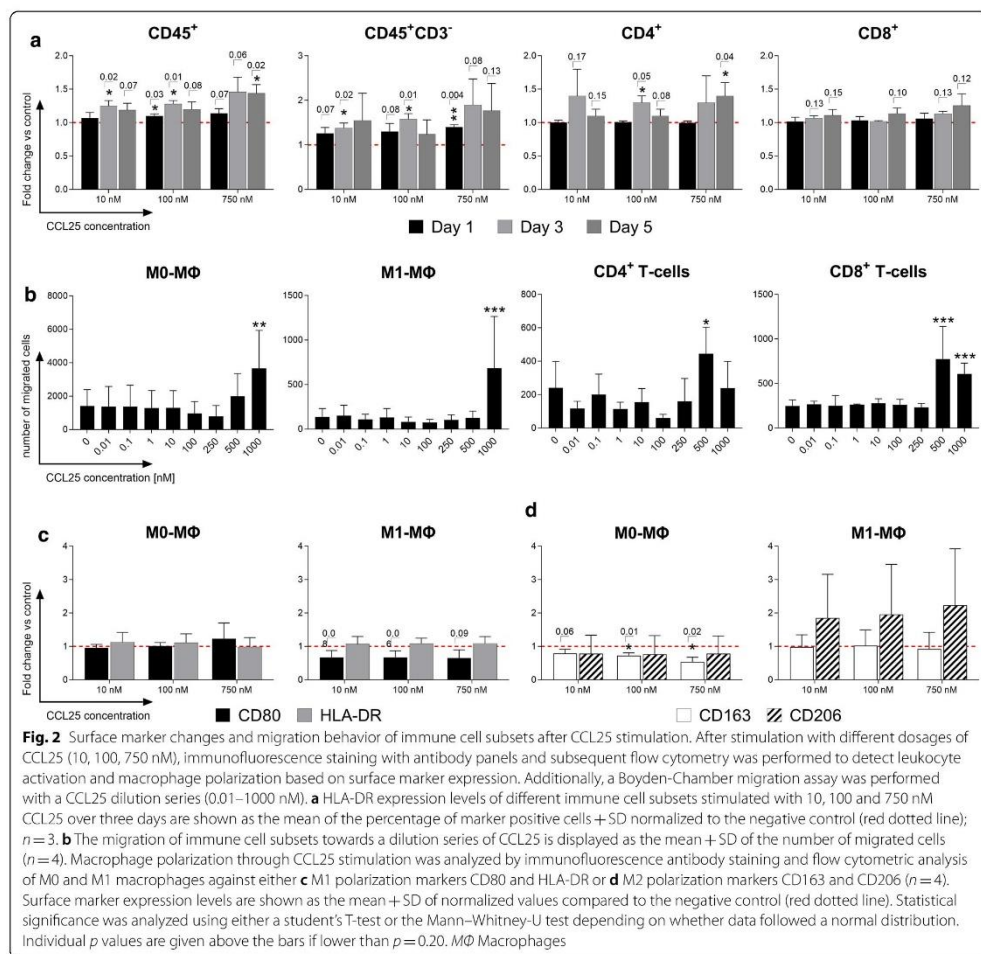
Flow cytometry was used to investigate the effects of CCL25 on the activation and polarization of immune cells. Macrophages were first analyzed for the differential expression of characteristic polarization markers for the

M1 (CD80 and HLA-DR) or M2 direction (CD163 and CD206). Analysis of the activation marker HLA-DR was then performed on PBMCs. While no statistically significant changes in the expression of either M1 or M2 type characteristic polarization markers on macrophages were detected (data not shown), PBMCs showed a very clear HLA-DR upregulation when exposed to all three concentrations of CCL25 (Fig. 2a). CD45<sup>+</sup>CD3<sup>-</sup> negative cells (all mononuclear leukocytes besides T-cells) exhibited the strongest reaction, with a dose-dependent increase up to a 1.8-fold change compared to the negative control. Also, CD4<sup>+</sup> cells reacted in a dose-dependent fashion

with a significant HLA-DR upregulation to CCL25 stimulation. Cytotoxic CD8<sup>+</sup> T-cells showed weaker changes in the expression level of HLA-DR than CD4<sup>+</sup> cells and did not reach a statistically significant difference compared to the unstimulated negative control.

**Macrophages and T-cells show dose dependent migration towards CCL25**

Assessing CCL25's capabilities to recruit leukocytes from foreign tissues, different macrophage and T-cell subsets were examined in a Boyden-Chamber migration assay employing a CCL25 concentration range from 0.01 to



1000 nM (Fig. 2b). After CCL25 stimulation, both unpolarized M0- and M1-polarized macrophages reacted with a dose-dependent increase in migration. While migration towards CCL25 in unpolarized M0-macrophages already started at concentrations of 500 nM, M1 macrophages only showed significant migration towards the highest tested concentration of 1000 nM. T-cells also showed a strong increase in migration towards CCL25 concentrations of 500–1000 nM. The migration of CD8<sup>+</sup> T-cells appeared to be stronger than that of CD4<sup>+</sup> T-cells.

#### Macrophages do not polarize or change their polarization upon CCL25 stimulation

M0- and M1-polarized macrophages were stimulated with 10, 100 and 750 nM CCL25, and then analyzed for their expression of surface markers specific for M1 or M2 macrophage polarization via flow cytometry (Fig. 2c). M0 macrophages showed no change in CD80 and HLA-DR (M1 markers), no significant change in CD206 and a significant decrease in CD163 (M2 marker) expression. In summary, no clear trend in the polarization mediated by CCL25 could be identified.

#### Immune cell stimulation by CCL25-loaded and unloaded particles leads to increased IL-8 and MCP-1 secretion

Similar to the previous CCL25 stimulation assay, human leukocytes were incubated with undegraded CCL25-loaded (CL) and unloaded (NL) PLGA particles in two different concentrations (0.5% w/v and 0.05% w/v) to distinguish between the effect of CCL25 and intact particle, as well as to check the integrity of the loaded particles. Cytokine levels of PBMC cultures treated with both particle types increased for IL-8 and MCP-1 compared to the untreated negative control, peaking around the third day of stimulation (Fig. 3a). The strongest reaction for IL-8, albeit not statistically significant, was shown by the 0.5% w/v NL particles on the third day with a mean increase of  $6.48 \pm 6.38$ -fold change in secretion ( $p = 0.14$ ). In relation to the negative control, the mean increase in IL-8 for 0.5% w/v CL particles was, at 4.2, much lower than for the NL particles. Stimulation with 0.05% w/v of either CL or NL particles induced very similar fold changes for IL-8 secretion with the CL particles causing a slightly higher IL-8 secretion on the third day than the NL particles (CL =  $5.2 \pm 3.98$ ; NL =  $4.26 \pm 4.84$ ). Interestingly, all stimulation groups reached a very similar level of IL-8 secretion on the fifth day, with around four times that of the negative control. For MCP-1, all groups except the 0.05% w/v concentration of the NL particles showed high increases in secretion on the third day. The highest mean increase was seen in 0.05% w/v CL particles ( $4.5 \pm 3.3$ -fold change;  $p = 0.22$ ) followed by the 0.5% w/v NL particles ( $4.3 \pm 3.3$ -fold change;  $p = 0.35$ ). As seen

with IL-8, MCP-1 secretion on day 5 equalized to similar levels at about 1.5-fold of the negative control, but only the 0.5% w/v concentration of the CL particle reached statistical significance ( $1.7 \pm 0.5$ -fold change;  $p = 0.02$ ). Macrophages also responded to CCL25 stimulation by increasing secretion of IL-8 but did not increase secretion of MCP-1 or other cytokines (Fig. 3b). M1-polarized macrophages reacted similarly to 0.5% and 0.05% w/v of either CL or NL particles, with a slight increase in IL-8 secretion (CL: 0.5% w/v:  $1.49 \pm 0.68$ ; 0.05% w/v:  $1.48 \pm 0.76$ ; NL: 0.5% w/v:  $1.83 \pm 0.72$ ; 0.05% w/v:  $1.55 \pm 0.35$ ). Unpolarized M0 macrophages reacted with a much stronger overall secretion of IL-8 and an observable difference between CCL25-loaded and unloaded particles (CL: 0.5% w/v:  $4.42 \pm 3.4$ ; 0.05% w/v:  $3.37 \pm 4.0$ ; NL: 0.5% w/v:  $2.73 \pm 3.2$ ; 0.05% w/v:  $3.11 \pm 3.0$ ).

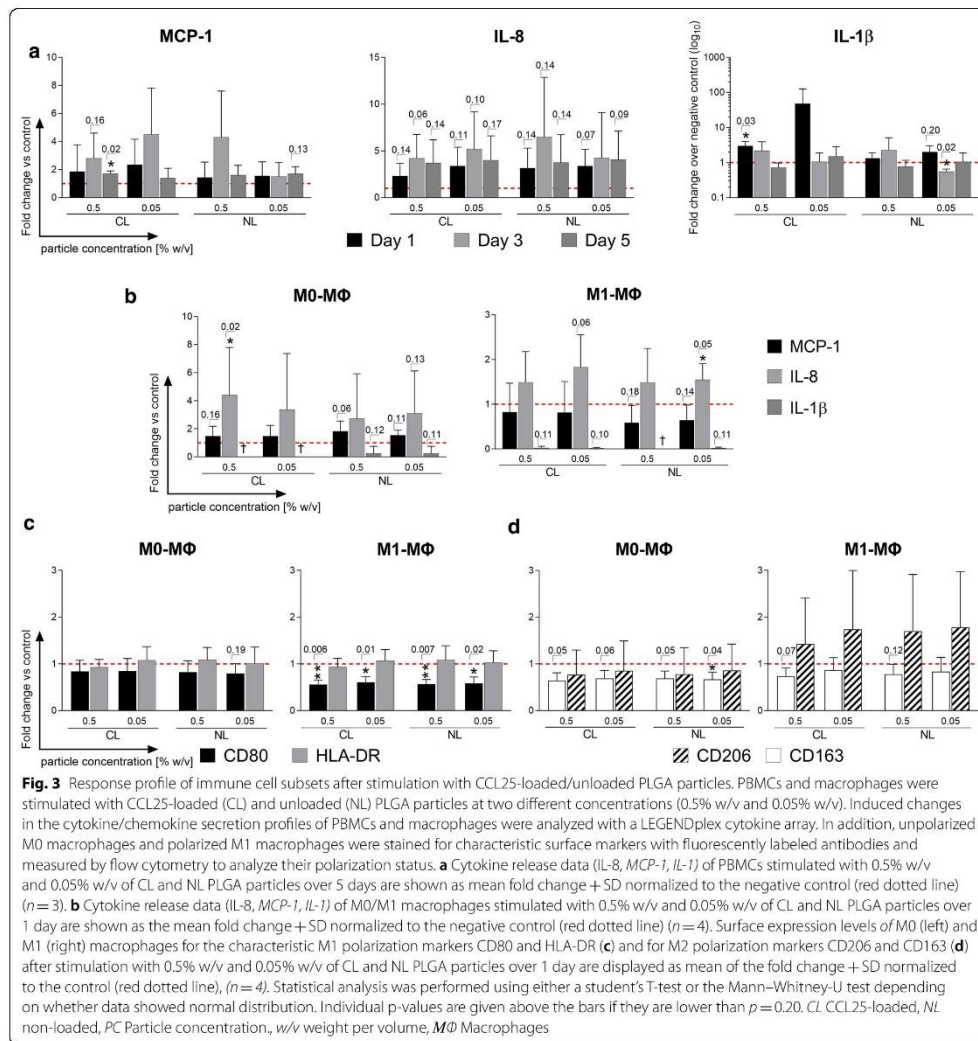
#### Both CCL25-loaded and unloaded particles modulate the M1 macrophage phenotype

Next, we determined whether the unloaded or CCL25-loaded particles could influence the polarization status of human macrophages in vitro and even reverse the development of a pro-inflammatory M1 phenotype. Both the CL and NL particle groups caused a significant reduction of CD80 expression, a typical M1 marker, in cultures of M1-polarized macrophages by a mean of  $1.52 \pm 0.07$  (Fig. 3c). However, the second M1 marker assayed, HLA-DR, showed no significant changes in expression level. At the same time, expression of the characteristic M2 surface marker CD206 in co-cultures of already polarized M1 macrophages with the particles trended towards an increase with a fold change of  $1.50 \pm 1.57$ . Expression of the M2 Marker CD163 trended towards a decrease of around 1.20 in both groups with the 0.5% w/v particles reaching p-values of 0.07 and 0.12, respectively (Fig. 3d). Unpolarized M0 macrophages also showed a slight reduction of CD80 and CD163 after particle incubation, but no increase in CD206 (Fig. 3b, d). No significant differences between the loaded and unloaded particles were observed.

#### Immune cell stimulation with supernatants of CCL25-loaded particles causes an increase in IL-8, MCP-1 and IL-1 $\beta$ secretion

To distinguish between the effects of particle fragments and the enclosed CCL25 on the leukocytes, CL and NL particles were both allowed to degrade over either 21 or 63 days. The supernatants of degraded particles were applied to the PBMCs in functional in vitro assays, and the cytokine secretion profile was determined at day 3 and 5 after supernatant stimulation (Fig. 4a). PBMC cultures treated with particle supernatants showed higher secretion levels of IL-8, MCP-1 and IL-1 $\beta$  compared to the control.





In the CL group, IL-8 secretion was increased 4.6-fold ( $\pm 5.3$ ,  $p=0.22$ ) after treatment with the 21-day supernatant and 5.3-fold ( $\pm 7.3$ ,  $p=0.45$ ) with the 63-day supernatant. The latter NL supernatants only induced a 5.14-fold ( $\pm 7.4$ ,  $p=0.49$ ) increase in IL-8 levels, which does not reach statistical significance. IL-1 $\beta$  secretion increased in a statistically insignificant manner by roughly the same amount in the CL and NL particle groups after three days

(CL: 21d:  $1.75 \pm 1.85$ ; 63d:  $1.81 \pm 1.68$ ; NL: 21d:  $1.54 \pm 1.47$ ; 63d:  $1.6 \pm 1.58$ ). However, after five days, secretion of IL-1 $\beta$  in PBMCs stimulated with the 21-day CL supernatant increased by a statistically significant amount ( $1.77 \pm 0.27$ ;  $p=0.02$ ), while for the corresponding NL particle supernatants, the IL-1 $\beta$  secretion tended to drop down to the levels of the negative control ( $0.95 \pm 0.46$ ). The same dynamics were observed for MCP-1 secretion, with a strong increase

(See figure on next page.)

**Fig. 4** Reaction of immune cell subsets after stimulation with supernatant from degraded CCL25-loaded/unloaded PLGA particles. CCL25-loaded (CL) and unloaded (NL) PLGA particles were allowed to degrade for either 21 or 63 days and particle supernatant was collected and used for in vitro stimulation assays with human PBMCs and macrophages. Changes in the cytokine/chemokine release pattern of PBMCs and macrophages were analyzed with a LEGENDplex cytokine array. Additionally, macrophages were analyzed by immunofluorescence staining and flow cytometry for the expression of surface markers indicating activation or polarization. **a** Cytokine array of PBMCs stimulated over 5 days with 21- and 63-day CL and NL PLGA particle supernatants. Cytokines with detectable differences in fold change are IL-8, MCP-1 and IL-1 $\beta$ . Data is shown as the mean fold change  $\pm$  SD normalized to the negative control (red dotted line) ( $n = 3$ ). **b** Cytokine array of M0/M1 macrophages stimulated over 1 day with 21- and 63-day CL and NL PLGA particle supernatants. Cytokines with detectable differences in fold change are IL-8 and MCP-1. Data is shown as mean fold change  $\pm$  SD normalized to the negative control (red dotted line) ( $n = 4$ ). **c** The migration of immune cell subsets towards a dilution series of particle degradation supernatant is displayed as the mean  $\pm$  SD of the number of migrated cells ( $n = 4$ ). **d/e** Flow cytometric analysis of M0/M1 macrophage polarization surface markers after 1 day of stimulation with 21- and 63-day CL and NL PLGA particle supernatants. Increased CD80 and HLA-DR indicates M1 polarization (d), while increased CD163 and CD206 indicates M2 polarization (e). Results are displayed as mean of the fold change  $\pm$  SD normalized to the control (red dotted line), ( $n = 4$ ). Statistical analysis was performed using either a student's T-test or the Mann-Whitney-U test depending on whether data followed normal distribution. Individual  $p$ -values are given above the bars if lower than  $p = 0.20$ . CL CCL25-loaded, NL non-loaded, NC negative control, M $\Phi$  Macrophage

after three days in all groups, and with high levels maintained on the fifth day in the CL particle supernatant group. At the same time, MCP-1 secretion decreased in the NL particle supernatant group (Fig. 4a). Again, macrophages were also analyzed in the same way, but only showed higher secretion levels for IL-8. The 21-day and 63-day old CL particle supernatants caused a 1.4-fold ( $\pm 0.5$ ,  $p = 0.32$ )/1.43 ( $\pm 0.83$ ,  $p = 0.44$ ) increase in cultures of M0 macrophages and a 1.15 ( $\pm 0.29$ ,  $p = 0.43$ ) / 1.29 ( $\pm 0.04$ ,  $p = 0.03$ ) increase in M1 macrophages, respectively (Fig. 4b). Interestingly, IL-1 $\beta$  secretion from M1-polarized macrophages was significantly lower in all CL and NL supernatant groups.

#### Supernatants of both loaded and unloaded particles cause no significant increases in immune cell migration

To assess the chemoattractive potential of the particle components, the supernatants of degraded particles (21 and 63 days) were used as stimuli in a Boyden-Chamber migration assay with the different leukocyte subsets (Fig. 4c). Stimulation was performed in a 1000-factor dilution series to distinguish between the effects of CCL25 and PLGA fragments. When testing CD4<sup>+</sup> T-cells, undiluted supernatants of both particle groups reduced the migration tenfold, which is a statistically significant decrease. Also, M1 macrophages showed a statistically significant reduction in migration at 1:10 and 1:100 dilutions of the particle supernatants, but only in the NL group. The other tested immune cell subsets (M0 macrophages, CD8<sup>+</sup> T-cells) showed no significant differences in migration in response to the particle supernatants compared to the control (Fig. 4c).

#### Supernatants of both loaded and unloaded particles increase HLA-DR expression on macrophages

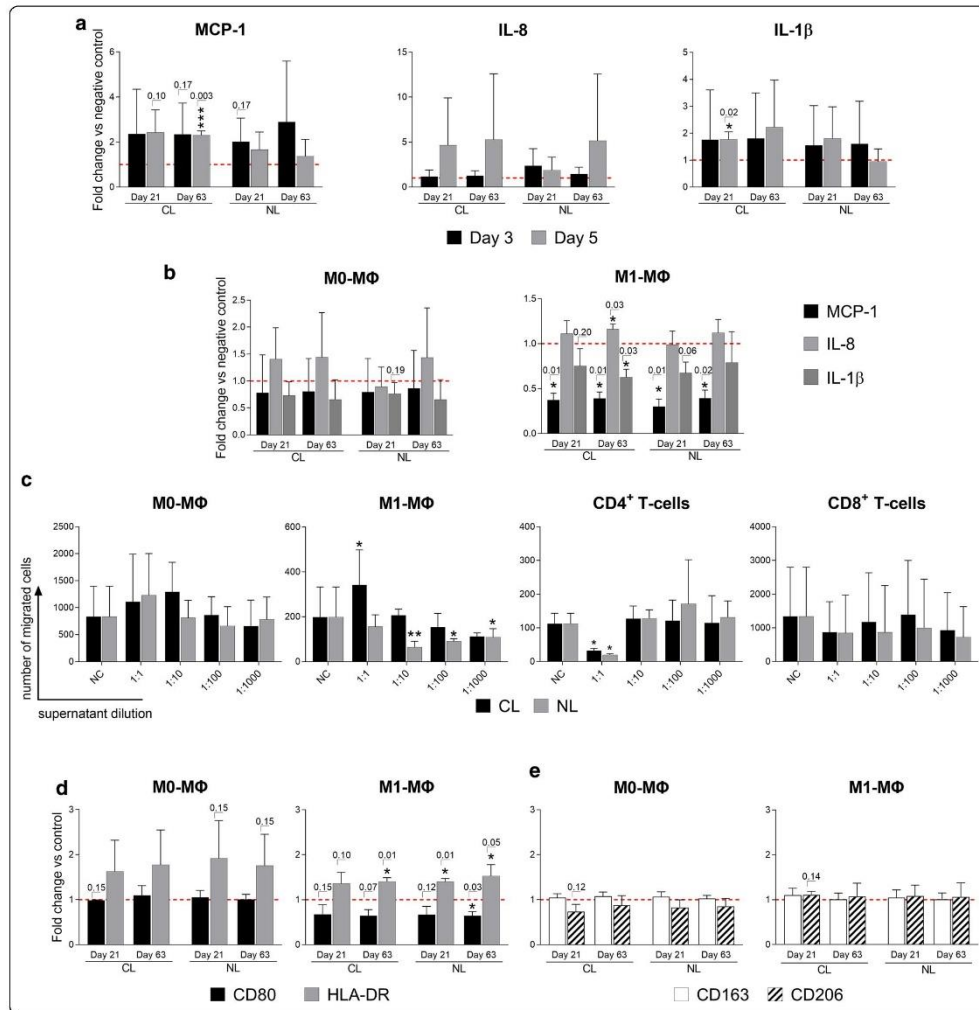
To assess the capacity of the particle supernatants to modulate the activation or polarization state of human macrophages, the surface expression levels of the

characteristic markers were analyzed by flow cytometry. After treatment of M1-polarized macrophages with CL and NL particle supernatants, HLA-DR expression was significantly increased with a mean fold change of  $1.4 \pm 0.2$  (Fig. 4d). However, there was no observable difference between the groups treated with CCL25-loaded and unloaded particle supernatant and the timespan of degradation. Meanwhile, the M1 marker CD80 decreased by a mean fold change of  $1.3 (\pm 0.17)$ . M0-polarized macrophages also increased expression of HLA-DR after supernatant stimulation from either CL or NL particles, but did not reach statistical significance. However, changes in the expression level of the M2 markers CD206 and CD163 induced by the particle supernatant treatment were not observable in either M0 or M1 phenotypes (Fig. 4d).

#### Discussion and limitations

The objective of this study was to analyze the inflammatory potential of a novel therapy for OA based on CCL25-loaded PLGA particles. We wanted to examine the reaction of leukocytes involved in innate and adaptive immune responses towards each individual component of the potential therapeutic agent to better assess which subcomponents are potentially critical and at what doses. For this purpose, human PBMCs isolated from whole blood and macrophages generated in vitro were exposed to different dosages of (i) pure CCL25, (ii) CCL25-loaded PLGA particles and (iii) their supernatants after varying time points of particle degradation. We subsequently analyzed the changes in pro-inflammatory cytokine secretion, the leukocyte activation and macrophage polarization by monitoring characteristic cell surface markers and investigated immune cell migration. Our results provided new insights regarding the inflammatory potential of a possible PLGA-based delivery chemokine therapy for the treatment of OA. Crucially, the CCL25





receptor CCR9 was found to be expressed on all analyzed leukocyte subsets, which makes a reaction upon contact with this chemokine very likely and underlines the need for a thorough analysis of this interaction.

The dose-dependent reaction of different leukocyte subsets to stimulation with CCL25 was remarkably clear. While the immune cells reacted only slightly to CCL25 concentrations of 10 and 100 nM, stimulation with 750 nM CCL25 caused a strong secretion of MCP1, IL-8,

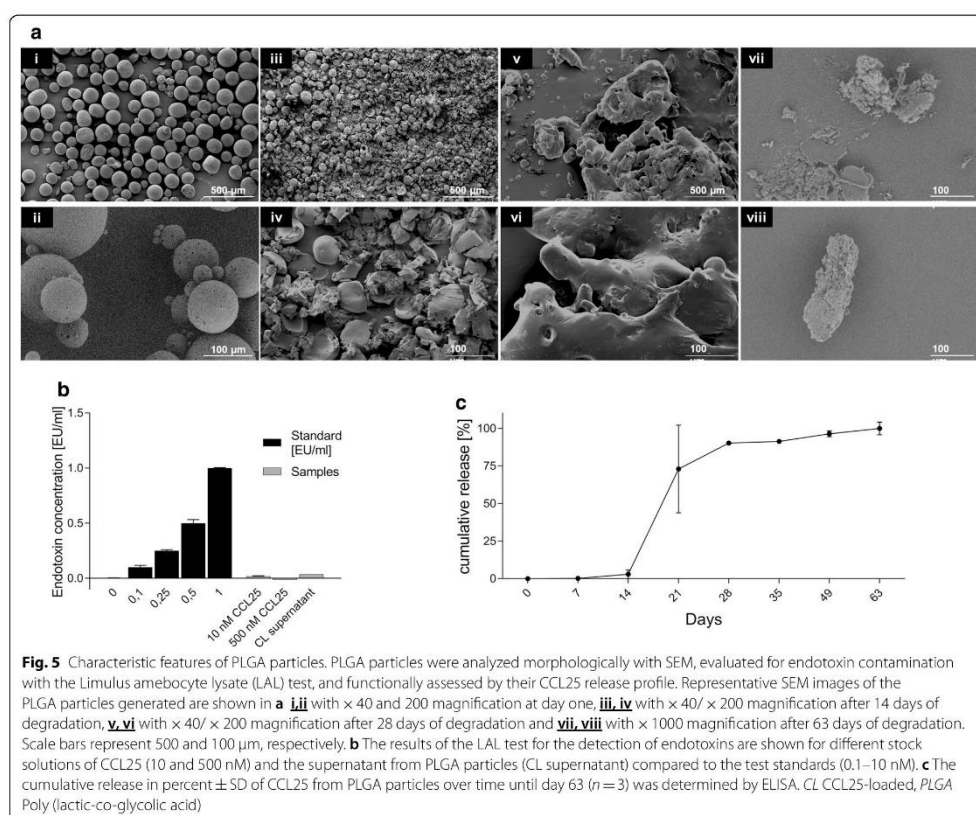
TNF- $\alpha$ , IL-1 $\beta$ , IL-6 and IFN- $\gamma$  from PBMCs. This combination of cytokines indicates a general, uncontrolled leukocytic activation. Except for IFN- $\gamma$ , secretion levels of all cytokines start to drop down after 5 days of stimulation. However, these cytokines were considered to be among the main biological drivers in the pathogenesis of OA. Especially MCP-1 and IL-8 are reported to correlate with clinical levels of pain and knee swelling. Concerningly, these two cytokines exhibited the largest

increase in expression for all dosages of CCL25 in both PBMCs and macrophages [27–29]. In an *in vivo* situation, this high level might subsequently cause an increase in inflammation by damaging the surrounding tissue and possibly further recruiting more immune cells to the site. Flow cytometric analysis of HLA-DR expression revealed a high sensitivity, especially for monocytes and CD4<sup>+</sup> T-cells, to CCL25 stimulation, with visible increases in expression even at low concentrations of 10 nM CCL25. This most likely contributes to the strong cytokine secretion in PBMCs through the simultaneous activation of both monocytes and CD4<sup>+</sup> T-cells, resulting in an amplification effect. This would also explain why macrophages alone do not respond as strongly as PBMCs, as they were cultured in isolation from other cell types and probably not exposed to a strong paracrine co-stimulus. CCL25 also exhibited the critical potential of recruiting leukocytes, which was expected given the physiologic role of CCL25 in T-cell homing [30]. Previous studies already demonstrated the capability of injected CCL25 to recruit T-cells to the site of injection [31]. Beginning at a certain concentration, unpolarized M0 macrophages and M1 polarized macrophages as well as CD4<sup>+</sup> and CD8<sup>+</sup> T-cells started to strongly migrate towards CCL25 concentration gradients. The critical dose for migration *in vitro* was between 500–1000 nM, which roughly corresponds to the concentrations that also triggered cytokine secretion. The level of HLA-DR expression induced by CCL25 stimulation correlates with the CCR9 expression profile, with monocytes revealing the highest CCR9 expression and HLA-DR upregulation, while CD8<sup>+</sup> T-cells showed the lowest CCR9 expression and HLA-DR upregulation. It is also likely that the strong HLA-DR upregulation observed is due to co-stimulation by secreted cytokines. Since the macrophages were cultivated as monocultures, they could not acquire a co-stimulus from other leukocytes. This might explain that they show no HLA-DR upregulation, despite carrying high amounts of CCR9 on their surface. In summary, CCL25, starting at concentrations of 250–500 nM, has a strong potential to trigger inflammatory processes by recruiting and activating leukocytes and inducing cytokine secretion, especially in a heterogeneous cell environment such as chronically inflamed tissue or blood.

When analyzing the immune cell responses to the CCL25-loaded PLGA particles, the induced response was much weaker compared to the direct CCL25 stimulation. The CCL25-loaded particles themselves triggered the release of cytokines such as IL-8, MCP-1 and IL-1 $\beta$  in PBMCs, and IL-8 in the M0 and M1 macrophage subsets. The increase of IL-8 and MCP-1 was slightly stronger and achieved more statistical significance in the CCL25-loaded particle group. IL-1 $\beta$  only increased

on the first day of stimulation with loaded particles. Overall, however, the difference between the loaded and unloaded particles was minute. It is very likely, that the reaction was mostly caused by the PLGA, with a marginal CCL25 contribution. The observed increase in IL-8 secretion could be induced by the acidic degradation of the PLGA, which has been shown to cause IL-8 production in other cells [32, 33]. The influence of CCL25-loaded particles on the polarization of macrophages did not show a very clear polarization trend towards either a more pro-inflammatory M1-type or the pro-regenerative M2-type. However, the decrease of CD80 and increase of CD206 point in the direction of increased M2 polarization. Macrophage polarization towards the pro-regenerative M2 macrophage direction by PLGA has been recently described by others [34, 35]. M2 macrophage polarization is thought to be a highly favorable feature of tissue engineering devices to decrease inflammation and promote healing [36, 37]. This in turn underlines the suitability of PLGA as a delivery platform for regenerative therapeutics. Overall, these results are in line with the existing literature. PLGA has been used clinically as a surgical suture material for years and is not known to cause major inflammatory side effects other than the aforementioned acidic degradation. On the contrary, the promotion of M2 macrophage polarization might even prove advantageous to minimize an already existing inflammation.

After stimulation with supernatants from the degraded CCL25-loaded particles, PBMCs showed a much stronger reaction induction of cytokine secretion than after the stimulation with undegraded but loaded particles. Considering the release pattern exhibited by the particles (Fig. 5c), supernatants at day 21 and 63 contain roughly 75% and 100% of released chemokine, respectively. This amounts to a maximum of 352 nM (63 days) 35.2 nM (21 days) of CCL25. The supernatants contained both the degraded PLGA fragments and the chemokine CCL25, and triggered release of IL-8 and MCP-1 by immune cells as well as IL-1 $\beta$  in addition to the particles. Notably, the supernatants of CCL25 loaded particles caused a higher and longer secretion of these cytokines. IL-1 $\beta$  is a highly potent pro-inflammatory cytokine, of which only a few nanograms are sufficient to cause massive local inflammation and tissue degradation, especially in human joint tissue [38–41]. These findings must be considered in the context of the *in vivo* situation. CCL25 as well as PLGA would also be degraded enzymatically over time, meaning that particle supernatants generated *in vitro* contained much more CCL25 and undegraded fragments than would occur in a therapeutic situation. Further, compared to the direct stimulation with CCL25, the supernatants of the degraded particles did not cause



an increase in HLA-DR expression on immune cells or enhance their migration. This does suggest that, even though the theoretical concentration of CCL25 in the supernatants amounted up to 352 nM, due to the protein degradation (average half-time of proteins in aqueous phases is about 5–7 days) [42] the proportion of active CCL25 always remains below the presumed critical concentration of 100 nM where definitive inflammatory activation of immune cells becomes visible. However, the concentration of CCL25 previously applied in vivo and identified as beneficial was approximately 1–5 nM [13]. Concerning cytokine release and leukocyte chemoattraction, the first concentrations which prove to be critical lie slightly above 100 nM. Our findings suggest that the intra-articular concentration should never exceed these values, which can be assured by controlled release from an implant with a slow release kinetic. Since the leukocyte responses to CCL25-loaded PLGA particles

that were observed in vitro did not differ much from the unloaded particles, it can be expected that particles carefully loaded with CCL25 are most likely safe to use. In fact, the secretion of IL-8 and MCP-1 after stimulation of leukocytes by polylactic scaffolds has been previously described by Caires et al. [43] as potentially beneficial for healing by aiding in MSC recruitment. Nevertheless, it must be assured that the release device used is tear resistant. A sudden release of large amounts of CCL25 could prove highly counterproductive in the therapy of OA, as it increases rather than reduces intraarticular inflammation.

The strength of this study is the broad spectrum of different analytic methods and leukocyte subsets employed, which made it possible to draw a differentiated picture of the inflammatory potential of the different components of a CCL25-loaded particle for potential OA treatment. The study is limited by the relatively low number



of human immune cell donors and the strong variability which impeded the generation of statistically valid statements due to high standard deviations. Nevertheless, the analysis of different leukocyte subgroups as well as differently polarized macrophages allowed detailed insights into the type and extent of the expected inflammatory reaction and sheds light on the complex mechanisms of signal transduction of the chemokine CCL25 in the context of a potential clinical application.

### Conclusion

Delayed intra-articular release of CCL25 is a promising approach for a regenerative therapeutic to treat cartilage degeneration in OA. PLGA appears to have only mild few pro-inflammatory properties and may even induce beneficial M2 macrophage polarization. However, high doses of CCL25 indeed do carry the risk of inducing an extensive inflammatory response by immune cells present in joint tissue. We demonstrated for the first time, that externally applied CCL25 is capable to induce secretion of proinflammatory cytokines, including TNF- $\alpha$ , IL-1 $\beta$ , and IFN- $\gamma$  in PBMCs, HLA-DR upregulation on monocytes and CD4+ T cells, and enhanced migration of CD4+ T-cells and macrophages. Although the previously determined targeted therapeutic doses of CCL25 of about 1 nM are well below the measured inflammatory cutoff of 100 nM—spontaneous disruption of the particles could release a large amount into the joint cavity and produce serious side effects. Due to these potentially dangerous side effects, our results suggest very high-quality requirements for any CCL25 delivery device. Essentially, each batch must be tested for structural integrity in the frame of tests for spontaneous degradation and resistance to mechanical stress.

### Methods

#### Production of CCL25-loaded PLGA microparticles and sampling

To enclose the hydrophilic chemokine CCL25 (Peprotech, Rockyhill USA) within the biodegradable polymer PLGA (Sigma-Aldrich, St. Louis USA), a water-in-oil-in-water ( $w_1/o/w_2$ ) double emulsion with subsequent solvent evaporation was performed according to a previously published method [15]: PLGA polymer (Resomer<sup>®</sup>, RG 503—Evonik Industries, Essen, Germany) was dissolved (100 mg polymer in 0.7 ml methylene chloride) and served as organic (o) phase. The internal aqueous phase ( $w_1$ ) was comprised of 1  $\mu$ g CCL25 per mg PLGA that was dissolved in 66.5 ml lactose (300 mM)/BSA (0% or 5% w/w)/Tris-HCl (10 mM)-EDTA (1 mM) buffer. For preparation of the  $w_1/o$  primary emulsion, the  $w_1$ -phase was emulsified in the o-phase either by vortex mixing at 2500 rpm for 1 min or by sonication for 10 s at

7 W. For fabrication of big-sized microparticle formulations, the primary emulsion was subsequently emulsified into 80 ml of the external aqueous  $w_2$  phase (5% (w/v) poly(vinylalcohol) (PVA, MW 67,000, Sigma-Aldrich)). In order to yield small-sized microparticles of formulation, the primary emulsion was first emulsified in 2 ml 5% PVA by vortex mixing at 2500 rpm for 3 min and the resulting  $w_1/o/w_2$  double emulsion was further poured into 30 ml 1% PVA. The double emulsions were stirred continuously for 3 h for solvent evaporation. The solidified microparticles were centrifuged and rinsed three times with distilled water. In addition to CCL25-loaded particles (CL-particles), a batch with non-loaded particles (NL-particles) was also produced to serve as negative control. After production, the particles were freeze-dried over-night and stored at 4 °C. The release samples were generated by incubating the particles at 37 °C in a shaker at 25 rpm. Sampling was performed after centrifugation for 5 min at 600g by collecting the supernatant, which was stored at -20 °C. The samples were transferred into pre-weighed tubes and the collected volume was determined with a precision scale. It was assumed that 1 g supernatant equaled 1 ml. After collection of the supernatant, fresh medium was added to the particle solution, and they were placed back in the shaker. The samples were collected every seven days beginning with day 7 and every 14 days from day 35 to day 63.

#### Morphological analysis of PLGA particles

To ensure sufficient quality of produced particles, size and surface morphology was analyzed using light microscopy and scanning electron microscopy (SEM). A small amount of each PLGA batch was dispersed in Aquatex<sup>™</sup> (Millipore Sigma, Burlington USA) and 100 to 500 particles were photographed. Light microscopy images were captured with the software ProgRes Capture Pro<sup>™</sup> (Jenoptik, Jena, Germany) and analyzed in ImageJ (Version 1.8.0.112). The diameters of 10%, 50%, 90% and 99% ( $D_{V10}$ ,  $D_{V50}$ ,  $D_{V90}$ ,  $D_{V99}$ ) of the particles were obtained.  $D_{V50}$  of produced particles was at ~84  $\mu$ m, which is within the previously reported range of optimal size for maximal CCL25 release [15]. Pictures of SEM were taken with an SEM JFM-6000 electron microscope (Jeol, Akishima, Japan) at day one and day 63 using the backscattered electrons (BSE) detector at 200 $\times$  and 1000 $\times$  magnification. SEM analysis revealed round particles, which exhibit few pore formations on an otherwise smooth surface. After 63 days, the shape of the previously round particles was completely lost, leaving only fragments or deformed particles, showing the degradation process is a requirement for functioning CCL25 release (Fig. 5a).

### Endotoxin detection

Immune cell reactions are highly inducible by endotoxins. To determine if cellular reactions to all tested samples (CCL25, CCL25-loaded PLGA particles and supernatants of CCL25-loaded PLGA particles) would be distorted by the presence of endotoxins, an endotoxin assay was performed with all stimulation components (10 nM and 500 nM stock solution; supernatants of particle release) (Fig. 5b). Gram-negative bacterial endotoxin was analyzed by the Pierce™ LAL Chromogenic Endotoxin Quantitation kit (Thermo Fisher Scientific, Waltham, USA) according to manufacturer instructions. Absorbance at 410 nm was measured on a SpectraMax™ plate reader (Molecular Devices, San Jose, USA). All values remained under 0.1 EU/ml, showing the absence of endotoxin in the samples.

### CCL25 determination

The amount of CCL25 released from the PLGA micro-particles was measured using the human CCL25/TECK DuoSet® Enzyme linked immunosorbent assay (ELISA) kit (R&D Systems, Minneapolis, USA). The optical density was measured at 450 nm and 570 nm using the Synergy™ HT Multi-Detection Microplate Reader (BioTek, Winooski, USA; Fig. 5c). The optical imperfections in the plate were corrected for by subtracting the background at 570 nm from the readings at 450 nm. The data were evaluated considering the qualitative (blank plus three times the standard deviation of the blank) and quantitative (blank plus nine times the standard deviation of the blank) borders of the ELISA. CCL25 release started slowly on day 14, with more than 90% of total CCL25 detected between day 21 and day 28. The strongest release was observed between days 14 and 21. Recovery of CCL25 amounted to 77% of incorporated CCL25.

### Isolation and cultivation of human immune cell subsets

Peripheral blood mononuclear cells (PBMCs) were isolated from buffy coats and human peripheral blood from healthy volunteers using protocols approved by the ethics committee of the Charité Universitätsmedizin Berlin (EA2/139/10; EA1/226/14) via density gradient centrifugation using Biocoll (BioTek, Winooski, USA). Lymphocytes and monocytes were isolated from PBMCs via positive selection with antibody-labeled magnetic MicroBeads (Miltenyi Biotec, Bergisch Gladbach, Germany) and MACS-columns. 20 µl CD4, CD8 (for the isolation of CD4<sup>+</sup> and CD8<sup>+</sup> T-lymphocytes, respectively) or CD14 (for the isolation of monocytes) MicroBeads per 10<sup>7</sup> cells were added to label the corresponding cell subtypes. To generate unpolarized (M0) macrophages, CD14<sup>+</sup> monocytes were resuspended in complete cell culture medium (VLE-RPMI, 0.1% AB serum, 1% Penicillin/

Streptomycin) containing M-CSF (50 ng/ml Miltenyi Biotec, Bergisch Gladbach, Germany), seeded into 6-well cell culture plates, and incubated at 37 °C and 5% CO<sub>2</sub>. After six days of stimulation in culture, monocytes were differentiated into M0 macrophages. To polarize them further towards pro-inflammatory M1 type macrophages, the cells were detached from the cell culture plates using 0.5 ml Accutase (Innovative Cell Technologies Inc., San Diego, USA). Then, two million cells were seeded in 6-wells in complete medium supplemented with 20 ng/ml IFN-γ (Peprotech, Rocky Hill, USA) and 100 ng/ml lipopolysaccharide (LPS; Sigma-Aldrich, St. Louis–USA) to enable polarization within 48 to 72 h towards the M1 macrophage type.

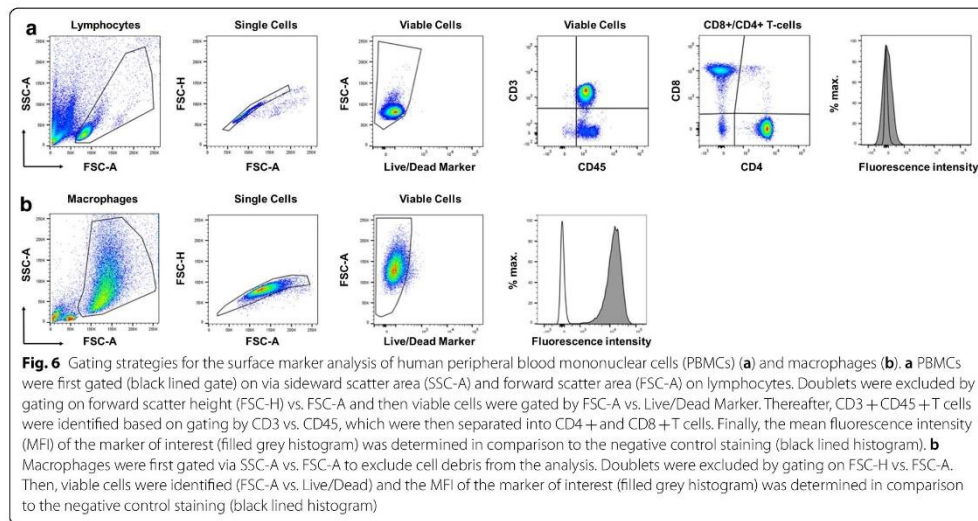
### Stimulation of immune cell subsets

For the analysis of the immune cell secretome, PBMCs of three different donors were seeded in 6-well plates, containing two million cells per well in 2 ml of cell complete culture medium. Cells were incubated with the following stimuli: (i) different concentrations of CCL25 (10, 100 and 750 nM), (ii) 10 and 1 mg of CCL25-loaded and unloaded particles, and (iii) the supernatants of loaded and unloaded particles that were previously degraded over 21 or 63 days (5 mg/ml). Assuming full degradation, the maximum achievable concentration in (ii) would amount to 352 and 35.2 nM, respectively. Regarding (iii), the theoretical concentration of CCL25 in the supernatants would amount to 75% of total released chemokine at 21 days, and 100% at 63 days (Fig. 5c). This is also why these timepoints were chosen for the supernatants. One well was always left unstimulated to serve as a negative control. 200 µl of cell culture supernatants were harvested and stored after 1, 3 and 5 days for further analysis at – 80 °C. The same stimulation setting was used for the macrophages, which were only cultivated for 48 h, since expression profiles of macrophages already change after 24 h of culture. For the flow cytometric analysis of PBMCs, 0.2 million cells were seeded in 96-well plates containing 200 µl of complete cell culture medium.

### Analysis of surface marker expression on immune cells by flow cytometry

Non-adherent PBMCs were resuspended by pipetting, and adherent cells were harvested using either a 0.05% trypsin solution with EDTA or Accutase (both Gibco, Life technology, Thermo Fisher Scientific) and transferred to 1 ml Micronic tubes (Micronic). Briefly, cells were washed once with cold PBS and resuspended in a final volume of 50 µl antibody mix in cold FACS buffer (PBS supplemented with 1% FCS) containing the antibody in the appropriate titrated concentration for 30 min at 4 °C in the dark. Incubating cells with only staining buffer





served as a control. The purity of isolated immune cells was determined using the antibodies CD3 FITC, CD4 PE, CD8 PE, CD14 PE and CD15 FITC. CCR9 expression was investigated separately on all cell types using an antibody against CCR9 (CD199 APC). The PBMCs contained 60% T-lymphocytes (CD3<sup>+</sup>), 46% CD4<sup>+</sup> T-lymphocytes, 26% CD8<sup>+</sup> T-lymphocytes and 19% monocytes (CD14<sup>+</sup>). Additionally, the PBMCs exhibited a minor contamination with CD15<sup>+</sup> granulocytes (2%). The purified CD4<sup>+</sup> T-lymphocytes were shown to be 86% CD4<sup>+</sup> with small amounts of CD8<sup>+</sup> (7%), CD14<sup>+</sup> (4%) and CD15<sup>+</sup> (2%) cells. The purity of the isolated CD8<sup>+</sup> T-lymphocytes was found to be 99%. The surface marker changes on macrophages were analyzed with the antibodies CD14 APCy7 and CD16 PerCPCy5.5 (general monocyte/macrophage markers), CD80 PE and HLA-DR PECy7 (M1 macrophage polarization markers), and CD206 APC (M2 polarization marker). PBMCs were also stained with HLA-DR PECy7. Additionally, the LIVE/DEAD<sup>TM</sup> Fixable Aqua Dead Cell Stain Kit (Thermo Fisher Scientific, Waltham, USA) was used to exclude dead cells. All antibodies were purchased from BioLegend, Miltenyi Biotec and Becton Dickinson; dilutions were prepared accordingly to the manufacturers recommendations. After antibody incubation, the samples were washed with cold FACS buffer, resuspended in 1% paraformaldehyde (PFA; Roth, Karlsruhe, Germany) in FACS buffer and transferred to 5 ml FACS tubes (Falcon). Samples were kept at 4 °C in the dark until measurement. Data was acquired using a FACS Canto II device with FACS Diva software

(Becton Dickinson, San Jose, CA, USA). Data analysis was performed using FlowJo software (TreeStar Inc., Ashland, OR, USA). Gating strategies for PBMCs and macrophages are shown in Fig. 6.

#### Cytokine detection

A LEGENDplex<sup>TM</sup> human inflammation panel (13-plex) assay (BioLegend, San Diego, USA) was performed according to the manufacturer's instructions to investigate the secretion of different cytokines (IFN- $\gamma$ , TNF- $\alpha$ , MCP-1, IL-6, IL-8, IL-10) from the cultivated and polarized macrophages and PBMCs after stimulation. Briefly, lyophilized human inflammation panel standard cocktail was reconstituted with 250  $\mu$ l assay buffer for 10 min and a standard series from 2.4 pg/ml to 10,000 pg/ml was prepared. The pre-mixed beads bottle was vortexed for 2 min before use. 25  $\mu$ l of the following reagents were pipetted into each microtube: assay buffer, standard or samples, mixed beads, and detection antibodies. All samples were measured on a FACS Canto II flow cytometer and analyzed using the LEGENDplex<sup>TM</sup> software (BioLegend, San Diego, USA).

#### Chemotaxis assay

Migration was investigated using a modified Boyden-Chamber migration assay. 96-multiwell format Chemotax plates with polycarbonate membranes (MERCK Millipore, Burlington, USA) were used. The pore sizes were chosen for each cell type individually to enable active migration without cells passing through the pores

passively. Diameters of 3  $\mu\text{m}$  were chosen for T-cells, 5  $\mu\text{m}$  for monocytes and PBMCs, and 8  $\mu\text{m}$  for macrophages. Except for the macrophages, which were cultivated, polarized and detached as described previously, all cell types were freshly isolated. A CCL25 dilution series (0.01–1000 nM) in complete cell culture medium without M-CSF was prepared on ice to enable comparison of the chemotactic effect between particles, supernatants and pure CCL25. The buffer of the tested release samples was exchanged as described above. To address the possibility of an inhibitory effect of the release samples on the migration of the immune cell types, the samples were tested undiluted and in 1:10, 1:100 and 1:1000 dilutions. Since a chemotactic reaction of the immune cells could also be attributed to the PLGA fragments in the samples, NL release samples from the same days were tested as a comparison. To quantify the number of migrated cells, an image of each well was taken with the software ProgRes Capture Pro<sup>SM</sup> (Jenoptik, Jena, Germany). The cell numbers in each picture were determined using the ImageJ plug-in Cell ImageAnalyzer v4.5. The program subtracted the red value from the green value in the RGB color mode, yielding a grey-scale image. The particle analyzer counted the cells using different thresholds for the detection, starting from the adjusted 'Max-Entropy Threshold' in ImageJ.

#### Statistical analysis

*Microsoft Excel* (2011) was used to test datasets for normal distribution using the Lilliefors-corrected Kolmogorov-Smirnov-Test. Normally distributed datasets were analyzed using a paired student's t-test to detect significant changes of receptor expression, cytokine secretion and cell migration of CCL25 stimulated immune cell subsets compared to negative controls. Datasets which were not normally distributed were tested for significant changes with the non-parametric Mann-Whitney-U-Test. Since only one statistical test was performed on every dataset, a Bonferroni-Holms corrected p-value of  $0.05/1=0.05$  was considered as significant. Due to the low risk of a multiple comparison problem, no additional post-hoc-tests were performed. The p-values of the individual analyses are given in the result graphs; results are illustrated with their individually calculated standard deviations.

#### Acknowledgements

We thank Mrs. Anja Fleischmann for technical assistance in the data acquisition.

#### Authors' contributions

JS was involved in the conception, design, data acquisition and analysis as well as manuscript writing. NS, MS and KF were mainly involved in study conception and data acquisition (cell culture, flow cytometry, migration assays). LS was involved in data analysis and manuscript writing. MS, MS, JR and TD were mainly involved in study conception, design, and data interpretation. The

views and opinions expressed within this manuscript are those of all authors. All authors read and approved the final manuscript.

#### Funding

Open Access funding enabled and organized by Projekt DEAL. This research project was funded by the BIH Centre for Regenerative Therapies (Funding of Federal Ministry of Education and Research; BMBF Grant #13GW0099).

#### Availability of data and materials

The datasets used and analyzed during the current study are available from the corresponding author on reasonable request. In general, data generated or analyzed during this study are included in this published article and its additional information files.

#### Declarations

##### Ethics approval and consent to participate

Study was approved by ethics committee of Charité-Universitätsmedizin Berlin, (Internal Review Number EA2/139/10; EA1/226/14) after informed consent.

##### Consent for publication

Not applicable.

##### Competing interests

Michael Sittinger, Kristin Fröhlich and Jochen Ringe are inventors of the following patents: US 9533297B2; EP 2645998B1.

##### Author details

<sup>1</sup>Tissue Engineering Laboratory, BIH Center for Regenerative Therapies, Department for Rheumatology and Clinical Immunology & Berlin Institute of Health at Charité-Universitätsmedizin Berlin, BCRT, Charitéplatz 1, 10117 Berlin, Germany. <sup>2</sup>Institute of Medical Immunology and Berlin Institute of Health Center for Regenerative Therapies, Institute of Medical Immunology, Charité-Universitätsmedizin Berlin, corporate member of Freie Universität Berlin and Humboldt-Universität zu Berlin, Augustenburger Platz 1, 13353 Berlin, Germany. <sup>3</sup>DZHK (German Center for Cardiovascular Research), partner site Berlin, Germany.

Received: 7 January 2021 Accepted: 10 March 2021

Published online: 25 March 2021

#### References

1. Aigner T, et al. Suppression of cartilage matrix gene expression in upper zone chondrocytes of osteoarthritic cartilage. *Arthritis Rheum Off J Am Coll Rheumatol*. 1997;40:562–9.
2. Rezus E, et al. The link between inflammation and degenerative joint diseases. *Int J Mol Sci*. 2019;20:614.
3. Ichiseki T, et al. Intraarticularly-injected mesenchymal stem cells stimulate anti-inflammatory molecules and inhibit pain related protein and chondrolytic enzymes in a moniodoacetate-induced rat arthritis model. *Int J Mol Sci*. 2018;19:203.
4. Jo CH, et al. Intra-articular injection of mesenchymal stem cells for the treatment of osteoarthritis of the knee: a proof-of-concept clinical trial. *Stem Cells*. 2014;32:1254–66.
5. Ryan CNM, Doulgkeroglou MN, Zeugolis DI. Electric field stimulation for tissue engineering applications. *BMC Biomed Eng*. 2021. <https://doi.org/10.1186/s42490-020-00046-0>.
6. Shen X, et al. Sequential and sustained release of SDF-1 and BMP-2 from silk fibroin-nanohydroxyapatite scaffold for the enhancement of bone regeneration. *Biomaterials*. 2016;106:205–16.
7. Hu Y, et al. Exogenous stromal derived factor-1 releasing silk scaffold combined with intra-articular injection of progenitor cells promotes bone-ligament-bone regeneration. *Acta Biomater*. 2018;71:168–83.
8. Andreas K, Sittinger M, Ringe J. Toward in situ tissue engineering: chemokine-guided stem cell recruitment. *Trends Biotechnol*. 2014;32:483–92.



9. Muylaert DEP, et al. Early in-situ cellularization of a supramolecular vascular graft is modified by synthetic stromal cell-derived factor-1 $\alpha$  derived peptides. *Biomaterials*. 2016;76:187–95.
10. Yang A, et al. IL-8 enhances therapeutic effects of BMSCs on bone regeneration via CXCR2-mediated PI3K/Akt signaling pathway. *Cell Physiol Biochem*. 2018;48:361–70.
11. Stich S, et al. Human periosteum-derived progenitor cells express distinct chemokine receptors and migrate upon stimulation with CCL2, CCL25, CXCL8, CXCL12, and CXCL13. *Eur J Cell Biol*. 2008;87:365–76.
12. Ullah M, Eucker J, Sittlinger M, Ringe J. Mesenchymal stem cells and their chondrogenic differentiated and dedifferentiated progeny express chemokine receptor CCR9 and chemotactically migrate toward CCL25 or serum. *Stem Cell Res Ther*. 2013;4:99.
13. Ringe J, et al. CCL25-Supplemented hyaluronic acid attenuates cartilage degeneration in a guinea pig model of knee osteoarthritis. *J Orthop Res*. 2019. <https://doi.org/10.1002/jor.24312>.
14. Glasson SS, Chambers MG, Van Den Berg WB, Little CB. The OARSI histopathology initiative - recommendations for histological assessments of osteoarthritis in the mouse. *Osteoarthr Cartil*. 2010. <https://doi.org/10.1016/j.joca.2010.05.025>.
15. Fröhlich K, et al. Delayed release of chemokine CCL25 with bioresorbable microparticles for mobilization of human mesenchymal stem cells. *Acta Biomater*. 2018. <https://doi.org/10.1016/j.actbio.2018.01.036>.
16. Andreas K, et al. Biodegradable insulin-loaded PLGA microspheres fabricated by three different emulsification techniques: Investigation for cartilage tissue engineering. *Acta Biomater*. 2011. <https://doi.org/10.1016/j.actbio.2010.12.014>.
17. Fang Y, et al. Characterizing the release mechanism of donepezil-loaded PLGA microspheres in vitro and in vivo. *J Drug Deliv Sci Technol*. 2019. <https://doi.org/10.1016/j.jddst.2019.03.029>.
18. Washington MA, et al. Monomer sequence in PLGA microparticles: Effects on acidic microclimates and in vivo inflammatory response. *Acta Biomater*. 2018. <https://doi.org/10.1016/j.actbio.2017.10.043>.
19. Han FY, Thurecht KJ, Whittaker AK, Smith MT. Bioerodible PLGA-based microparticles for producing sustained-release drug formulations and strategies for improving drug loading. *Front Pharmacol*. 2016. <https://doi.org/10.3389/fphar.2016.00185>.
20. Foldager CB, Indzu. Danish medical journal: Advances in autologous chondrocyte implantation and related techniques for cartilage repair; 2013.
21. Athanasiou KA, Niederauer GG, Agrawal CM. Sterilization, toxicity, biocompatibility and clinical applications of poly(lactic acid)/poly(glycolic acid) copolymers. *Biomaterials*. 1996. [https://doi.org/10.1016/0142-9612\(96\)85754-1](https://doi.org/10.1016/0142-9612(96)85754-1).
22. Siepmann J, Elkharrak Z, Siepmann F, Klose D. How autocatalysis accelerates drug release from PLGA-based microparticles: A quantitative treatment. *Biomacromol*. 2005. <https://doi.org/10.1021/bm050228k>.
23. Siegel SJ, et al. Effect of drug type on the degradation rate of PLGA matrices. *Eur J Pharm Biopharm*. 2006. <https://doi.org/10.1016/j.ejpb.2006.06.009>.
24. Biasi, P. Correction to: Poly(lactic acid)/poly(lactic-co-glycolic acid)-based microparticles: an overview (*Journal of Pharmaceutical Investigation*, (2019), 49, 4, (337–346), <https://doi.org/10.1007/s40005-019-00453-z>). *Journal of Pharmaceutical Investigation* (2019) <https://doi.org/10.1007/s40005-019-00457-9>.
25. Spinnen J, Ringe J, Sittlinger M. CCL25 chemokine-guided stem cell attraction: an assessment of possible benefits and risks. *Regen Med*. 2018;13:833–44.
26. Grevenstein D, et al. Excellent histological results in terms of articular cartilage regeneration after spheroid-based autologous chondrocyte implantation (ACI). *Knee Surgery Sport Traumatol Arthrosc*. 2020. <https://doi.org/10.1007/s00167-020-05976-9>.
27. Nees TA, et al. Synovial cytokines significantly correlate with osteoarthritis-related knee pain and disability: inflammatory mediators of potential clinical relevance. *J Clin Med*. 2019;8:1343.
28. Schlaak JF, Pfers I, Meyer ZBK, Märker-Hermann E. Different cytokine profiles in the synovial fluid of patients with osteoarthritis, rheumatoid arthritis and seronegative spondylarthropathies. *Clin Exp Rheumatol*. 1996;14:155.
29. Kapoor M, Martel-Pelletier J, Lajeunesse D, Pelletier J-P, Fahmi H. Role of proinflammatory cytokines in the pathophysiology of osteoarthritis. *Nat Rev Rheumatol*. 2011;7:33.
30. Campbell DJ, Butcher EC. Intestinal attraction: CCL25 functions in effector lymphocyte recruitment to the small intestine. *J Clin Invest*. 2002;110:1079–81.
31. Chen H, et al. Intratumoral delivery of CCL25 enhances immunotherapy against triple-negative breast cancer by recruiting CCR9+ T cells. *Sci Adv*. 2020;6:eax4690.
32. Xu L, Fidler IJ. Acidic pH-induced elevation in interleukin 8 expression by human ovarian carcinoma cells. *Cancer Res*. 2000;60:4610–6.
33. Shan J, Oshima T, Fukui H, Watari J, Miwa H. Acidic deoxycholic acid and chenodeoxycholic acid induce interleukin-8 production through p38 mitogen-activated protein kinase and protein kinase A in a squamous epithelial model. *J Gastroenterol Hepatol*. 2013;28:823–8.
34. Chen X, et al. A core-shell structure QRu-PLGA-RES-DS NP nanocomposite with photothermal response-induced M2 macrophage polarization for rheumatoid arthritis therapy. *Nanoscale*. 2019;11:18209–23.
35. Huang J, et al. Asiaticoside loading into poly(lactic-co-glycolic acid) electrospun nanofibers attenuates host inflammatory response and promotes M2 macrophage polarization. *J Biomed Mater Res Part A*. 2020;108:69–80.
36. Alvarez MM, et al. Delivery strategies to control inflammatory response: Modulating M1–M2 polarization in tissue engineering applications. *J Control Release*. 2016;240:349–63.
37. Das A, et al. Monocyte and macrophage plasticity in tissue repair and regeneration. *Am J Pathol*. 2015;185:2596–606.
38. Dinarello CA. Overview of the IL-1 family in innate inflammation and acquired immunity. *Immunol Rev*. 2018;281:8–27.
39. Zelenka M, Schäfers M, Sommer C. Intraneural injection of interleukin-1 $\beta$  and tumor necrosis factor- $\alpha$  into rat sciatic nerve at physiological doses induces signs of neuropathic pain. *Pain*. 2005;116:257–63.
40. Ren K, Torres R. Role of interleukin-1 $\beta$  during pain and inflammation. *Brain Res Rev*. 2009;60:57–64.
41. Kardos D, et al. Investigation of cytokine changes in osteoarthritic knee joint tissues in response to hyperacute serum treatment. *Cells*. 2019;8:824.
42. Feng Y, et al. Effects of temperature, water content and pH on degradation of Cry1Ab protein released from Bt corn straw in soil. *Soil Biol Biochem*. 2011. <https://doi.org/10.1016/j.soilbio.2011.04.011>.
43. Caires HR, et al. Macrophage interactions with poly(lactic acid) and chitosan scaffolds lead to improved recruitment of human mesenchymal stem/stromal cells: a comprehensive study with different immune cells. *J R Soc Interface*. 2016;13:20160570.

#### Publisher's Note

Springer Nature remains neutral with regard to jurisdictional claims in published maps and institutional affiliations.



- 8.3. **Amler A-K, Dinkelborg PH, Schlauch D, Spinnen J, Stich S, Lauster R, Sittinger M, Nahles S, Heiland M, Kloke L, Rendenbach C, Beck-Broichsitter B, Dehne T (2021).**  
Comparison of the Translational Potential of Human Mesenchymal Progenitor Cells from Different Bone Entities for Autologous 3D Bioprinted Bone Grafts  
*Int J Mol Sci.* 2021 Jan 14;22(2):796.

Journal Data Filtered By: **Selected JCR Year: 2019** Selected Editions: SCIE,SSCI  
 Selected Categories: **"BIOCHEMISTRY and MOLECULAR BIOLOGY"** Selected  
 Category Scheme: WoS

**Gesamtanzahl: 297 Journale**

Rank	Full Journal Title	Total Cites	Journal Impact Factor	Eigenfactor Score
1	CELL	258,178	38.637	0.564970
2	NATURE MEDICINE	85,220	36.130	0.168730
3	Annual Review of Biochemistry	20,499	25.787	0.024820
4	MOLECULAR CELL	69,148	15.584	0.166260
5	Molecular Cancer	15,448	15.302	0.023990
6	PROGRESS IN LIPID RESEARCH	6,139	15.083	0.005730
7	TRENDS IN BIOCHEMICAL SCIENCES	18,416	14.732	0.032060
8	TRENDS IN MICROBIOLOGY	13,604	13.546	0.022780
9	Signal Transduction and Targeted Therapy	1,182	13.493	0.003380
10	Nature Chemical Biology	22,084	12.587	0.060130
11	MOLECULAR PSYCHIATRY	22,227	12.384	0.054730
12	Molecular Plant	11,432	12.084	0.028530
13	NATURAL PRODUCT REPORTS	11,239	12.000	0.013610
14	NATURE STRUCTURAL & MOLECULAR BIOLOGY	27,178	11.980	0.056800
15	NUCLEIC ACIDS RESEARCH	201,649	11.501	0.403470
16	TRENDS IN MOLECULAR MEDICINE	10,618	11.099	0.018720
17	GENOME RESEARCH	41,755	11.093	0.076940
18	MOLECULAR BIOLOGY AND EVOLUTION	50,486	11.062	0.084810
19	CELL DEATH AND DIFFERENTIATION	21,095	10.717	0.029600
20	Redox Biology	10,157	9.986	0.023810

Rank	Full Journal Title	Total Cites	Journal Impact Factor	Eigenfactor Score
21	EMBO JOURNAL	64,724	9.889	0.059690
22	CURRENT OPINION IN CHEMICAL BIOLOGY	10,968	9.689	0.017770
23	PLANT CELL	54,927	9.618	0.048640
24	CURRENT BIOLOGY	63,256	9.601	0.133170
25	MOLECULAR ASPECTS OF MEDICINE	6,207	9.577	0.005750
26	Molecular Systems Biology	8,914	8.991	0.017390
27	Cell Systems	3,822	8.673	0.029290
28	MATRIX BIOLOGY	6,878	8.572	0.011920
29	ONCOGENE	66,303	7.971	0.068320
30	Cell Chemical Biology	3,326	7.739	0.015770
31	CRITICAL REVIEWS IN BIOCHEMISTRY AND MOLECULAR BIOLOGY	3,675	7.634	0.006380
32	EMBO REPORTS	14,976	7.497	0.030290
33	BIOCHIMICA ET BIOPHYSICA ACTA-REVIEWS ON CANCER	5,650	7.365	0.007800
34	PLOS BIOLOGY	31,650	7.076	0.060300
35	Essays in Biochemistry	2,383	6.966	0.005060
36	CURRENT OPINION IN STRUCTURAL BIOLOGY	11,035	6.908	0.021890
37	CELLULAR AND MOLECULAR LIFE SCIENCES	26,128	6.496	0.037010
38	Science Signaling	12,736	6.467	0.026590
39	ANTIOXIDANTS & REDOX SIGNALING	21,119	6.323	0.024660
40	Molecular Ecology Resources	10,868	6.286	0.019630
41	FREE RADICAL BIOLOGY AND MEDICINE	42,665	6.170	0.036960
42	BIOMACROMOLECULES	38,863	6.092	0.031320

Selected JCR Year: 2019; Selected Categories: "BIOCHEMISTRY and MOLECULAR BIOLOGY"

Rank	Full Journal Title	Total Cites	Journal Impact Factor	Eigenfactor Score
43	Computational and Structural Biotechnology Journal	1,954	6.018	0.004980
44	CYTOKINE & GROWTH FACTOR REVIEWS	5,935	5.982	0.007380
45	Advances in Carbohydrate Chemistry and Biochemistry	634	5.800	0.000340
46	EXPERIMENTAL AND MOLECULAR MEDICINE	5,536	5.418	0.010300
47	AMERICAN JOURNAL OF RESPIRATORY CELL AND MOLECULAR BIOLOGY	12,243	5.373	0.016040
48	RNA Biology	6,589	5.350	0.015820
49	Acta Crystallographica Section D-Structural Biology	21,750	5.266	0.018220
50	MOLECULAR ECOLOGY	38,951	5.163	0.050800
51	INTERNATIONAL JOURNAL OF BIOLOGICAL MACROMOLECULES	47,121	5.162	0.057240
52	BIOCHEMICAL SOCIETY TRANSACTIONS	12,651	5.160	0.016140
53	HUMAN MOLECULAR GENETICS	39,652	5.100	0.064170
54	Journal of Genetics and Genomics	2,271	5.065	0.004310
55	Cell and Bioscience	1,898	5.026	0.004210
56	Antioxidants	2,568	5.014	0.004170
57	FASEB JOURNAL	43,126	4.966	0.043730
58	International Review of Cell and Molecular Biology	2,167	4.934	0.004350
59	Open Biology	2,886	4.931	0.009590
60	Journal of Integrative Plant Biology	5,005	4.885	0.006830
61	Advances in Microbial Physiology	1,227	4.875	0.000960
61	Nucleic Acid Therapeutics	1,030	4.875	0.003610

Selected JCR Year: 2019; Selected Categories: "BIOCHEMISTRY and MOLECULAR BIOLOGY"

Rank	Full Journal Title	Total Cites	Journal Impact Factor	Eigenfactor Score
63	JOURNAL OF NUTRITIONAL BIOCHEMISTRY	11,460	4.873	0.011150
64	STRUCTURE	15,145	4.862	0.026940
65	International Journal of Biological Sciences	6,262	4.858	0.009710
66	BIOORGANIC CHEMISTRY	5,712	4.831	0.006730
67	Genes & Diseases	1,081	4.803	0.003310
68	JOURNAL OF MOLECULAR BIOLOGY	56,952	4.760	0.040330
69	BIOFACTORS	3,769	4.734	0.002930
70	BIOELECTROCHEMISTRY	4,944	4.722	0.004950
71	Reviews of Physiology Biochemistry and Pharmacology	805	4.700	0.000670
72	JOURNAL OF ENZYME INHIBITION AND MEDICINAL CHEMISTRY	5,415	4.673	0.005420
73	BIOESSAYS	10,189	4.627	0.016560
74	INTERNATIONAL JOURNAL OF MOLECULAR SCIENCES	77,286	4.556	0.143760
75	APOPTOSIS	6,539	4.543	0.005880
76	BIOCHIMICA ET BIOPHYSICA ACTA-MOLECULAR AND CELL BIOLOGY OF LIPIDS	10,266	4.519	0.016350
77	ACS Chemical Neuroscience	6,881	4.486	0.015300
78	JOURNAL OF LIPID RESEARCH	24,223	4.483	0.022420
79	ACS Chemical Biology	12,884	4.434	0.035490
80	FEBS Journal	18,845	4.392	0.025250
81	JOURNAL OF PHOTOCHEMISTRY AND PHOTOBIOLOGY B-BIOLOGY	12,794	4.383	0.013640
82	BIOCHIMICA ET BIOPHYSICA ACTA-MOLECULAR BASIS OF DISEASE	15,965	4.352	0.024200

Selected JCR Year: 2019; Selected Categories: "BIOCHEMISTRY and MOLECULAR BIOLOGY"



Article

# Comparison of the Translational Potential of Human Mesenchymal Progenitor Cells from Different Bone Entities for Autologous 3D Bioprinted Bone Grafts

Anna-Klara Amler<sup>1,2,†</sup>, Patrick H. Dinkelborg<sup>3,4,\*</sup>, Domenic Schlauch<sup>1,2</sup>, Jacob Spinnen<sup>4</sup>, Stefan Stich<sup>4</sup>, Roland Lauster<sup>1</sup>, Michael Sittinger<sup>4</sup>, Susanne Nahles<sup>3</sup>, Max Heiland<sup>3</sup>, Lutz Kloke<sup>2</sup>, Carsten Rendenbach<sup>3</sup>, Benedicta Beck-Broichsitter<sup>3</sup> and Tilo Dehne<sup>4</sup>

- <sup>1</sup> Department of Medical Biotechnology, Technische Universität Berlin, 13355 Berlin, Germany; aka@cellbricks.com (A.-K.A.); D.schlauch@campus.tu-berlin.de (D.S.); roland.lauster@tu-berlin.de (R.L.)
  - <sup>2</sup> Cellbricks GmbH, 13355 Berlin, Germany; lk@cellbricks.com
  - <sup>3</sup> Charité-Universitätsmedizin Berlin, Corporate Member of Freie Universität Berlin, Humboldt Universität zu Berlin, Department of Oral and Maxillofacial Surgery, and Berlin Institute of Health, 13353 Berlin, Germany; susanne.nahles@charite.de (S.N.); max.heiland@charite.de (M.H.); carsten.rendebach@charite.de (C.R.); benedicta.beck-broichsitter@charite.de (B.B.-B.)
  - <sup>4</sup> Charité-Universitätsmedizin Berlin, Corporate Member of Freie Universität Berlin, Humboldt Universität zu Berlin, Department of Rheumatology, and Berlin Institute of Health, 10117 Berlin, Germany; jacob.spinnen@charite.de (J.S.); stefan.stich@charite.de (S.S.); michael.sittinger@charite.de (M.S.); tilo.dehne@charite.de (T.D.)
- \* Correspondence: patrick.dinkelborg@charite.de; Tel.: +49-030-450-655249  
† These authors contributed equally to this work.



**Citation:** Amler, A.-K.; Dinkelborg, P.H.; Schlauch, D.; Spinnen, J.; Stich, S.; Lauster, R.; Sittinger, M.; Nahles, S.; Heiland, M.; Kloke, L.; et al. Comparison of the Translational Potential of Human Mesenchymal Progenitor Cells from Different Bone Entities for Autologous 3D Bioprinted Bone Grafts. *Int. J. Mol. Sci.* **2021**, *22*, 796. <https://doi.org/10.3390/ijms22020796>

Received: 30 November 2020  
Accepted: 11 January 2021  
Published: 14 January 2021

**Publisher's Note:** MDPI stays neutral with regard to jurisdictional claims in published maps and institutional affiliations.



**Copyright:** © 2021 by the authors. Licensee MDPI, Basel, Switzerland. This article is an open access article distributed under the terms and conditions of the Creative Commons Attribution (CC BY) license (<https://creativecommons.org/licenses/by/4.0/>).

**Abstract:** Reconstruction of segmental bone defects by autologous bone grafting is still the standard of care but presents challenges including anatomical availability and potential donor site morbidity. The process of 3D bioprinting, the application of 3D printing for direct fabrication of living tissue, opens new possibilities for highly personalized tissue implants, making it an appealing alternative to autologous bone grafts. One of the most crucial hurdles for the clinical application of 3D bioprinting is the choice of a suitable cell source, which should be minimally invasive, with high osteogenic potential, with fast, easy expansion. In this study, mesenchymal progenitor cells were isolated from clinically relevant human bone biopsy sites (explant cultures from alveolar bone, iliac crest and fibula; bone marrow aspirates; and periosteal bone shaving from the mastoid) and 3D bioprinted using projection-based stereolithography. Printed constructs were cultivated for 28 days and analyzed regarding their osteogenic potential by assessing viability, mineralization, and gene expression. While viability levels of all cell sources were comparable over the course of the cultivation, cells obtained by periosteal bone shaving showed higher mineralization of the print matrix, with gene expression data suggesting advanced osteogenic differentiation. These results indicate that periosteum-derived cells represent a highly promising cell source for translational bioprinting of bone tissue given their superior osteogenic potential as well as their minimally invasive obtainability.

**Keywords:** bioprinting; tissue engineering; gelatin methacrylate; regenerative medicine; segmental bone defect; mesenchymal progenitor cell; osteogenic differentiation; stereolithography; biomaterial

## 1. Introduction

Segmental bone defects are usually caused by trauma, resection due to benign or malignant tumors, chronic infection, osteonecrosis, or osteodegenerative diseases. They cause severe disabilities in patients [1]. Clinical management of segmental bone defects remains highly challenging, with autologous bone grafts being the gold standard procedures. For smaller defects, autologous free non-vascularized bone grafts or bone graft substitutes can be used, as vascularization is not required. For larger defects, free osteomyocutaneous or myo-osseous free flaps with microsurgical anastomosis can provide



vascularized grafts [2–4]. The existing methods of reconstructive surgery have many limitations, depending on the underlying pathology and the defect site and size [5]. The rates of perioperative complications, postoperative comorbidities, and functional impairments of donor and recipient site vary from 20 to 50% of all cases, which underlines the need for alternative treatment procedures [6,7].

Advancements in the field of tissue engineering have the potential to offer alternative approaches for the reconstruction of bone defects. Tissue engineering is an interdisciplinary field applying various concepts of life sciences and biotechnological engineering for the manufacture of artificial tissues and organs, offering a diverse toolbox for the construction of personalized human tissues [8]. One of the latest developments is 3D bioprinting, the adaptation of 3D printing for direct fabrication of biological constructs containing living cells. It allows for rapid fabrication of complex structures and manufacturing of more physiological models and customized tissue implants containing multiple cell types and delicate features [9–12].

For the successful clinical implementation of cell-containing 3D bioprinted bone constructs, selecting the right cell source is essential [13–16]. The cell source should ideally combine low morbidity of the initial biopsy, an easy harvesting method, rapid expansion, and the ability to differentiate into bone-forming cells [16]. Mesenchymal stem or progenitor cells (MPCs) can be isolated from different body tissues and extensively expanded *in vitro* while maintaining their undifferentiated, multipotent condition, and have already been investigated in clinical trials [13,17]. MPCs derived from bone marrow and adipose tissue are the ones that have mainly been used for bioprinting artificial bone tissue [13,16,18]. However, the possibility of failure of cell extraction and the inconsistent tissue ossification and speed are barriers to using this procedure in a clinical setting [19,20]. The associated costs and risks may outweigh the long-term benefits.

Periosteum-derived MPCs (P-MPCs) are a promising alternative. They can be obtained via minimally invasive periosteal shaving, and have recently shown high performance in cell-based regenerative therapy of cartilage and bone defects [21]. However, the substantial osteogenic potential of these cells has never before been studied in any bioprinting applications.

We therefore set out to directly compare the osteogenic potential of a panel of human bone-, bone-marrow-, and periosteum-derived mesenchymal progenitor cells, extracted from clinically relevant biopsy sites in a 3D bioprinted environment, and discuss their potential use in a clinical context.

## 2. Results

### 2.1. Bioprinting and Cultivation of Printed Constructs

A panel of human MPC cells was isolated from clinically relevant harvesting sites and expanded (Figure 1a, Table 1). By means of computer-assisted design (CAD) software, a simplified 3D model was designed and exported as a stereolithography (STL) file (Figure 1b). Directly before printing, cells were added to the bioink, which was based on methacrylated gelatin (Figure 1c). Cell-laden constructs were bioprinted using a projection-based stereolithographic printing platform in which precise solidification of hydrogels was achieved by projecting photomasks onto the printing dish, resulting in the fabrication of a three-dimensional construct (Figure 1d,e).

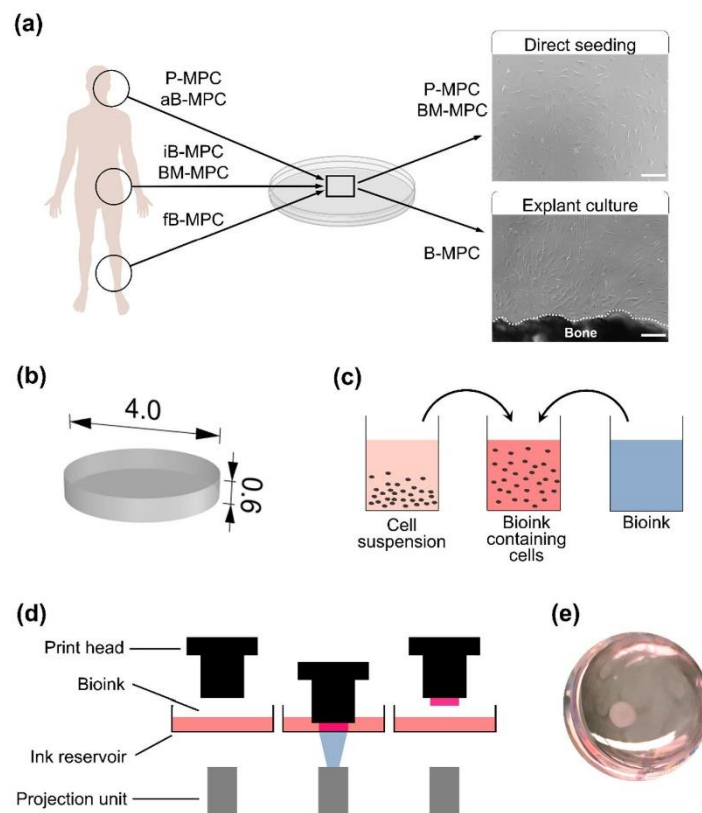


**Figure 1.** Experimental setup. (a) Human mesenchymal progenitor cells were isolated from different body tissues (alveolar bone (aB-MPC), fibula bone (fB-MPC), iliac crest bone (iB-MPC), iliac crest bone marrow (BM-MPC), periosteum of the mastoid (P-MPC)). Scale bar = 200  $\mu$ m. (b) A 3D model was designed with computer-assisted design (CAD) software and exported as a stereolithography (STL) file. Measurements are given in mm. (c) Preparation of bioink prior to bioprinting. (d) The bioprinting process. The print head is lowered into the ink reservoir and the bioink is solidified by projecting photomasks. (e) A photograph showing the completed print in a culture plate.

Subsequently, bioprinted constructs were cultivated in osteogenic medium for 28 days. Microscopic images on day 0 showed homogenous distribution in cell-laden constructs (Figure 2). While cell-free bioprints retained their size and discoid shape over the entire cultivation period, shrinkage and central retractions were observed in cell-laden constructs. During cultivation, the P-MPC-laden constructs became progressively less translucent, while the other bioprints retained uniform translucency.

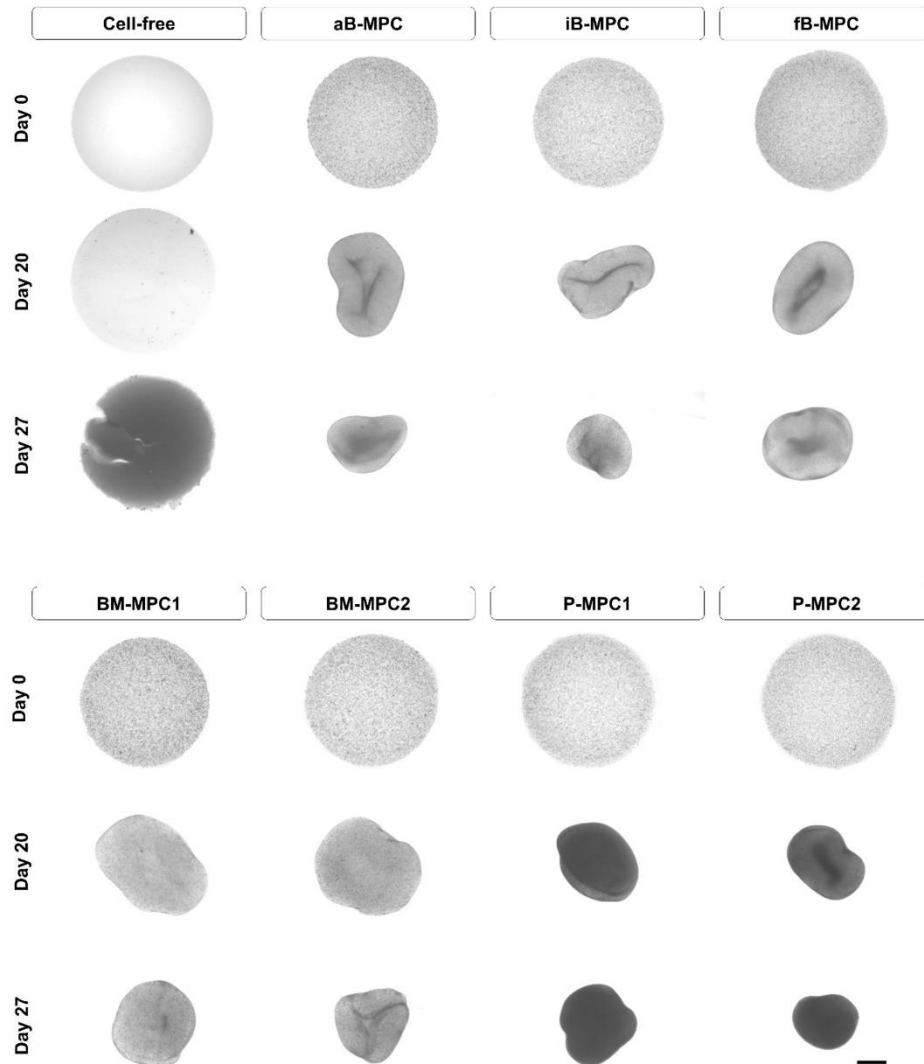


**Figure 2.** Cultivation of the printed constructs. Microscopic images were taken on days 0, 20, and 27 of cultivation. Scale bar = 1000  $\mu\text{m}$ .

### 2.2. Viability and Metabolic Activity

In all cell-laden printed constructs, live/dead staining demonstrated that the vast majority of the cells remained viable throughout the 28 days of culture. Over the entire cultivation period, only a small portion of the cells was found dead (Figures 3a and A1).

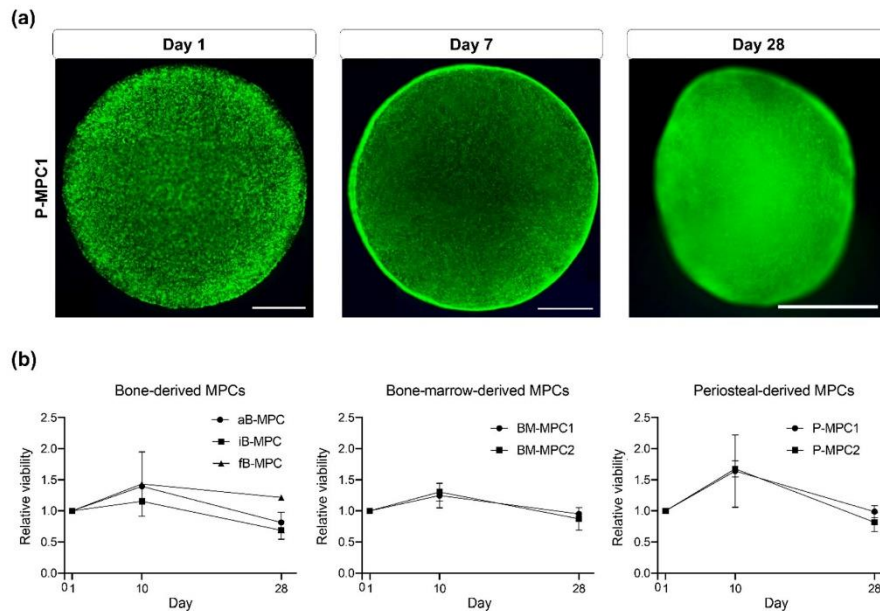


**Figure 3.** Viability of cells in bioprints. (a) Fluorescence microscopy images of propidium iodide/fluorescein diacetate stained constructs showing living cells in green and dead cells in red on days 1, 7, and 28. Representative images shown for P-MPC1. Scale bar = 1000  $\mu\text{m}$ . (b) Results of alamarBlue<sup>TM</sup> assay on days 1, 10, and 28 of cultivation. Viability was normalized to the respective value for each cell type on day 1.  $n = 2$ .

A unique feature of bone is its biomechanical properties achieved through the mineralization of the extracellular matrix (ECM). The secretion of ECM depends on the metabolic activity of bone-forming cells. Metabolic activity as a biomarker of viability was assessed using the established alamarBlue<sup>TM</sup> assay, in which non-fluorescent resazurin is reduced to highly fluorescent resorufin by metabolically active and therefore viable cells [22]. In general, metabolic activity of the bioprinted constructs peaked on day 10 at comparable levels for all subgroups (Figure 3b, Supplementary Material).

### 2.3. Mineralization

Calcification and thus hardening of the bone matrix is accomplished through deposition of mineralized nodules by osteoblasts. This is achieved by incorporating nanoscale calcium phosphate crystals into the osteoid—a soft matrix consisting mainly of collagen I fibrils, previously secreted by the cells [23–25].

Cryosections of the printed constructs were analyzed for deposition of minerals by the cells by staining the hydroxyapatite portion using OsteoImage<sup>TM</sup> Mineralization Assay (Figure 4). On day 28, the bioprints containing periosteal cells showed a strong uniform signal, while constructs containing BM-MPCs and aB-MPCs displayed formation of nodule-like structures. Only single nodules were visible for iB-MPCs, while no signal was detected for fB-MPCs and for cell-free constructs. On day 1, no signal was detected for any samples.



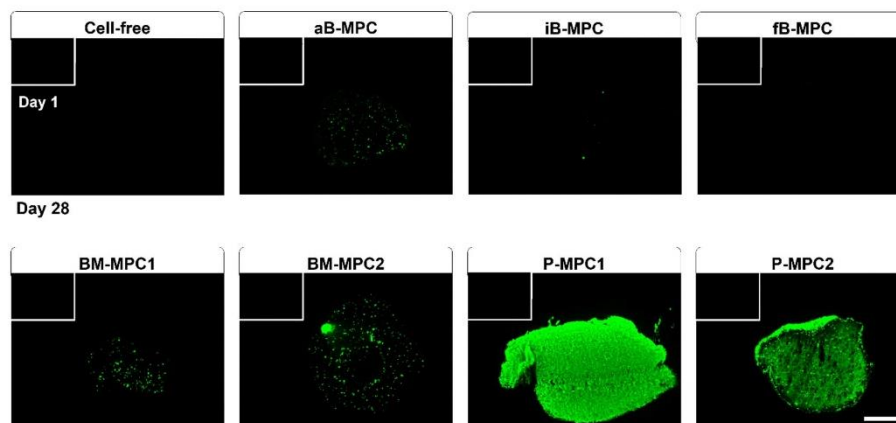


**Figure 4.** Mineralization of printed constructs. Histological staining on day 1 (white bordered rectangle) and day 28, using OsteoImage™ Mineralization Assay. Scale bar = 500  $\mu$ m.

#### 2.4. Gene Expression Analysis

To assess the osteogenic differentiation of printed constructs at the gene expression level, quantitative real-time PCR was performed. Expression of mRNA was normalized to the housekeeping gene TATA-box binding protein (TBP). Alkaline phosphatase (ALPL) is a membrane-bound enzyme involved in bone mineralization through hydrolyzing pyrophosphate, and is a marker for osteogenic differentiation [26,27]. Similarly, collagen I is considered an early bone differentiation marker [28]. It is required for matrix mineralization, as it accounts for most of the organic material in the bone matrix, with collagen type 1 alpha 1 chain (*COL1A1*) is the predominant collagen [29,30]. *RUNX2* encodes for the Runt-related transcription factor 2, one of the key regulators of osteogenic differentiation, also known as Cbfa1 [28]. The ubiquitously expressed protein osteonectin, encoded by *SPARC* (secreted protein acidic and cysteine rich), plays a role in the mineralization of the bone matrix and is often used as a late marker of osteogenic differentiation [31]. Osteopontin (*SPP1*; secreted phosphoprotein 1) is one of the SIBLING proteins (small integrin-binding ligand, N-linked glycoproteins) and is also associated with bone mineralization [32].

All the genes of the selected osteogenic marker panel were detected for all cell types. However, expression levels and patterns sometimes differed. Expression of *ALPL* displayed an upward trend over the 28 days of cultivation for all cell types, although this increase was only significant for aB-MPCs (Figure 5, Supplementary Material). A similar increase was observed for expression of *COL1A1* in constructs containing B-MPCs and for BM-MPC donor 2, while BM-MPC donor 1 showed no significant differences. In contrast, bioprints with P-MPCs were found to significantly decrease in *COL1A1* expression from day 1 to day 7 and to remain at a lower level on day 28. Overall, expression levels of both aB-MPCs and iB-MPCs differed significantly from almost all other groups on day 28. *RUNX2* expression levels remained stable over the course of the experiment for all conditions except aB-MPCs, where a significant increase was observed. Constructs containing P-MPCs also exhibited stable expression for *SPARC* and *SPP1*, with lowest expression levels compared to all other conditions on day 28. Donor 1 and 2 samples of BM-MPCs exhibited differences in expression patterns, as for both genes, expression decreased for BM-MPC1, whereas an increase was observed for BM-MPC2. Therefore, BM-MPCs showed a higher donor variability compared to P-MPCs. Expression of *SPARC* increased for all B-MPC bioprints, while for *SPP1*, only aB-MPCs displayed higher gene expression on day 28, with iB-MPCs and fB-MPCs remaining stable overall.

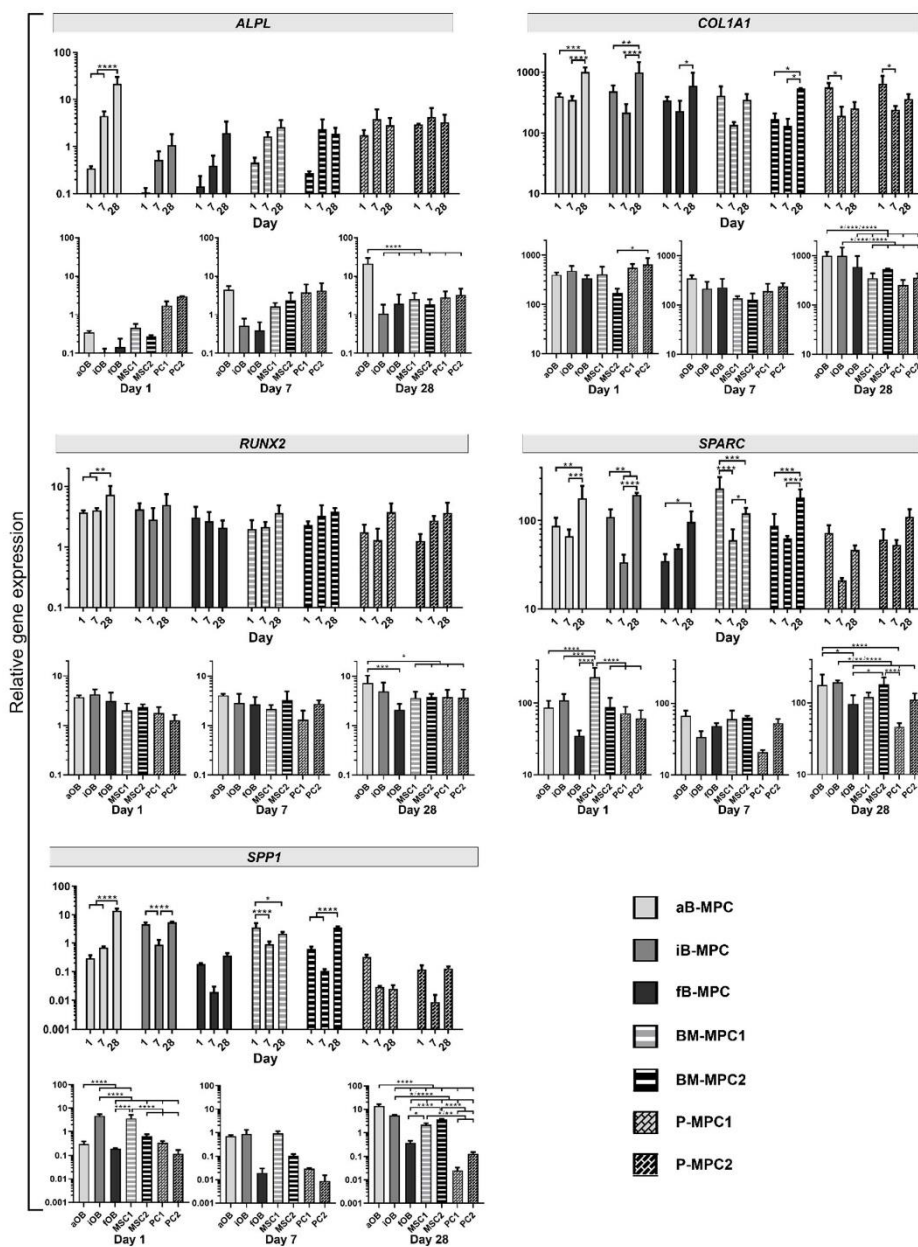


**Figure 5.** Gene expression analysis. Relative gene expression of differentiation markers *ALPL* (alkaline phosphatase), *COL1A1* (collagen type I alpha chain), *RUNX2* (Runt-related transcription factor 2), *SPARC* (secreted protein acidic and cysteine rich) and *SPP1* (secreted phosphoprotein 1) in bioprinted constructs on days 1, 7, and 28, normalized to TATA-box binding protein (TBP) expression. Asterisks mark statistically significant differences in the data. Data are presented as mean  $\pm$  standard deviation.  $n = 3$ .



### 3. Discussion

In this study, we successfully bioprinted human MPCs isolated from different clinically relevant harvesting sites, and compared their behavior under osteogenic cultivation conditions. For the clinical implementation of cell-containing 3D bioprinted bone constructs, the choice of the right cell source and the adequate bioink are important factors. Methacrylated gelatin (GelMA) based bioink was used to fabricate cell-laden constructs, since it has been shown to be advantageous for cell behavior. As it is an ECM-based material, it naturally presents an arginylglycylaspartic (RGD) amino acid motifs and can be modified by cells [33–35]. Here, embedded MPCs were able to contract the gels (Figure 2), implying strong adhesion of the cells to their surrounding matrix. However, similar contraction of the print matrix was not observed for prints with different geometry, suggesting dependence on the overall structure (Figure A2). The multi-layered architecture might improve structural integrity, as we have shown in previous studies [36].

Viability, as measured by alamarBlue™ assay, increased on day 10, followed by a decrease at the end of cultivation, at comparable levels for all cell types (Figure 3). This could be explained by impaired diffusion of the dye through the hydrogel after day 10 (as embedded cells secrete matrix components, including collagen), as well as by the change in construct shape from discoid to spheroid, resulting in a reduced surface area. Changes in measured viability could also result from lowered metabolic activity, as cells lose their highly active proliferative status during differentiation [37]. This is consistent with results from gene expression analysis (Figure 5).

The transcription factor RUNX2 is needed for both differentiation and functioning of osteogenic cells [38–40]. Accordingly, gene expression levels remained stable for almost all cell types (Figure 5). A significant increase was observed only for aB-MPCs, hinting at differentiation from early progenitor status to osteoblast-like cells over the course of the experiment. Expression of *COL1A1* is strongly upregulated at the stage prior to matrix mineralization, and its fibril formation is essential for further matrix maturation of bone occurring physiologically in vivo [41]. Hence, bone-derived MPCs appear to be at an early differentiation stage, as an increase of *COL1A1* expression levels was observed over the 28 days of cultivation. These findings are consistent with the OsteoImage™ staining, where little or no mineralization was detected (Figure 4). Accordingly, expression of *ALPL*, one of the early bone differentiation marker genes, was significantly upregulated only in aB-MPCs, while all constructs containing BM-MPCs and P-MPCs showed stable expression levels. In contrast, a downregulation of *COL1A1* expression was observed for P-MPCs. This supports the hypothesis of advanced osteogenic differentiation, since *COL1A1* is usually downregulated during this process [42].

Similarly to collagen, the expression of *SPARC* is upregulated as cells move toward an osteoblast phenotype, and then is subsequently downregulated again [43]. Upregulation of *SPARC* was found for all B-MPC constructs, as well as for BM-MPC2, whereas downregulation was detected for BM-MPC1 and for both P-MPC donors. In contrast, the matrix protein osteopontin, encoded by *SPPL1*, is expressed at later stages of osteogenic differentiation and persists at a high level [39]. Again, upregulation was observed for all B-MPC constructs, as well as for BM-MPC2, while expression levels were stable or slightly diminished for P-MPC and BM-MPC1 constructs. Results from gene expression analysis are further substantiated by high mineralization levels for P-MPC constructs, in contrast to moderate mineralization levels for BM-MPC constructs and little to no mineralization for B-MPC constructs, as shown by OsteoImage™ staining (Figure 4).

Directly comparing B-MPCs from different bone entities, cells obtained from the fibula showed the lowest osteogenic potential, since they displayed no mineralization and low expression levels of osteogenic marker genes. Alveolar B-MPCs showed stronger mineralization of the print matrix than those acquired from explant cultures of iliac crest bone. However, donor variability should be considered [44].

To the best of our knowledge, this is the first study that includes periosteum-derived MPCs for the fabrication of artificial bone tissue by 3D bioprinting. Our findings are

supported by several other studies, which have shown that periosteal cells are superior in bone and cartilage regeneration compared to bone marrow or other mesenchymal cell sources [45–47]. The reported higher proliferation rate of periosteum-derived cells compared to other cell sources is advantageous, as it allows for reduction of the time needed for expansion before transplantation [21]. Furthermore, the periosteum can be removed in a much less invasive way than the other sources of MPCs from various convenient locations, which may facilitate clinical implementation [48,49].

Biocompatible scaffolds secondarily colonized with cartilage or osteoprogenitor cells are already clinically applied in the reconstruction of small cartilage and bone defects [4,50,51]. However, their applicability in large segmental bone defects is limited, as cellular nutrition can only be achieved by diffusion. Implementation of vascularization is currently one of the biggest challenges in the field of tissue engineering. It is crucial for the scale-up of fabricated constructs, and therefore for their potential for transplantation, since diffusion limits need to be overcome to ensure supply with nutrients and oxygen and removal of waste products [52–54]. Recently, Thomas et al. presented an enzyme-based system for rapid fabrication of vasculature-like structures for multi-material stereolithographic bioprinters [55]. Perfusable channels can be printed in a bulk material using hyaluronic acid-based ink, which is first solidified and then digested using hyaluronidase. These channels can optionally be lined with endothelial cells by embedding the cells in the channel ink and subsequently releasing them via enzymatic digestion of the surrounding matrix, allowing cell attachment to the resulting channel walls. This system could readily be adapted to our application, allowing bigger constructs to be fabricated. Furthermore, the introduction of endothelial cells can have a positive effect on the osteogenic maturation of tissues, as has been shown before [36,56,57].

Further differentiation of printed cells might be observed by prolonging the cultivation time. This would be particularly interesting for bone-derived cells, as gene expression and mineralization data indicate an early differentiation stage. Moreover, loading the hydrogel with cell attractants like growth factors or chemokines could enhance the *in vitro* maturation of the bioprinted constructs and be advantageous for subsequent transplantation, as has been shown before [58–62]. This should be validated in follow-up *in vivo* studies.

For successful translation, several challenges need to be met. Autologous transplants require a large number of cells, necessitating sophisticated cell isolation and expansion workflows. Furthermore, the material and its printed structure need to promote engraftment after implantation. For GelMA, the material used in this study, previous publications have reported promising results [62,63]. Another aspect to consider is the ease of handling of the fabricated constructs in the surgical procedure. Prior to clinical application, long-term *in vitro* testing, as well as *in vivo* studies, must be completed, proving biocompatibility for prolonged time periods.

Although much larger artificial bone grafts are required to restore segmental bone defects, the purpose of this study was to compare the osteogenic potential of MPCs from different bone entities in 3D bioprinted constructs first. Therefore, a simplified design was chosen, allowing for screening of MPCs originating from four bone entities (alveolar, fibula, iliac crest, and mastoid) using three different extraction and harvesting methods (explant culture, bone marrow aspiration, and periosteal shaving with subsequent seeding). To facilitate investigation of a large number of relevant bone sites, a total of only seven donors were analyzed. For better significance, the number of donors per bone entity should be increased. However, homogenous results were still observed from MPCs in the different entities when exposed to the same fabrication and cultivation protocols within our study.

In addition to the origin of the osteogenic cell source, the biomechanical characteristics of different implant types should also be thoroughly assessed in the future. However, this was beyond the scope of this study, since these properties are highly dependent on the construct size, and more sensible data could be obtained by bioprinting structures resembling the prospective implant features more closely.



## 4. Materials and Methods

### 4.1. Photoink Synthesis

Methacrylated gelatin (GelMA) was synthesized as described previously [64,65]. After dissolution at 10% *w/v* in phosphate-buffered saline (PBS), type A gelatin from porcine skin (300 bloom) was heated to 50 °C, and methacrylic anhydride was added dropwise at 0.1 mL g<sup>-1</sup> gelatin. The reaction was allowed to continue for three hours under constant stirring. After adjusting the pH to 7.4, dialysis of GelMA was performed for four days against distilled water through a 12–14 kDa cut-off membrane to remove the remaining methacrylate and salts. After lyophilization at 1 mbar and –60 °C, GelMA was stored at –20 °C. Methacrylation was measured by <sup>1</sup>H-NMR using a Bruker Avance III at 500 MHz (Bruker Corporation, Billerica, MA, USA). Lithium phenyl-2,4,6-trimethylbenzoyl phosphinate (LAP) was used as a photoinitiator. Synthesis was performed as previously published [66,67]. All synthesis reagents were purchased from Sigma-Aldrich (Saint Louis, MO, USA).

### 4.2. Cell Isolation and Culture

#### 4.2.1. Ethical Statement

All subjects gave their informed consent for inclusion before they participated in the study. The study was conducted in accordance with the Declaration of Helsinki, and the protocol was approved by the Ethics Committee of Charité-Universitätsmedizin Berlin (EA4/049/13, EA2/068/14).

#### 4.2.2. Bone Marrow MPCs

Adult human BM-MPCs were isolated from iliac crest bone marrow aspirates according to a protocol published previously [68]. Heparinized aspirates were diluted in BM-MPC medium and seeded directly in tissue culture flasks (1 mL undiluted aspirate per 175 cm<sup>2</sup>). BM-MPC medium was composed of Dulbecco's modified Eagle's medium (DMEM) containing 1 g L<sup>-1</sup> glucose, 2 mM L-alanyl-L-glutamine, 100 U mL<sup>-1</sup> penicillin, 100 µg mL<sup>-1</sup> streptomycin, 20 mM HEPES (all Merck, Berlin, Germany), 10% fetal calf serum (FCS, HyClone™, GE Healthcare, Chicago, IL, USA), and 2 ng mL<sup>-1</sup> basic fibroblast growth factor (FGF2, PeproTech, Rockyhill, CT, USA). Adherent cells were propagated in medium that was exchanged three times a week; non-adherent mononuclear cells were removed by media exchange. Cells were maintained at 37 °C in a humidified atmosphere with 5% CO<sub>2</sub>, and were trypsinized upon reaching a confluence of 90% by means of a 0.05% trypsin-EDTA solution (Merck, Berlin, Germany).

#### 4.2.3. Bone-Derived MPCs

Adult primary human bone-derived MPCs were isolated from cancellous bone of patients undergoing free vascularized fibula tissue transfer, free vascularized iliac crest tissue transfer, or dental implantation, following slightly modified protocols published previously [44,69]. The bone tissue was repeatedly washed with PBS to remove blood components under a sterile workbench. Subsequently, the explants were minced and seeded in tissue culture flasks containing cell culture medium. The cell culture medium was composed of DMEM containing 1 g L<sup>-1</sup> glucose, 2 mM L-alanyl-L-glutamine, 100 U mL<sup>-1</sup> penicillin, 10 µg mL<sup>-1</sup> streptomycin, 20 mM HEPES (all Merck, Berlin, Germany), 10% FCS (HyClone™, GE Healthcare, Chicago, IL, USA), and 2 ng mL<sup>-1</sup> basic fibroblast growth factor (FGF2, PeproTech, Rockyhill, CT, USA). Explants were cultured in a humidified incubator at 37 °C with 5% CO<sub>2</sub>. Cells started to grow out within 3–7 days and reached critical confluency on or after day 14. Non-adherent cells were removed by media exchange, which was conducted three times a week. At confluency, the culture was expanded by trypsinization by means of 0.05% trypsin-EDTA solution (Merck, Berlin, Germany).

#### 4.2.4. Periosteum-Derived MPCs

Periosteal tissues (0.5 cm<sup>2</sup>) were harvested according to a method previously described [46] from the human mastoid of two patients undergoing mastoidectomy. In brief, the periosteal flap was rinsed with Hank's solution (Merck, Berlin, Germany) three times, minced and digested for 3 h in DMEM/Ham's F12 medium (Merck, Berlin, Germany) containing 10,000 U mL<sup>-1</sup> collagenase II (Merck, Berlin, Germany), 10% human allogenic serum (German Red Cross, Berlin, Germany), 2.5% HEPES (Biochrom, Berlin, Germany), 100 U mL<sup>-1</sup> penicillin, and 10 µg mL<sup>-1</sup> streptomycin (Biochrom, Berlin, Germany). Subsequently, the cells were harvested, resuspended in DMEM/Ham's F12 medium containing 10% human allogenic serum, plated in cell culture flasks, and allowed to attach for about 4–6 days. Non-adherent cells were removed by exchange of medium. Adherent growing periosteum-derived MPCs (P-MPCs) were sub-cultured under standard cell culture conditions. At 90% confluence, P-MPCs were detached by treatment with 0.05% trypsin-EDTA, replated, and sub-cultured in DMEM medium containing 10% FCS.

**Table 1.** Cell types used for bioprinting.

Construct	Cell Type	Biopsy Site	Biopsy Method	Expansion Method
Cell-free	–	–	–	–
aB-MPC	Bone-derived MPC	Alveolar bone	Bone explantation	Explant outgrowth
iB-MPC		Iliac crest		
fB-MPC	Bone marrow MPC	Fibula	Fine needle aspiration	Direct seeding
BM-MPC1		Iliac crest bone marrow		
BM-MPC2	Periosteal MPC	Mastoid	Periosteum explantation	Seeding after tissue digestion
P-MPC1				
P-MPC2				

A summary of the cells types used and their sources are given in Table 1. Cells were characterized by flowcytometrical analyses of cell surface antigens as described previously (Figure A3) [70]. All cells were used at passage 3. Consumables were obtained from Corning Inc. (Corning, CA, USA) unless stated otherwise.

#### 4.3. Bioprinting

3D models were designed using Rhinoceros 6 software (Robert McNeel and Associates, Seattle, WA, USA) and exported as an STL file. Photomasks were generated using the printer's software. Photoink was prepared by dissolving lyophilized GelMA in PBS and then diluting it to the final concentration of 8% *w/w* while adding 0.1% *w/w* LAP. To fabricate cell-laden constructs, cells were detached from the culture dish and added to the ink at  $20 \times 10^6$  cells mL<sup>-1</sup> directly before printing. Bioprinting was performed using a proprietary stereolithographic printing platform, as described previously [10,55]. Briefly, precise solidification of hydrogels was achieved by projecting photomasks onto the printing dish, resulting in the fabrication of a three-dimensional construct.

#### 4.4. Bioprint Cultivation

The printed constructs were cultivated for 28 days in osteogenic medium (DMEM with 1 g L<sup>-1</sup> glucose, 10% FCS, 2.5% HEPES, 100 U mL<sup>-1</sup> penicillin, 10 µg mL<sup>-1</sup> streptomycin, 100 nM dexamethasone (Sigma-Aldrich, Saint Louis, MO, USA), 0.05 mM L-ascorbic acid 2-phosphate (Sigma-Aldrich, Saint Louis, MO, USA), and 10 mM β-glycerophosphate (Sigma-Aldrich, Saint Louis, MO, USA)) in 24-well ultra-low attachment multiple well plates. Medium exchange was performed three times a week. Images were taken using the BIOREVO BZ-9000 microscope (Keyence, Osaka, Japan) and CK40 (Olympus, Hamburg, Germany).

#### 4.5. Assessment of Viability

##### 4.5.1. alamarBlue™ Assay

To evaluate cell viability after printing, alamarBlue™ assay was used according to the manufacturer's recommendations (Thermo Fisher Scientific, Waltham, MA, USA). AlamarBlue™ was diluted 1:10 in DMEM containing 10% FCS (AB medium). The medium was removed and each construct was incubated in 500 µL AB medium for 4 h at 37 °C and 5% CO<sub>2</sub>. After the incubation period, 4 × 100 µL of each well was transferred to a 96-well plate. Fluorescence was measured in a plate reader with the following wavelength filter settings—540 nm for excitation and 590 nm for emission. AB medium without any cells served as a blank measurement. Two bioprinted constructs per condition were analyzed and measured in technical quadruplicates.

##### 4.5.2. Live/Dead Staining

Whole constructs were examined for viability using propidium iodide/fluorescein diacetate staining (PI/FDA; Sigma-Aldrich, Saint Louis, MO, USA) on days 1, 7, and 28 of osteogenic maintenance. After washing with PBS (Merck, Berlin, Germany), staining was performed, first in an FDA solution (3 µg mL<sup>-1</sup>; 15 min, 37 °C) and then in a PI staining solution (100 µg mL<sup>-1</sup>; 2 min; room temperature). For microscopy, an Olympus CKX41 combined with a reflected fluorescence microscopy system was used (Olympus, Hamburg, Germany). The staining results were photodocumented using the ProgRes® speed XT core 5 camera and ProgRes® CapturePro 2.10 software (both Jenoptik, Jena, Germany).

##### 4.6. Mineralization

The printed constructs were washed in PBS and fixated for 15 min at room temperature using 4% formalin (ROTI® Histofix; Roth, Karlsruhe, Germany). After washing in PBS, the printed constructs were embedded in an optimal cutting temperature (OCT) compound (Sakura Finetek, Alphen aan den Rijn, Netherlands) and incubated at 37 °C for 35 min. Samples were shock-frozen in liquid nitrogen and stored at -80 °C until further use. Following this, 10 µm cryosections were produced using the CM1950 cryostat (Leica Microsystems, Wetzlar, Germany). To assess the mineralization of the printed matrix, samples were stained using the OsteoImage™ Mineralization Assay (Lonza, Basel, Switzerland) according to the manufacturer's protocol. Briefly, sections were permeabilized with acetone for 10 min at -20 °C, washed two times with PBS and once with a wash buffer, incubated with the staining reagent for 30 min at room temperature, washed three times with a wash buffer, and mounted using ImsolMount (ImmunoLogic, Duiven, Netherlands). Images were taken using the BIOREVO BZ-9000 microscope (Keyence, Osaka, Japan).

##### 4.7. Real-Time PCR

To assess the relative gene expression levels of bone-specific marker genes, a semi-quantitative real-time PCR was performed. Three bioprints per condition were pooled, isolated, and analyzed. Isolation of total mRNA was performed using the ARCTURUS® PicoPure™ RNA isolation kit, following the manufacturer's protocol (Thermo Fisher Scientific, Waltham, MA, USA). mRNA was quantified using NanoDrop® ND-1000 spectrophotometer, and transcribed to cDNA using the iScript™ cDNA synthesis kit (Bio-Rad, Munich, Germany) according to the manufacturer's protocol. Real-time PCR was performed using the CFX96 real-time PCR system (Bio-Rad, Munich, Germany). Primer (10 µM), cDNA (equivalent to 6 ng total mRNA), and SensiFAST™ SYBR® No-ROX qPCR master mix (Bioline, Luckenwalde, Germany) were mixed in a total volume of 20 µL. After each PCR run, a melting curve analysis was performed to exclude non-specific amplification. Three replicates of each sample were measured. The relative expression of marker genes was normalized to the housekeeping gene TATA-box binding protein (*TBP*). The primer sequences are given in Table 2.



**Table 2.** Sequences of primers used for real-time PCR.

Gene	Accession Number	Description	For	Rev
ALPL	NM_000478	Alkaline phosphatase	cccacttcatctggaaccgc	ccgtgggtcaattctgcctcc
COL1A1	NM_000088	Collagen type I alpha 1 chain	gccgtgacctcaagatgtg	gccgaaccagacatgcctc
RUNX2	NM_001015051	Runt-related transcription factor 2	tcacaaatcctcccaagtagc	ggcgggacacctactctcatac
SPARC	NM_003118	Secreted protein acidic and cysteine rich	gcagaagctgcgggtgaagaa	ctcgaaaaagecgggtggtgc
SPP1	NM_000582	Secreted phosphoprotein 1	cactgatttcccacggacct	ccattcaactcctcgtttcc
TBP	NM_003194	TATA-box binding protein	ccttgctctaccaccaac	tcgtctcctgaatcccttagaagatg

#### 4.8. Statistical Analysis

Statistical analyses were performed using GraphPad Prism 8 (San Diego, CA, USA). All values are given as mean  $\pm$  standard deviation. AlamarBlue™ assay and real-time PCR data were analyzed using two-way ANOVA with Tukey's multiple comparison test (Supplementary Material). P values smaller than or equal to 0.05 were considered significant.

#### 5. Conclusions

In our work we compared osteogenic cells from different bone entities in terms of their applicability in biofabrication of autologous bone implants. Our findings suggest that periosteum-derived MPCs are the most suitable cell source for 3D bioprinted bone constructs based on microscopic observations, viability, mineralization capacity, and gene expression analysis, indicating an advanced differentiation stage with strong mineralization of the surrounding matrix. Additionally, these cells are readily obtainable via minimally invasive periosteal shaving and show high proliferation rates, making them ideal candidates for translational applications. The unique combination of these advantages makes the use of periosteum-derived MPCs a promising approach for the fabrication of autologous 3D bioprinted bone grafts.

**Supplementary Materials:** The following are available online at <https://www.mdpi.com/1422-0067/22/2/796/s1>. The data presented in this study are available from the corresponding author upon request.

**Author Contributions:** Conceptualization, A.-K.A., P.H.D., D.S., J.S., R.L., M.S., S.N., M.H., L.K., C.R., B.B.-B. and T.D.; methodology, A.-K.A., P.H.D., D.S., T.D.; validation, A.-K.A., P.H.D., D.S., J.S., S.S., R.L., M.S., S.N., M.H., L.K., C.R., B.B.-B., T.D.; formal analysis, A.-K.A., P.H.D., D.S., J.S., R.L., M.S., S.N., M.H., L.K., C.R., B.B.-B., T.D.; investigation, A.-K.A., P.H.D., D.S., T.D.; data curation, A.-K.A., P.H.D., D.S., T.D.; writing—original draft preparation, A.-K.A., P.H.D.; writing—review and editing, A.-K.A., P.H.D., D.S., J.S., S.S., R.L., M.S., S.N., M.H., L.K., C.R., B.B.-B., T.D.; visualization, A.-K.A., P.H.D. and T.D.; supervision, A.-K.A., P.H.D., R.L., M.S., S.N., M.H., L.K., C.R., B.B.-B. and T.D.; project administration, A.-K.A., P.H.D. and T.D. All authors have read and agreed to the published version of the manuscript.

**Funding:** This work was supported by the European Union Framework Programme (EU 953134—INKplant). We acknowledge support from the German Research Foundation (DFG) and the Open Access Publication Fund of Charité—Universitätsmedizin Berlin.

**Institutional Review Board Statement:** The study was conducted in accordance with the Declaration of Helsinki, and the protocol was approved by the Ethics Committee of Charité-Universitätsmedizin Berlin (EA4/049/13, EA2/068/14).

**Informed Consent Statement:** Informed consent was obtained from all subjects involved in the study.

**Data Availability Statement:** The data presented in this study are available in the supplementary material. PCR data is available from the corresponding author upon request.

**Acknowledgments:** We thank Alexander Thomas and Christopher Palmer for their critical revision of the manuscript. We also thank Anja Fleischmann for her excellent technical assistance.

**Conflicts of Interest:** A.-K.A. and D.S. are employees of Cellbricks GmbH. L.K. is the founder of Cellbricks GmbH. All other authors declare no conflict of interest.

### Abbreviations

3D	Three-dimensional
<sup>1</sup> H-NMR	Proton nuclear magnetic resonance
a	Alveolar bone
AB	alamarBlue™
B-MPC	Bone-derived mesenchymal progenitor cell
BM-MPC	Bone-marrow-derived mesenchymal progenitor cell
CAD	Computer-aided design
CO <sub>2</sub>	Carbon dioxide
DMEM	Dulbecco's modified Eagle's medium
ECM	Extracellular matrix
EDTA	Ethylenediaminetetraacetic acid
f	Fibular bone
FCS	Fetal calf serum
FGF	Fibroblast growth factor
GelMA	Methacrylated gelatin
HEPES	Hydroxyethyl piperazineethanesulfonic acid
i	Iliac-crest bone
kDa	Kilodalton
LAP	Lithium phenyl-2,4,6-trimethylbenzoylphosphinate
min	Minute
mL	Milliliter
MHz	Megahertz
MPC	Mesenchymal progenitor cell
mRNA	Messenger ribonucleic acid
μL	Microliter
nm	Nanometer
PBS	Phosphate-buffered saline
PI/FDA	Propidium iodide/fluorescein diacetate
P-MPC	Periosteum-derived mesenchymal progenitor cell
RGD	Tripeptide Arg-Gly-Asp
STL	Stereolithography

## Appendix A

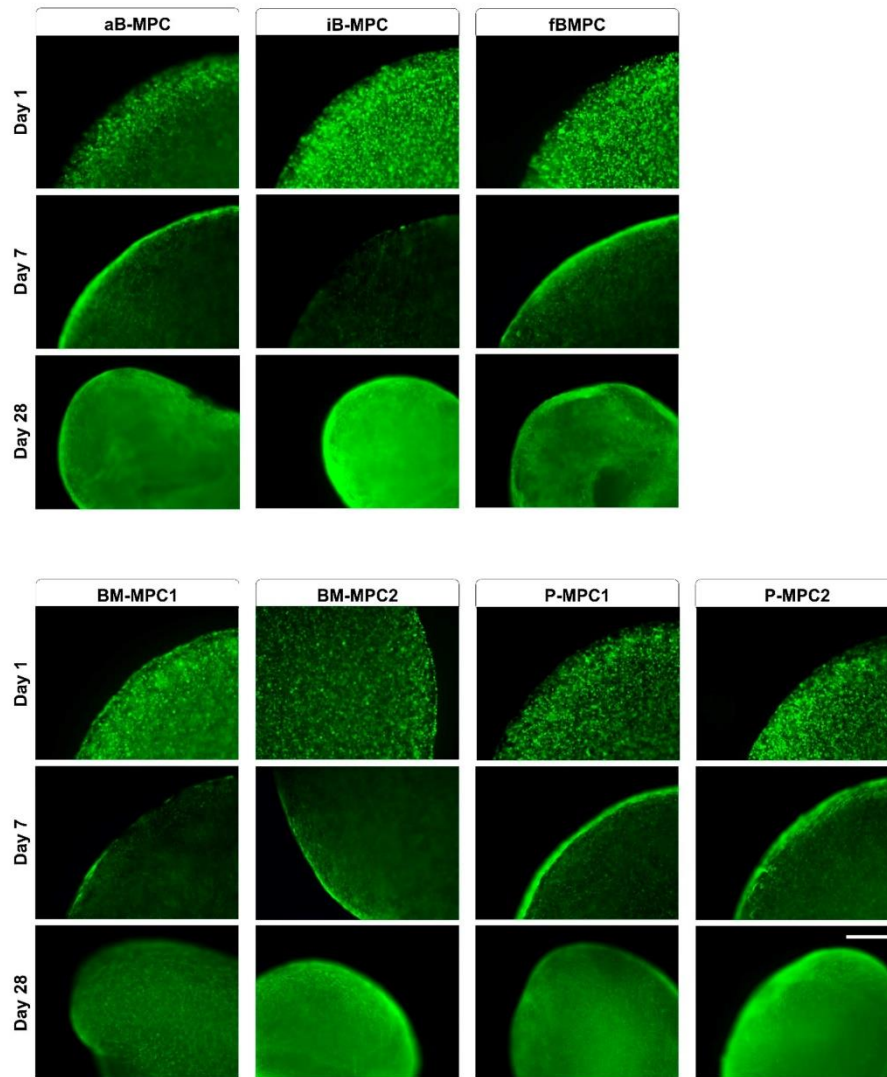


**Figure A1.** Viability of bioprints. Fluorescence microscopy images of constructs stained with PI/FDA showing living cells in green and dead cells in red on days 1, 7, and 28. Scale bar = 500  $\mu\text{m}$ .

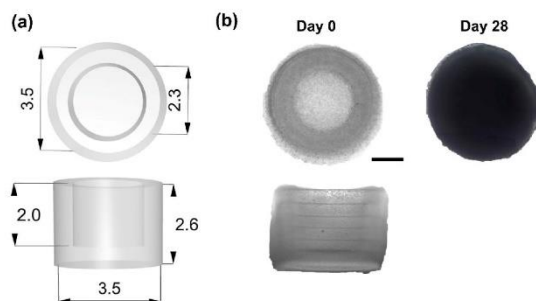


**Figure A2.** Bioprinting of a scaled-up construct containing P-MPCs. (a) CAD model of the bioprinted construct. Measurements are given in mm. (b) Microscopic images of bioprints on days 0 and 28 of cultivation. Scale bar = 1000  $\mu$ m.

(a)

% pos gated	P-MPC		BM-MPC		B-MPC		
	1	2	1	2	1	2	3
CD14	0.03	0.01	0	0.92	0.03	0.61	
CD34	0.96	0.58	0.01	0.04	0.01	0.16	
CD45	0.04	0	0.16	0.17	0.01	0.16	0.75
CD44	99.96	99.97	99.98	99.96	97.81	98.35	
CD73	99.95	99.98	99.99	99.95	100	99.71	99.8
CD90	99.49	99.15	84.43	96.76	95.2	93.91	86.8
CD105	99.97	99.99	99.84	99.81	99.94	97.31	98.3
CD166	99.96	99.98	99.23	99.67	99.92	86.69	

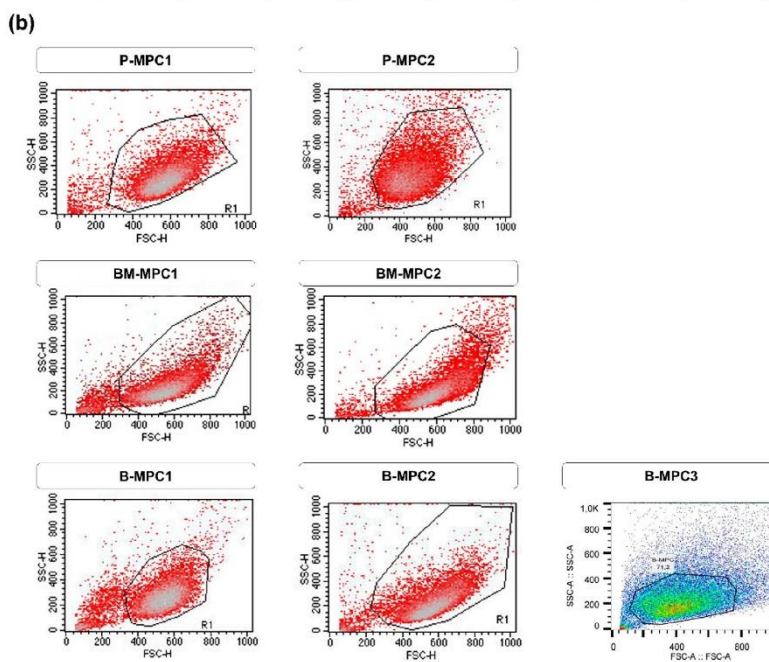


**Figure A3.** Flowcytomterical analyses of MPCs. (a) Results from flowcytomterical analyses of cell surface antigen patterns of isolated MPCs. (b) Side versus forward scatter density plots of analyzed MPCs.



## References

- Reichert, J.C.; Saifzadeh, S.; Wullschlegler, M.E.; Epari, D.R.; Schütz, M.A.; Duda, G.N.; Schell, H.; Van Griensven, M.; Redl, H.; Hutmacher, D.W. The challenge of establishing preclinical models for segmental bone defect research. *Biomater* **2009**, *30*, 2149–2163. [CrossRef] [PubMed]
- Rendenbach, C.; Hölterhoff, N.; Hischke, S.; Kreutzer, K.; Smeets, R.; Assaf, A.T.; Heiland, M.; Wikner, J. Free flap surgery in Europe: An interdisciplinary survey. *Int. J. Oral Maxillofac. Surg.* **2018**, *47*, 676–682. [CrossRef] [PubMed]
- Homma, Y.; Zimmermann, G.; Hernigou, P. Cellular therapies for the treatment of non-union: The past, present and future. *Injury* **2013**, *44*, S46–S49. [CrossRef]
- McKay, W.F.; Peckham, S.M.; Badura, J.M. A comprehensive clinical review of recombinant human bone morphogenetic protein-2 (INFUSE® Bone Graft). *Int. Orthop.* **2007**, *31*, 729–734. [CrossRef] [PubMed]
- Beck-Broichsitter, B.E.; Garling, A.; Koehne, T.; Barvencik, F.; Smeets, R.; Mehl, C.; Jeschke, A.; Wiltfang, J.; Becker, S.T. 3D-tracking the regenerative potential of the mandible with micro-CTs. *Oral Maxillofac. Surg.* **2015**, *19*, 29–35. [CrossRef] [PubMed]
- Rendenbach, C.; Steffen, C.; Hanken, H.; Schlurmann, K.; Henningsen, A.; Beck-Broichsitter, B.; Kreutzer, K.; Heiland, M.; Precht, C. Complication rates and clinical outcomes of osseous free flaps: A retrospective comparison of CAD/CAM versus conventional fixation in 128 patients. *Int. J. Oral Maxillofac. Surg.* **2019**, *48*, 1156–1162. [CrossRef] [PubMed]
- Rendenbach, C.; Rashad, A.; Hansen, L.; Kohlmeier, C.; Dyck, M.L.; Suling, A.; Assaf, A.T.; Amling, M.; Heiland, M.; Wikner, J.; et al. Functional donor site morbidity longer than one year after fibula free flap: A prospective biomechanical analysis. *Microsurgery* **2018**, *38*, 395–401. [CrossRef] [PubMed]
- Hoffman, T.; Khademhosseini, A.; Langer, R. Chasing the Paradigm: Clinical Translation of 25 Years of Tissue Engineering. *Tissue Eng. Part A* **2019**, *25*, 679–687. [CrossRef] [PubMed]
- Baltazar, T.; Merola, J.; Catarino, C.; Xie, C.B.; Kirkiles-Smith, N.C.; Lee, V.; Hotta, S.; Dai, G.; Xu, X.; Ferreira, F.C.; et al. Three Dimensional Bioprinting of a Vascularized and Perfusable Skin Graft Using Human Keratinocytes, Fibroblasts, Pericytes, and Endothelial Cells. *Tissue Eng. Part A* **2020**, *26*, 227–238. [CrossRef] [PubMed]
- Lam, T.; Ruppelt, A.; Thomas, A.; Amler, A.-K.; Noichl, B.P.; Lauster, R.; Kloke, L. Bioprinting Perfusion-Enabled Liver Equivalents for Advanced Organ-on-a-Chip Applications. *Genes* **2018**, *9*, 176. [CrossRef]
- Rathan, S.; Dejob, L.; Schipani, R.; Haffner, B.; Möbius, M.E.; Kelly, D.J. Fiber Reinforced Cartilage ECM Functionalized Bioinks for Functional Cartilage Tissue Engineering. *Adv. Healthc. Mater.* **2019**, *8*, e1801501. [CrossRef] [PubMed]
- Lam, T.; Dehne, T.; Krüger, J.P.; Hondke, S.; Endres, M.; Thomas, A.; Lauster, R.; Sittlinger, M.; Kloke, L. Photopolymerizable gelatin and hyaluronic acid for stereolithographic 3D bioprinting of tissue-engineered cartilage. *J. Biomed. Mater. Res. Part. B Appl. Biomater.* **2019**, *107*, 2649–2657. [CrossRef] [PubMed]
- Genova, T.; Roato, I.; Carossa, M.; Motta, C.; Cavagnetto, D.; Mussano, F. Advances on Bone Substitutes through 3D Bioprinting. *Int. J. Mol. Sci.* **2020**, *21*, 7012. [CrossRef]
- Orciani, M.; Fini, M.; Di Primio, R.; Mattioli-Belmonte, M. Biofabrication and Bone Tissue Regeneration: Cell Source, Approaches, and Challenges. *Front. Bioeng. Biotechnol.* **2017**, *5*, 17. [CrossRef] [PubMed]
- Midha, S.; Dalela, M.; Sybil, D.; Patra, P.; Mohanty, S. Advances in three-dimensional bioprinting of bone: Progress and challenges. *J. Tissue Eng. Regen. Med.* **2019**, *13*, 925–945. [CrossRef]
- Scognamiglio, C.; Soloperto, A.; Ruocco, G.; Cidonio, G. Bioprinting stem cells: Building physiological tissues one cell at a time. *Am. J. Physiol. Cell Physiol.* **2020**, *319*, C465–C480. [CrossRef]
- Neumann, K.; Dehne, T.; Endres, M.; Erggelet, C.; Kaps, C.; Ringe, J.; Sittlinger, M. Chondrogenic differentiation capacity of human mesenchymal progenitor cells derived from subchondral cortico-spongious bone. *J. Orthop. Res.* **2008**, *26*, 1449–1456. [CrossRef]
- Leberfinger, A.N.; Ravnic, D.J.; Dhawan, A.; Ozbolat, I.T. Concise Review: Bioprinting of Stem Cells for Transplantable Tissue Fabrication. *Stem Cells Transl. Med.* **2017**, *6*, 1940–1948. [CrossRef]
- Secunda, R.; Vennila, R.; Mohanashankar, A.M.; Rajasundari, M.; Jeswanth, S.; Surendran, R. Isolation, expansion and characterisation of mesenchymal stem cells from human bone marrow, adipose tissue, umbilical cord blood and matrix: A comparative study. *Cytotechnology* **2015**, *67*, 793–807. [CrossRef]
- El-Jawhari, J.J.; Kleftouris, G.; El-Sherbiny, Y.; Saleeb, H.; West, R.M.; Jones, E.; Giannoudis, P.V. Defective Proliferation and Osteogenic Potential with Altered Immunoregulatory phenotype of Native Bone marrow-Multipotential Stromal Cells in Atrophic Fracture Non-Union. *Sci. Rep.* **2019**, *9*, 1–16. [CrossRef] [PubMed]
- Ferretti, C.; Mattioli-Belmonte, M. Periosteum derived stem cells for regenerative medicine proposals: Boosting current knowledge. *World J. Stem Cells* **2014**, *6*, 266–277. [CrossRef]
- Rampersad, S.N. Multiple Applications of Alamar Blue as an Indicator of Metabolic Function and Cellular Health in Cell Viability Bioassays. *Sensors* **2012**, *12*, 12347–12360. [CrossRef] [PubMed]
- Garant, P.R. *Oral Cells and Tissues*; Quintessence Publishing Company: Chicago, IL, USA, 2003.
- Schroeder, H.E. *The Periodontium. The Handbook of Microscopic Anatomy*; Springer: Berlin/Heidelberg, Germany, 1986; Volume 5.
- Kuhn, L.T. Bone mineralization. In *Encyclopedia of Materials: Science and Technology*, 2nd ed.; Buschow, K.H.J., Cahn, R.W., Flemings, M.C., Ilshner, B., Kramer, E.J., Mahajan, S., Veyssièrè, P., Eds.; Elsevier: Amsterdam, The Netherlands, 2001; pp. 787–794.
- Orimo, H. The Mechanism of Mineralization and the Role of Alkaline Phosphatase in Health and Disease. *J. Nippon. Med. Sch.* **2010**, *77*, 4–12. [CrossRef] [PubMed]



27. Lee, J.S.; Kim, M.E.; Seon, J.K.; Kang, J.Y.; Yoon, T.R.; Park, Y.-D.; Kim, H.K. Bone-forming peptide-3 induces osteogenic differentiation of bone marrow stromal cells via regulation of the ERK1/2 and Smad1/5/8 pathways. *Stem Cell Res.* **2018**, *26*, 28–35. [[CrossRef](#)] [[PubMed](#)]
28. Kirkham, G.R.; Cartmell, S.H. Genes and Proteins Involved in the Regulation of Osteogenesis. In *Topics in Tissue Engineering*; Ashammakhi, N., Reis, R.L., Chiellini, E., Eds.; Oulu University: Oulu, Finland, 2007; Volume 3.
29. Atala, A.; Yoo, J.J. *Essentials of 3D Biofabrication and Translation*; Academic Press: Cambridge, MA, USA, 2015.
30. Sodek, J.; McKee, M.D. Molecular and cellular biology of alveolar bone. *Periodontol.* **2000**, *24*, 99–126. [[CrossRef](#)]
31. Altmann, B.; Löchner, A.; Swain, M.; Kohal, R.-J.; Giselbrecht, S.; Gottwald, E.; Steinberg, T.; Tomakidi, P. Differences in morphogenesis of 3D cultured primary human osteoblasts under static and microfluidic growth conditions. *Biomaterials* **2014**, *35*, 3208–3219. [[CrossRef](#)]
32. Wein, M.; Huelter-Hassler, D.; Nelson, K.; Fretwurst, T.; Nahles, S.; Finkenzyler, G.; Altmann, B.; Steinberg, T. Differential osteopontin expression in human osteoblasts derived from iliac crest and alveolar bone and its role in early stages of angiogenesis. *J. Bone Miner. Metab.* **2018**, *37*, 105–117. [[CrossRef](#)]
33. McBeth, C.; Lauer, J.; Ottersbach, M.; Campbell, J.; Sharon, A.; Sauer-Budge, A.F. 3D bioprinting of GelMA scaffolds triggers mineral deposition by primary human osteoblasts. *Biofabrication* **2017**, *9*, 015009. [[CrossRef](#)]
34. Park, J.Y.; Choi, J.-C.; Shim, J.-H.; Lee, J.-S.; Park, H.; Kim, S.W.; Doh, J.; Cho, D.-W. A comparative study on collagen type I and hyaluronic acid dependent cell behavior for osteochondral tissue bioprinting. *Biofabrication* **2014**, *6*, 035004. [[CrossRef](#)]
35. Liu, Y.; Chan-Park, M.B. A biomimetic hydrogel based on methacrylated dextran-graft-lysine and gelatin for 3D smooth muscle cell culture. *Biomaterials* **2010**, *31*, 1158–1170. [[CrossRef](#)]
36. Amler, A.-K.; Thomas, A.; Tüzüner, S.; Lam, T.; Geiger, M.-A.; Kreuder, A.-E.; Palmer, C.; Nahles, S.; Lauster, R.; Kloke, L. A 3D bioprinted human jawbone model. *Sci. Rep.*. Under Review.
37. Pattappa, G.; Heywood, H.K.; De Bruijn, J.D.; Lee, D.A. The metabolism of human mesenchymal stem cells during proliferation and differentiation. *J. Cell. Physiol.* **2011**, *226*, 2562–2570. [[CrossRef](#)]
38. Long, F. Building strong bones: Molecular regulation of the osteoblast lineage. *Nat. Rev. Mol. Cell Biol.* **2012**, *13*, 27–38. [[CrossRef](#)] [[PubMed](#)]
39. Miron, R.J.; Zhang, Y. Osteoinduction: A Review of Old Concepts with New Standards. *J. Dent. Res.* **2012**, *91*, 736–744. [[CrossRef](#)] [[PubMed](#)]
40. Ducey, P.; Starbuck, M.; Priemel, M.; Shen, J.; Pinero, G.; Geoffroy, V.; Amling, M.; Karsenty, G. A Cbfa1-dependent genetic pathway controls bone formation beyond embryonic development. *Genes Dev.* **1999**, *13*, 1025–1036. [[CrossRef](#)] [[PubMed](#)]
41. Czekanska, E.M.; Stoddart, M.J.; Ralphs, J.R.; Richards, R.G.; Hayes, J.S. A phenotypic comparison of osteoblast cell lines versus human primary osteoblasts for biomaterials testing. *J. Biomed. Mater. Res. Part. A* **2014**, *102*, 2636–2643. [[CrossRef](#)] [[PubMed](#)]
42. Stich, S.; Loch, A.; Leinase, I.; Neumann, K.; Kaps, C.; Sittinger, M.; Ringe, J. Human periosteum-derived progenitor cells express distinct chemokine receptors and migrate upon stimulation with CCL2, CCL25, CXCL8, CXCL12, and CXCL13. *Eur. J. Cell Biol.* **2008**, *87*, 365–376. [[CrossRef](#)] [[PubMed](#)]
43. Almela, T.; Al-Sahaf, S.; Bolt, R.; Brook, I.M.; Moharamzadeh, K. Characterization of Multilayered Tissue-Engineered Human Alveolar Bone and Gingival Mucosa. *Tissue Eng. Part. C Methods* **2018**, *24*, 99–107. [[CrossRef](#)]
44. Wein, M.; Fretwurst, T.; Nahles, S.; Duttonhoefer, F.; Tomakidi, P.; Steinberg, T.; Nelson, K. Pilot investigation of the molecular discrimination of human osteoblasts from different bone entities. *J. Cranio-Maxillofac. Surg.* **2015**, *43*, 1487–1493. [[CrossRef](#)] [[PubMed](#)]
45. Thitiset, T.; Damrongsakkul, S.; Bunaprasert, T.; Leraanaksiri, W.; Honsawek, S. Development of Collagen/Demineralized Bone Powder Scaffolds and Periosteum-Derived Cells for Bone Tissue Engineering Application. *Int. J. Mol. Sci.* **2013**, *14*, 2056–2071. [[CrossRef](#)]
46. Zheng, Y.-X.; Ringe, J.; Liang, Z.; Loch, A.; Chen, L.; Sittinger, M. Osteogenic potential of human periosteum-derived progenitor cells in PLGA scaffold using allogeneic serum. *J. Zhejiang Univ. Sci. B* **2006**, *7*, 817–824. [[CrossRef](#)] [[PubMed](#)]
47. Ringe, J.; Leinase, I.; Stich, S.; Loch, A.; Neumann, K.; Haisch, A.; Häup, T.; Manz, R.; Kaps, C.; Sittinger, M. Human mastoid periosteum-derived stem cells: Promising candidates for skeletal tissue engineering. *J. Tissue Eng. Regen. Med.* **2008**, *2*, 136–146. [[CrossRef](#)] [[PubMed](#)]
48. Chang, H.; Tate, M.L.K. Concise Review: The Periosteum: Tapping into a Reservoir of Clinically Useful Progenitor Cells. *Stem Cells Transl. Med.* **2012**, *1*, 480–491. [[CrossRef](#)] [[PubMed](#)]
49. Kim, Y.-K.; Nakata, H.; Yamamoto, M.; Miyasaka, M.; Kasugai, S.; Kuroda, S. Osteogenic Potential of Mouse Periosteum-Derived Cells Sorted for CD90 In Vitro and In Vivo. *Stem Cells Transl. Med.* **2016**, *5*, 227–234. [[CrossRef](#)] [[PubMed](#)]
50. Kreuz, P.C.; Steinwachs, M.; Erggelet, C.; Krause, S.J.; Ossendorf, C.; Maier, D.; Ghanem, N.; Uhl, M.; Haag, M. Classification of graft hypertrophy after autologous chondrocyte implantation of full-thickness chondral defects in the knee. *Osteoarthr. Cartil.* **2007**, *15*, 1339–1347. [[CrossRef](#)] [[PubMed](#)]
51. Trautvetter, W.; Kaps, C.; Schmelzeisen, R.; Sauerbier, S.; Sittinger, M. Tissue-Engineered Polymer-Based Periosteal Bone Grafts for Maxillary Sinus Augmentation: Five-Year Clinical Results. *J. Oral Maxillofac. Surg.* **2011**, *69*, 2753–2762. [[CrossRef](#)] [[PubMed](#)]
52. Murphy, S.V.; Atala, A. 3D bioprinting of tissues and organs. *Nat. Biotechnol.* **2014**, *32*, 773–785. [[CrossRef](#)]

53. Kaempfen, A.; Todorov, A.; Güven, S.; Largo, R.D.; Claude, J.; Scherberich, A.; Martin, I.; Schaefer, D.J. Engraftment of Prevascularized, Tissue Engineered Constructs in a Novel Rabbit Segmental Bone Defect Model. *Int. J. Mol. Sci.* **2015**, *16*, 12616–12630. [[CrossRef](#)]
54. Zhang, H.; Zhou, Y.; Yu, N.; Ma, H.; Wang, K.; Liu, J.; Zhang, W.; Cai, Z.; He, Y. Construction of vascularized tissue-engineered bone with polylysine-modified coral hydroxyapatite and a double cell-sheet complex to repair a large radius bone defect in rabbits. *Acta Biomater.* **2019**, *91*, 82–98. [[CrossRef](#)]
55. Thomas, A.; Orellano, I.; Lam, T.; Noichl, B.; Geiger, M.-A.; Amler, A.-K.; Kreuder, A.-E.; Palmer, C.; Duda, G.; Lauster, R.; et al. Vascular bioprinting with enzymatically degradable bioinks via multi-material projection-based stereolithography. *Acta Biomater.* **2020**, *117*, 121–132. [[CrossRef](#)]
56. Chiesa, I.; De Maria, C.; Lapomarda, A.; Fortunato, G.M.; Montemurro, F.; Di Gesù, R.; Tuan, R.S.; Vozzi, G.; Gottardi, R. Endothelial cells support osteogenesis in an in vitro vascularized bone model developed by 3D bioprinting. *Biofabrication* **2020**, *12*, 025013. [[CrossRef](#)] [[PubMed](#)]
57. Mikos, A.G.; Herring, S.W.; Ochareon, P.; Elisseeff, J.; Lu, H.H.; Kandel, R.; Schoen, F.J.; Toner, M.; Mooney, D.; Atala, A.; et al. Engineering Complex Tissues. *Tissue Eng.* **2006**, *12*, 3307–3339. [[CrossRef](#)] [[PubMed](#)]
58. Du, M.; Chen, B.; Meng, Q.; Liu, S.; Zheng, X.; Zhang, C.; Wang, H.; Li, H.; Wang, N.; Dai, J. 3D bioprinting of BMSC-laden methacrylamide gelatin scaffolds with CBD-BMP2-collagen microfibers. *Biofabrication* **2015**, *7*, 044104. [[CrossRef](#)] [[PubMed](#)]
59. Koolen, M.; Longoni, A.; Van Der Stok, J.; Van Der Jagt, O.; Gawlitta, D.; Weinans, H. Complete regeneration of large bone defects in rats with commercially available fibrin loaded with BMP-2. *Eur. Cells Mater.* **2019**, *38*, 94–105. [[CrossRef](#)] [[PubMed](#)]
60. Ringe, J.; Strassburg, S.; Neumann, K.; Endres, M.; Notter, M.; Burmester, G.-R.; Kaps, C.; Sittinger, M. Towards in situ tissue repair: Human mesenchymal stem cells express chemokine receptors CXCR1, CXCR2 and CCR2, and migrate upon stimulation with CXCL8 but not CCL2. *J. Cell. Biochem.* **2007**, *101*, 135–146. [[CrossRef](#)] [[PubMed](#)]
61. Endres, M.; Andreas, K.; Kalwitz, G.; Freymann, U.; Neumann, K.; Ringe, J.; Sittinger, M.; Häupl, T.; Kaps, C. Chemokine profile of synovial fluid from normal, osteoarthritis and rheumatoid arthritis patients: CCL25, CXCL10 and XCL1 recruit human subchondral mesenchymal progenitor cells. *Osteoarthr. Cartil.* **2010**, *18*, 1458–1466. [[CrossRef](#)]
62. Daly, A.C.; Pitacco, P.; Nulty, J.; Cunniffe, G.M.; Kelly, D.J. 3D printed microchannel networks to direct vascularisation during endochondral bone repair. *Biomaterials* **2018**, *162*, 34–46. [[CrossRef](#)]
63. Daly, A.C.; Cunniffe, G.M.; Sathy, B.N.; Jeon, O.; Alsberg, E.; Kelly, D.J. 3D Bioprinting of Developmentally Inspired Templates for Whole Bone Organ Engineering. *Adv. Healthc. Mater.* **2016**, *5*, 2353–2362. [[CrossRef](#)]
64. Van Den Bulcke, A.I.; Bogdanov, B.; De Rooze, N.; Schacht, E.H.; Cornelissen, M.; Berghmans, H. Structural and Rheological Properties of Methacrylamide Modified Gelatin Hydrogels. *Biomacromolecules* **2000**, *1*, 31–38. [[CrossRef](#)]
65. Shirahama, H.; Lee, B.H.; Tan, L.P.; Cho, N.-J. Precise Tuning of Facile One-Pot Gelatin Methacryloyl (GelMA) Synthesis. *Sci. Rep.* **2016**, *6*, 31036. [[CrossRef](#)]
66. Majima, T.; Schnabel, W.; Weber, W. Phenyl-2, 4, 6-trimethylbenzoylphosphinates as water-soluble photoinitiators. Generation and reactivity of O<sup>•</sup> P(C<sub>6</sub>H<sub>5</sub>)(O<sup>-</sup>) radical anions. *Die Makromol. Chem.* **1991**, *192*, 2307–2315. [[CrossRef](#)]
67. Fairbanks, B.D.; Schwartz, M.P.; Bowman, C.N.; Anseth, K.S. Photoinitiated polymerization of PEG-diacrylate with lithium phenyl-2,4,6-trimethylbenzoylphosphinate: Polymerization rate and cytocompatibility. *Biomaterials* **2009**, *30*, 6702–6707. [[CrossRef](#)] [[PubMed](#)]
68. Ullah, M.; Eucker, J.; Sittinger, M.; Ringe, J. Mesenchymal stem cells and their chondrogenic differentiated and dedifferentiated progeny express chemokine receptor CCR9 and chemotactically migrate toward CCL25 or serum. *Stem Cell Res. Ther.* **2013**, *4*, 99. [[CrossRef](#)] [[PubMed](#)]
69. Trentz, O.A.; Ariketh, D.; Sentilnathan, V.; Hemmi, S.; Handschin, A.E.; De Rosario, B.; Mohandas, P.V.A. Surface proteins and osteoblast markers: Characterization of human adipose tissue-derived osteogenic cells. *Eur. J. Trauma Emerg. Surg.* **2010**, *36*, 457–463. [[CrossRef](#)] [[PubMed](#)]
70. Kruger, J.P.; Enz, A.; Hondke, S.; Wichelhaus, A.; Endres, M.; Mittlmeier, T. Proliferation, migration and differentiation potential of human mesenchymal progenitor cells derived from osteoarthritic subchondral cancellous bone. *J. Stem Cells Regen. Med.* **2018**, *14*, 45–52. [[CrossRef](#)]

## 9. Curriculum Vitae

**Mein Lebenslauf wird aus datenschutzrechtlichen Gründen in der elektronischen Version meiner Arbeit nicht veröffentlicht**

## 10. Acknowledgements

I would like to express my sincere thanks to the entire laboratory for tissue engineering, which made this ambitious project possible in a short time - especially to Dr. Shabnam Hemmati and Anja Fleischmann, who, despite their own tasks, always supported me when I needed their help.

My special thanks go to Dr. Tilo Dehne, who was always supportive and had a clever solution ready, even in difficult situations. I would also like to thank Dr. Carsten Rendenbach, who accompanied me all the way with his life experience in complex situations and always encouraged me to go my own way.

Furthermore, I would like to thank Lennard Shopperly for always putting his meticulousness in the right place and at the same time standing by me as a good friend.

Moreover, I would like to thank Prof. Martina Seifert, who taught me with great patience a little love for detail.

Finally, I would like to thank Prof. Michael Sittinger, who was constantly convinced that I could manage the tasks ahead and always supported me with his full backing - even when I had unconventional ideas.